ABSTRACT

Title of Document: MICROFLUIDICS INTERFACING TO MASS SPECTROMETRY

YI ZHOU, Doctor of Philosophy, 2007

Directed By: Dr. Don L. Devoe, Associate Professor, Department of Mechanical Engineering

Polymer-based microfluidic systems have received considerable attention for high throughput chemical analysis. Recently, the ongoing development of microfluidics interfacing to high-accuracy mass spectrometry to identify large molecules had an important impact on biochemistry. A primary goal of this dissertation is the development of a microfluidic apparatus for performing microscale gel electrophoresis, coupled with integrated electrospray tips for either direct interfacing to mass spectrometry through ESI-MS, or coupling to MALDI-MS through the deposition of separated analyte onto a MALDI target for offline analysis. In this dissertation, microfabrication techniques for polymer-based microchip are developed. A novel electrospray interface is demonstrated with good performance. The optimization of multi-channel electrospray tips for multiplexed analysis from a single microfluidic chip was demonstrated. Gas-phased electrophoretic protein/peptide concentration on a pre-structured MALDI target was further demonstrated via theoretical and experimental analysis. The results for developing GE-ES using linear polymer gel validate the underlined principles and specify challenges involved in coupling GE to MS. Finally, cross-linked polyacrylamide gel was explored and characterized using in-situ photo- polymerization method in microchannels.

MICROFLUIDICS INTERFACING TO MASS SPECTROMETRY

By

YI ZHOU

Dissertation submitted to the Faculty of the Graduate School of the
University of Maryland, College Park, in partial fulfillment
of the requirements for the degree of
Doctor of Philosophy
2007

Advisory Committee:
Associate Professor Don DeVoe, Chair
Associate Professor Cheng S. Lee, Dean's Representative
Professor Amr Baz
Associate Professor Elias Balaras
Assistant Professor Adam Hsieh

Dedication

To my husband, my daughter and my parents, with love.

Acknowledgement

I would like to express my sincere gratitude to my supervisor, Professor Don L. Devoe. His wide knowledge and his logical way of thinking have been of great value for me. His insights, encouragement and personal guidance have provided a good basis for this dissertation work. Also, his research interest in BioMEMS expanded my prospective in my future career.

I am deeply grateful to my committee members, Professor Cheng S. Lee, Professor Amr Baz, Professor Elias Balaras and Professor Adam Hsieh, for their detailed and constructive advice throughout this dissertation work.

I wish to express my warm and sincere thanks to Dr. Yan Li and Dr. Ying-xin Wang who gave me valuable suggestions and friendly help during our discussions.

Finally I would like to thank my friends and colleagues at Maryland Microfluidics Lab, Lihua Li, Likun Zhu, Wei-Jen Cheng, Parshant Kumar, Lou Hromada, Chris Kimball and Nate Sniadecki for their assistance and suggestion in this work.

Table of Contents

Table of Figures

Table of Tables

Chapter 1 Introduction

1.1 Motivation

Proteomics, the large-scale study of proteins within a given biological sample, continues to drive the development of analytical technologies that must address substantially greater challenges than those faced in genomic analysis. Unlike DNA and RNA, no techniques exist for the direct amplification of proteins, thus detection sensitivity is paramount for the identification of low-abundance species from limited samples. At the same time, the dynamic range of typical proteomes can be over 10^{10} [1-4], making the analysis of low-abundance proteins particularly challenging. Sensitivity and dynamic range limitation dictate the need for effective separation of protein or peptide species prior to back-end analysis by mass spectrometry. Such separations can greatly reduce the dynamic range of individual sample fractions, enabling far more effective and complete analysis than would otherwise be possible. Sodium dodecyl sulfate polyacrylamide gel electrophoresis (SDS-PAGE) is a well-characterized technology for separating proteins with differences in molecular weights and charge states and is one of the most common bioseparation technologies [5-7]. Combining SDS-PAGE with isoelectric focusing (IEF), two-dimensional PAGE platform further extends the resolving power of the techniques [8], and has became the standard for proteomic analysis when thousands of constituent

species must be resolved in a single run. However, 2-D PAGE suffers from several limitations, including insufficient resolving power and mass accuracy for identification of typical protein species [9]. Smith et al. introduced a capillary electrophoresis - mass spectrometry (CE-MS) coupling technique [10] in 1987, with MS used for high mass resolution measurements of biomolecules separated by CE. In modern proteomic analysis, MS coupling is an essential tool, enabling accurate protein identification as well as quantification.

Since the concept of "micro total analysis systems" (μTAS) was proposed in the late 1980's [11], microfluidic systems have been widely applied in proteomics applications such as on-chip sample purification, digestion, concentration, and separation [12-14]. At an early stage, it was recognized that the flow rates used in microfluidics (from a few tens of nL/min to a few tens of μL/min) were comparable to those used in electrospray ionization-mass spectrometry (ESI-MS). ESI-MS has become a powerful technique for the analysis of a large array of small organic molecules, peptides, proteins, oligonucleotides, and nucleic acids because ESI-MS produces intact molecular ions directly from the solution phase [15-18]. As summarized in [13], it was believed that the development of microfabrication techniques allowed the integration of a high number of electrospray emitters on the same chip to increase the analysis throughput; other functions, such as sample preparation or separation, may be integrated on the same chip. These reasons excited an enormous research interest in integration of the coupling of high-throughput MS with other functions in proteomic analysis.

The advantages of microfluidics, such as short analysis time to limit diffusion, and high surface-to-volume ratio to reduce Joule heating, make it promising for proteomic studies. This thesis work addresses the use of microfluidic systems by implementation different analytical functions such as protein and peptide separation, coupled with MS. Specially, sample preparation off-line coupling with matrix-assisted laser deposition/ionization – mass spectrometry (MALDI-MS) can dramatically increase its throughout, which will be discussed in this thesis work.

1.2 Literature Review

1.2.1 Microfluidics/ ESI-MS Interfacing

1.2.1.1Electrospray Emitters

Microfabrication techniques offer various options for building electrospray emitters: materials (glass, silica, PDMS, polyimide, etc), size of the microchannel (from nanosprayer to microsprayer), shape of the outlet, surface chemistry, high-voltage delivery, etc [13].

A simple way to fabricate electrospray emitters is to insert a sharp capillary spray tip into microchannel exits by gluing [19], or using a liquid junction [20]. These devices suffer from large dead volume and are very difficult to use in the fabrication of high-density electrospray tips arrays since they are not fully integrated with the microchannel exits.

Directly spraying the liquid from a flat or blunt orifice was explored by different groups [21-23]. This method had the difficulty of establishing a stable Taylor cone since the

fluid out of the microchannel exit tended to spread over the surface. To prevent the liquid from spreading, the modifications to increase the hydrophobicity of the channel exits were reported, either by using a surface coating [21-22], or using highly hydrophobic polymer materials [23]. These approaches limited liquid spreading, but still would not maintain the stable positions of Taylor cones. In addition, the lifetime of the surface coating was limited since damage to coating during the electrospray process would occur.

The nib-shape emitters used to minimize the wetted area demonstrated good electrospraying characteristics, on silicon by plasma etching [24], on polycarbonate by laser ablation [25-26], on Su-8 involving the releasing of a sacrificial layer (Nickel) [27], or an additional layer such as parylene C [20] incorporated to form a sharp tip. These types of devices provided very good spray stability due to significantly reduction of liquid spreading, but required complicated fabrication processes or an additional layer, which hindered the mass production using batch processing.

Therefore, the crucial parameter that affects the generation of stable electrospray was high hydrophobicity of the outer walls to prevent the solution from wetting the outer wall and forming a big droplet.

In addition several traditional ways of applying the high voltage for electrospray were used: a platinum electrode plunged into the solution or a liquid junction used, or a conductive coating applied at the outer of the emitter. These methods had disadvantages which relied on either the sample conductivity or the lifetime of the conductive coating. An advantage of electrospray emitters in microfluidic chip format is that electrodes may be integrated on the same chip. For example, carbon-pasted electrodes [28] or gold-

coated copper electrodes [29] sat at the bottom of microchannels to apply the high voltage as close as desirable to the emitters.

1.2.1.2 CE-MS Integration

One of the major driving forces for the development of a MS chip is that a MS chip is not only an electrospray emitter, but also a tool for implementation of other functions such as sample preparation, or separations on the same chip [13].

When the electrospray emitter was integrated with CE, a solvent make-up flow was needed to generate a stable electrospray. Henion's group used a liquid junction at the outlet of CE microchannel to allow the application of make-up flow, sheath gas and high voltage to realize the integration of CE with a MS chip [30-32]. In microchip format, the make-up flow can be integrated either through a side-arm microchannel [19, 33-37], or through a porous microjunction [35].

In most microfluidic devices, a big droplet was easily formed at the outlet of microsprayer [37]. It resulted in the difficulty of directly coupling with MS with the upstream separation because of the limitation of dead volume, flow rate disturbances [35], band broadening etc.

At this point in time, all the research reported is still far from exploiting the full potential of on-chip CE-MS in terms of resolution and sensitivity [13].

1.2.2 Microfluidics/ MALDI-MS Interfacing

MALDI is a soft ionization technology in MS that is used to allow the ionization of solid phase analyte cocrystallized with an energy-absorbing matrix material on the surface of a supporting target plate. The term MALDI was coined in 1985 by Karas et al [38]. These researchers found that the amino acid alnine could be ionized more easily with a pulsed 266 nm laser if mixed with the amino acid tryptophan, which acted as an energy-absorbing matrix component. Modern MALDI-MS uses a nitrogen laser to ionize analytes cocrystallized with an organic matrix component [39], and performs a detection of generated ions typically using a time-of-flight (TOF) MS instrument.

MALDI-MS offers excellent detection limits and easily interpreted mass spectra [40], which can detect a wide range of sample between ca. 500Da and 300kDa while ESI-MS detects less than 100kDa. MALDI-MS is more tolerant of salts and other contaminations than ESI-MS. MAIDI-MS enables on-chip sample preparation steps to be fully decoupled from the MS-analysis [40]. While simultaneous ESI-MS from multiple microchannels is generally not practical, the off-line feature of MALDI-MS coupled with microfluidics may be feasible for parallel deposition of sample from multiplexed microchannels onto MALDI target.

1.2.2.1 MALDI sample preparation

The efficiency of MALDI-MS was highly sensitive to the sample preparation procedure such as the matrix/solvent system, substrate material, sample purification, sample crystallization techniques etc. It was reported that the formation of homogeneous

matrix/analyte co-crystals facilitated the overall ionization process, resulting in reduced matrix signal and stable and reproducible analyte ion yields. Several different methods for growing homogeneous analyte-doped matrix crystals have been described in the MS literature [41-52].

Briefly, the most common MALDI-MS sample preparation techniques included the dried droplet method [41], vacuum drying method [42], fast solvent evaporation [43-44], two-layer method [45-46] etc. These approaches involve using pipetting or spotting samples and matrix solution on MALDI target followed by either air-drying or vacuum drying or using highly evaporate solvents. Due to an inhomogeneous mixture of analytes throughout the sample, MALDI users often end up searching for "sweet spots" which result in high variable analyte ion production as the laser is moved across the sample surface [45, 47].

One strategy to improve the homogeneous sample is to reduce the diameter of deposited sample spot, which can be accomplished by modifying MAIDI target surfaces. For example, hydrophilic target material such as gold was deposited and patterned on top of a hydrophobic substrate such as Teflon [53], resulting in a reduction in sample spot size. Similarly, patterned hydrophobic regions can be surrounded hydrophilic target pads to improve MS analysis sensitivity and resolution [54-56]. SuNyx (Cologne, Germany) recently reported that a MALDI chip was fabricated by predepositing α-cyano-4-hydroxycinnamic acid (CHCA) matrix pads arrays with 300nm in diameter onto an ultra-hydrophobic surface, with detection limits in order of 0.5 amol [57].

In addition, purely physical concentrators have been demonstrated for increasing local analyte concentration on the MALDI target plates. Nanovial targets first employed a microfabricated target based on anisotropic bulk etching of silicon to form an array of inverted pyramidal structures [58], and then square vials with depths less than 300um to achieve a detection limit in the 10~50 amol range [59]. Similarly, high-density nanovial array has been fabricated on thermoplastic polymer by using direct milling and cold embossing techniques [60].

1.2.2.2 Microfluidics/MALDI Integration

One strategy for interfacing microfluidics to MALDI-MS is to deposit sample from a microfluidic chip onto a standard off-chip target plate. Directly spotting from a microfluidic chip is feasible but difficult to precisely control the spot volume, at the same time, it is not feasible for closely spaced array in multiplexed device.

As an alternative to direct spotting, microfluidic dispensers have been reported to deliver sub-nanoliter volumes of sample or matrix solution to MALDI targets [59-61], either combined with a microchip-based immobilized enzyme reactor for proteolytic digestion [59-60], or from a microfluidic 96-element SPE array designed for protein purification and enrichment prior to MALDI-MS [62].

While the above microfluidic piezoelectric deposition methods were applied for off-line MALDI analysis, many groups have demonstrated microfluidics coupled with MALDI-MS for online analysis. A typical method, using the centrifugal force to push the liquid into an open area to evaporate the solvent, successfully integrated sample concentration,

desalting, elution and crystallization on a compact disk [63]. A rotating ball acted as a mechanical transport mechanism to introduce sample deposited on its surface to the ionization chamber, this CE combined with on-line MALDI had been demonstrated in [64].

To interface planar microfluidics to MALDI-MS, manipulation of sample and matrix in the liquid phase may be combined with on-chip crystallization. A simple approach consisted of fabricating open microchannels such that the following CE separation cocrystalized solid-phase sample and matrix can be rastered by laser after the solvent evaporated in open channels [65]. Vacuum-driven reaction chips for microfluidics integrated to online MALD-MS analysis have been reported by Brivio et.al. [66]. Performing such analyses within the vacuum environment of a standard MALDI instrument without requiring more complex interfaces may be attractive for some applications.

The Gyrolab MALDI-CD technology (Gyros AB, Uppsala, Sweden) utilized centrifugal force to realize sample processing steps such as sample washing, elution, and sample/matrix cocrystallization on a microfluidic disk. Using BSA digest, protein identification has been successfully demonstrated with three typical peptides detected for a protein loading level of only 50 amol [67]. An array of nanovials packed with RP beads preincubated with protein digest was fabricated on a silicon wafer, to combine sample cleanup and enrichment with on-chip sample/matrix cocrystallization [68]. Wheeler et al. used an electrowetting-on-dielectric (EWOD) approach to manipulate, mix and deposit

sample and matrix on an EWOD surface coated with hydrophobic Teflon-AF as a MALDI target [69].

The analysis of low amount sample loading has become increased important in proteomics analysis. Because microfluidics can serve to limit on-chip analyte dispersion while enabling efficient sample deposition on MALDI target area matching to the laser spot size, these platforms offer a path towards improved integration and automation while providing high sensitivity MS analysis from limited sample [40].

1.3 Dissertation Objectives

Separation techniques combined with high accurate mass spectrometry have gradually shown great capacity for identification of proteins, with a major impact on bioanalysis. The literature provided only a few examples on how to successfully couple standard capillary gel electrophoresis (CGE) with MS, and essentially no insight into the specific challenges involved in coupling microchannel gel electrophoresis (μGE) to MS. In addition, many examples of electrospray tips showed the complicated fabrication or poor electrospray performance. Developing a novel electrospray tips using simple batch production fabrication technique with good performance is required to integrate μGE with MS in a microchip.

A primary goal of this dissertation is the development of a microfluidic apparatus for performing microscale gel electrophoresis coupled with integrated electrospray tips for either directly interfacing to mass spectrometry through ESI-MS, or off-line coupling to

MALDI-MS through the deposition of separated analyte onto a MALDI target. Further development of microfluidics interfacing to MALDI mass spectrometry was explored.

This dissertation includes the following:

- Development of novel ultra-rapid plastic microfluidic device fabrication technology;
- Development of a novel electrospray interface, which can be used for other application in biochemistry analysis;
- Development of a gas-phased protein/peptide electrophoretic concentration method for mass spectrometry;
- Development of a microchannel gel electrophoresis separation system coupled with mass spectrometry via electrospray interface.

Chapter 2 Background

This chapter introduced the basic principles involved in this dissertation work, including the principles of gel electrophoresis, free-radical polymerization and electrospray mechanism.

2.1 Gel Electrophoresis

2.1.1 Principle of Gel Electrophoresis

Electrophoresis is an analytical method frequently used in molecular biology and medicine for the separation and characterization of proteins, nucleic acids and subcellular-sized particles like viruses and small organelles.

Hjertén first described the mathematical treatment of gel electrophoresis [70]. Electrophoresis is defined as the movement of electrically charged particles or molecules in a conductive liquid medium, under the influence of an electric field [70]. This movement is due to the Lorentz force that is equal to the multiply of the net charge of the molecule, q, and the electric field, E. The resulting electrophoretic migration is countered by forces of friction such that the rate of migration is constant in a constant and homogeneous electric field:

$$\nu = \frac{qE}{f} \tag{2-1}$$

The electrophoretic mobility can be defined as

$$\mu_{EP} = \frac{\nu_{EP}}{E} \tag{2-2}$$

Proteins are usually denatured in the presence of a detergent such as SDS that coats the proteins with a negative charge. Generally, the amount of SDS bound is relative to the size of the protein (usually 1.4 gram SDS per gram of protein), so that the resulting denatured proteins have an overall negative charge, and all the proteins have a similar charge to mass ratio. Since the denatured protein acts like long rods instead of a complex tertiary shape, the rate at which the resulting SDS coated protein migrates in the free solution is not relative to its charge or shape.

CGE is performed in a capillary filled with a network of obstacles, most frequently cross-linked gels or entangled linear polymers. The space between obstacles forms pores through which the molecules migrate. The frictional force within a gel matrix is a combination of factors such as molecular weight, the viscosity of the medium, the effective pore size of the matrix etc. Hence, among molecules of the same charge-to-mass ratio, larger molecules move more slowly in the gel and the electrophoretic separation occurs by size. This mechanism is called as ‘sieving mechanism’. The position of a protein along the separation length gives a good approximation of its size, and the measured separation band intensity is a rough indicator of the amount of protein present in the sample.

2.1.2 Selecting the Right Gel

Researchers initially used highly cross-linked polyacrylamide (PA) in-situ polymerized within the lumen of the capillary [72]. Originally this gel cross-linked by thermal polymerization was not very effective for a variety of reasons: voids left within the capillary, difficult quality control etc. Recently, many groups explored more precise control on cross-linked gel formation via ultraviolet (UV) photo-initiated polymerization.

Meanwhile, a range of linear polymers have shown good utility for use in DNA sequencing and protein separation, including linear polyacrylamide (LPA) [73], poly (N, N-di-methylacrylamide) (PDMA) [74], and poly (ethylene oxide) (PEO) [75]. These types of gels were not as rigid as cross-linked PA, so they can be easily replaced. Moreover, production and characterization of polymer ex-situ has allowed researchers to adjust polymer physical and chemical properties.

The replaceable gel was first considered in this project because the gel can be easily replaced after each run. Substantial literature was available describing the use of PEO gels for capillary and microchannel protein separations, but little was available for LPA in these applications. In addition, PEO is significantly less toxic than LPA. PEO is a water-soluble liquid or low-melting solid depending on its molecular weight and has the structure ($HO\text{-}(CH_2\text{-}CH_2\text{-}O)_n\text{-}H$).

When the results using PEO gel was satisfactory, cross-linked PA was also explored in this project later. The following section will introduce the basic principle of PA polymerization.

2.1.3 Principle of Polyacrylamide Polymerization

PA gel, a typical polymer produced by free-radical chain polymerization, is formed by the co-polymerization of acrylamide (CH_2=CH-CO-NH_2), a water-soluble monomer, with a cross-linker to form a three-dimensional lattice. The most common cross-linker is N, N'-methylenebisacrylamide ('bisacrylamide' or 'BIS' for short, (CH_2=CH–CO–NH–CH_2–NH–CO–CH=CH_2)). BIS has two double bonds, which in polymerization reactions cross-link with adjacent chains of acrylamide. If polymerized in the absence of a cross-linking agent, acrylamide forms only linear polymers, resulting in viscous aqueous solutions rather than a gel.

The pore size of PA gel is determined by two parameters: total solid content (%T) and the ratio of cross-linker to acrylamide monomer (%C). The %T is the ratio of the sum of the weights of the acrylamide monomer and the cross-linker to the volume of solution, expressed as % w/v. The %C is the weight/weight percentage of total cross-linker weight in the sum of monomer and cross-linker weights. As the %T increases when the %C remains constant, the pore size of PA gel decreases. When the %T remains constant and the %C increases, the pore size follows a parabolic function: at high and low value of the %C, the pores are large; the minimum is at %C of 4~5% [76]. For example, 30% (%T) PA gel with 4.75% (%C) has been reported to have an average pore size of about 2nm [76].

The mechanism of PA polymerization takes place via free-radical polymerization, which is a chain reaction consisting of three sequential steps: initiation, propagation and termination [77-80].

During initiation, the active center of a free radical is often created by the division of a molecule (known as initiator) into two fragments along a single bond with the energy provided by thermal processes, microwave or UV radiation processes, or electron transfer (redox) processes. One advantage of UV radiation is that the formation of free radical occurs only where the UV light is incident, which can precisely control the polymerization region. Propagation is the rapid reaction of a radical with another monomer to form a covalent bond and the subsequent repetition to create the repeating chain. Finally termination takes place by joining two growing chains to form a single polymer molecule.

Since precise control of gel location is required in this project, UV-radiation was applied for in-situ polymerization.

A number of factors must be considered when choosing appropriate photoinitiator for the polymerization of a biomaterial. Light absorption is described by $a = \beta Cl$, where β is the extinction coefficient, C is the concentration of the species, and l is the light path length [81]. The extinction coefficient, β, a constant for a compound at a specific wavelength, is an experimental measure of the probability of absorption at that wavelength. The magnitude of the extinction coefficient depends upon the compound's chromophore, the chemical moiety responsible for the absorption of light.

Table 2-1 Wavelengths of maximum absorption and associated extinction coefficient for typical chromophores found in photolabile compounds [81]

Chromophore	λ_{max} (nm)	β_{max}
C=C	195	10,000
C=C	195	2,000
C=C–C=C	215	20,000
Benzene	185	60,000
	200	8,000
	255	200
RRC=O	190	900
	280	15
RCOOH	205	60
N=N	345	10
NO_2	270	18.5
S=O	210	1500

Specifically, the peak absorption wavelength and extinction coefficient of the initiator, the reactivity of the initiator toward the other species within the system, and the kinetics of the photoinitiator all determine the applicability of the system. Typical chromophores contain unsaturated functional groups such as C=C, C=O, NO_2, or N=N. Table 2-1 lists the wavelength of maximum absorption, and the extinction coefficient at this wavelength for some chromophores [81]. For example, Azo compounds can be used as photoinitiators, because the azo group (N=N) absorbs light which peaks at approximately 350 nm to produce two reactive carbon-centered radicals. 2, 2'-Azobisisobutyronitrile [AIBN, $(CH_3)_2C(CN)–N = N–C(CN)(CH_3)_2$] has been used with significant success [82-83]. However, the low light absorption and associated slow polymerization rate are main disadvantages of azo compounds.

Often, the free-radical polymerization rate can be simplified as [77, 79]

$$-\frac{1}{V_l}\frac{dN_{monomer}}{dt} = k_c[N_{monomer}]\sqrt{[I]} \qquad (2\text{-}3)$$

where N is the number of monomers in (kmol) and [] is the concentration in (kmol/m^3), I is the initiator, V_l is total liquid volume in m^3, kc is a constant that is a function of several factors such as the initiator efficiency, the initiation rate, the propagation rate and the termination rate.

The increase of the initiator concentration results in the reduction in the average polymer chain length, accompanied by a rise in gel turbidity and decrease in gel elasticity [84]. On the other hand, from the above equation, the decrease of the initiator concentration also causes slower polymerization, which is not desirable as dissolved oxygen in the monomer solution can begin to inhibit the reaction resulting in more porous or mechanically weak gels.

2.2 Electrospray

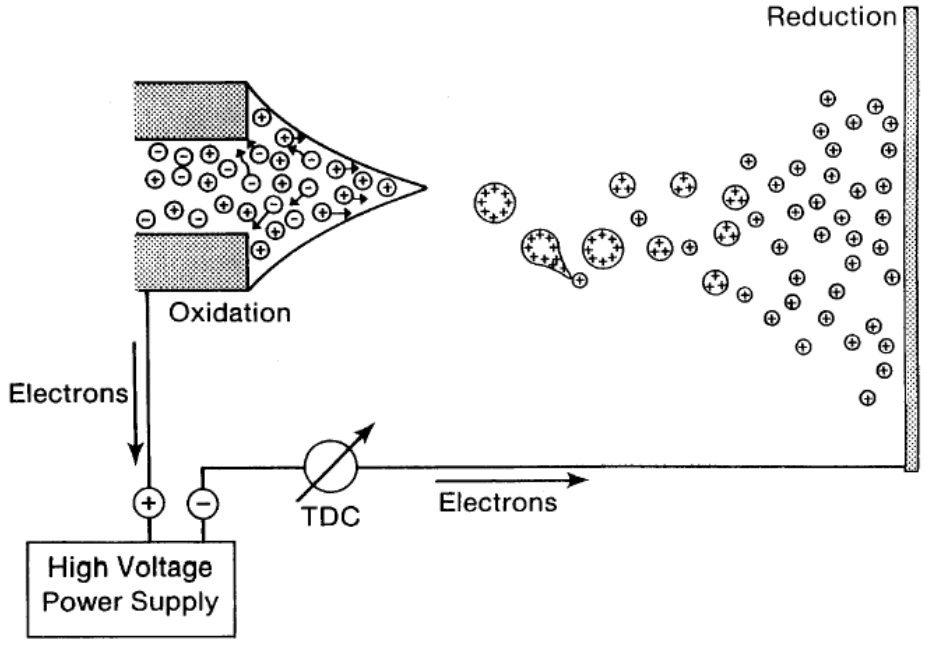

Figure 2-1 Basic Principle of Electrospray [90]

In 1968, Dole [85] first recognized the generation of gas-phase ions of macromeolecules by spraying a solution from the tip of an electrically charged capillary. Based on Dole's idea, Fenn and co-workers [86-88] developed electrospray as a true interface for mass spectrometry. Electrospray is a method by which a liquid is dispersed into small charged droplets by applying a high electric potential between a liquid in a capillary tip and a counter electrode. Today, the use of ESI to introduce sample for MS is a widely used technique for accurate mass identification in a wide range of biological, biochemical, pharmaceutical and medical research. In addition, the electrospray method may be employed to deposit single particles on a surface in nanotechnology [89].

The mechanism of electrospray ionization includes three main steps [90]. First, charged droplets are formed at the tip of the spray capillary due to the action of the electric field between the capillary tip and a counter electrode, as shown in Figure 2-1. Due to the electrophoretic motion of charged particles under electric field, the cations migrate towards the strongest point of the filed-- the capillary tip surface. Excess charges accumulate near the end of the capillary and cause the emerging liquid to elongate in the direction of the counter-electrode; however, the surface tension of the liquid holds the solution together. Under sufficiently high electric field, the balancing of these two opposing forces results in formation of the dynamic Taylor cone at the exit of the electrospray capillary. When the shear force is stronger than the surface tension, a liquid jet will emerge from which charged droplets are ejected.

The minimal potential required to generate a stable electrospray can be estimated using the equation [91-94]:

$$V_{on} = A_1 \ln(\frac{4d}{r_c})\sqrt{\frac{2}{\varepsilon_0}\gamma r_c \cos\theta} \quad (2\text{-}4)$$

Where V_{on} is electrospray onset voltage (V), A_1 is dimensionless constant, about 0.5~0.7; γ is the surface tension (Nm^{-1}); r_c is the capillary radius (m);θ is half angle of the Taylor cone apex; d is the distance between spray tip and counter electrode (m), and ε_0 is electrical permittivity in vacuum ($C^2N^{-1}m^{-2}$). The electric field strength is typically ~10^6-10^7 V/m [91-94].

When operated in a stable mode, charges emerging from the ESI tips produce a steady-state current with a magnitude proportional to the rate at which charge leaves the capillary in the form of droplets. The current depends on the flow rate of the droplets, surface tension of the solvent, specific conductivity of the solution, and the imposed electric field [95]. The ESI current provides a quantitative estimate of the maximum number of available charges that can be converted into gas-phase ions, and substantial fluctuations in the current are indicators of spray instability and /or electrical discharge.

The second step of electrospray ionization is solvent evaporation from ESI droplets. When the charged droplets travel towards the counter electrode, their radii decrease as the solvent evaporates, but their charges remain constant [95]. At a certain point called the Rayleigh limit, the Coulombic force overcomes the surface tension of the liquid and the droplet separates into several offspring droplets. This process, called as Coulombic fission, leads to very small highly charged droplets.

The final step in electrospray ionization process is gas-phase ion formation. Two main theories have been suggested, the charged residue mechanism (CRM) [85, 96, 97] and the ion evaporation mechanism (IEM) [98, 99] although the actual mechanism is not yet fully understood. The CRM explains that with ongoing solvent evaporation, electrically charged intact gas-phase ions finally can be obtained due to Coulombic fission. The IEM suggests that when the droplets have shrunk to a given size (<10nm), direct emission of ions from the droplets becomes possible. Lately, it appears that both mechanisms apply, but for different types of analytes.

Chapter 3 Polymer-based Microfluidics Fabrication

3.1 Introduction

Early work in microfluidic systems involved the fabrication of microchannels on silicon [100], glass [101], or quartz [102] using microelectronic fabrication technologies such as lithography, wet chemical or reactive ion etching, and thermal or anodic bonding. Disadvantages to these types of devices include expensive cost of substrate and fabrication processes, harmful chemicals involved in the fabrication processes, and poor surface properties of substrate e.g. molecules stick to silicon. Polymers were extensively reported by many groups as substitute substrate materials [103] due to their fair mechanical properties, good optical characteristics and good chemical resistance. Low cost raw materials and the development of suitable polymer fabrication technologies provide efficient tools for mass production of disposable microfluidic systems.

A wide variety of polymer materials, used for microfluidics including PDMS, PC, PMMA, polyamide (PA), poly (p-xylenen) (parylene), cyclic olefin copolymer (COC), polyethylene (PE), and polystyrene (PS), were well reviewed in [103].

The polymers differ in their mechanical properties, optical characteristics, temperature stability, chemical resistance and biological characteristics. When choosing a polymer substrate, the properties of the materials are important for both the fabrication process

and the successful application of the device. Different fabrication techniques have different specific constrains with regard to the properties of the materials. For example, with hot embossing and injection molding, the glass transition temperature and melt temperature are critical parameters for successful fabrication. When using optical detection, optical properties of polymer materials are also critical. In biomedical engineering, the properties including chemical resistances, hydrophobicity and surface chemistry are important considerations.

3.1.1 Optical Properties of Plastic Materials

The optical properties of plastic materials such as light transparency at a desired wavelength and low background fluorescence are important when they are used in microfluidics.

Photoinitiated polymerization occurs within a microchannel surrounded by bulk polymer. Therefore, the polymer material must be light transparent at a desired wavelength, e.g., a range of 230~350nm. Figure 3-1 shows the UV spectra of various materials, including PC (curve #1), PMMA (curve #2), PDMS (curve #3), PS (curve #4), COC (curve #5), hydrogenated polystyrene (PS-H) (curve #6), Borofloat glass (curve #7) and quartz (curve #8) [104]. From Figure 3-1, quartz is transparent in the entire range (230~350nm), while PC is completely opaque in this range and therefore it is not suitable for photografting or photoinitiated polymerization. PDMS exhibits the best transparency among polymers in the far-UV range. The UV transparency of COC is very close to that

of PDMS, even exceeds that of glass. PS-H is also sufficiently transparent and enables acceptable grafting. PS has lower transparency than PS-H.

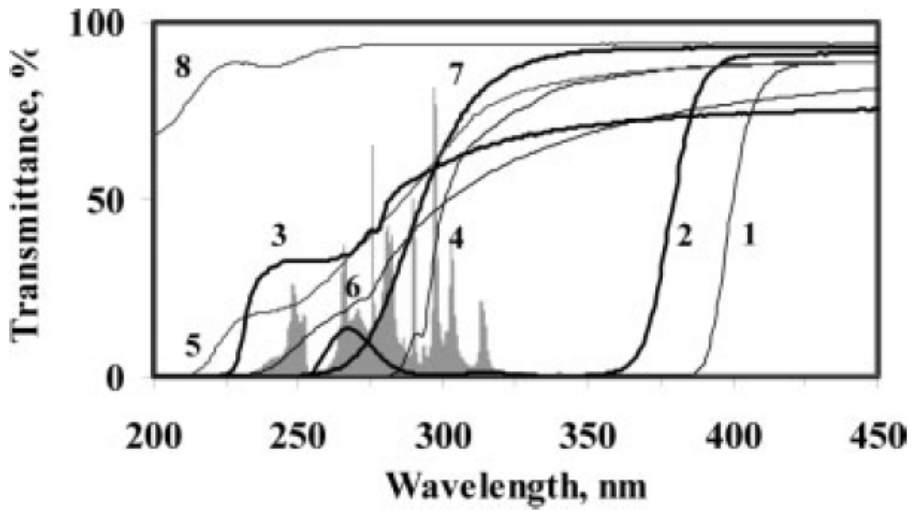

Figure 3-1 UV spectra of various Materials (1) PC; (2) PMMA (3) PDMS; (4) PS; (5) COC; (6) PS-H; (7) Boro float glass and (8) Quartz [104].

Plastic materials exhibit significant fluorescence background when excited by near- UV (even visible spectrum) radiation. Seliskar et. al [105] reported the autofluorescence of various plastic materials in buck materials and in chips. They concluded that PDMS has the lowest autofluorescence. Other materials such as PC, PMMA, and COC have autofluorescence levels ~3 to 5 times higher than Borofloat glass. Thick PC (such as 2mm in thickness) showed very high fluorescence while thin PC (such as 250 μm in thickness) showed a comparable fluorescence with PMMA and COC.

In the option of optical properties of plastic materials, PDMS exhibits excellent properties while polycarbonate did not display favorable properties.

3.1.2 Physical Properties of Polymers

There are two basic types of polymers: thermoplastic and thermoset. A thermoplastic polymer consists of uncrosslinked or weakly linked chain molecules. When the thermoplastic polymers are heated, the molecule spread farther apart. If the polymer molecules are cross-linked (chemically bonded), the polymer is called as thermoset. Thermoset polymers cannot be softened, melt or flow when they are heated. These materials have to be cast into a permanent shape.

PC, PMMA, and COC are the most popular polymers for microfabrication by means of hot embossing and inject molding. Table 3-1[103] summarizes the basic physical properties of some commonly used polymer materials.

Table 3-1 Basic Physical Properties of Various Materials [103]

Polymer	Density (10^3 kg/m^3)	Glass Temp (°C)	Permanent temp. of use (°C)	Thermal conductivity ($Wm^{-1}k^{-1}$)	Linear expansion coefficient ($10^{-6}K^{-1}$)	Heat distortion temp. (°C)
PC	1.2	150	115-130	0.21	65	148-150
PMMA	1.18-1.19	106	82-98	0.186	70-90	80-110
COC	1.01	138			60	123
PS	1.05	80-100	70	0.18	70	78-99
PDMS	0.985	<-125	-55	0.002		

Biomolecules (such as DNA, proteins and olugonucleotides etc) tend to adhere to polymer surfaces, either by forming a chemical bond (‘chemisorption’), or through Van der Waals forces (‘physisoption’). A key goal in the development of polymer-based microfluidic device is the ability to control and manipulate the surface chemistry of the plastic to impart desired characteristic of the devices.

Hydrophobic material, being water-repellent, has low surface tension and lacks active groups in its surface to form hydrogen bonds with water. For a given droplet on a solid surface, contact angle, relating to the surface tension by the Young's equation, is the angle formed between the surface of a solid and the line tangent to the droplet radius from the point of contact with the solid surface. This angle can be measured by a contact angle goniometer. An angle greater than 90° indicates that the solid surface repels the liquid and the solid material has high hydrophobicity. An angle between 0° and 90° results from the liquid spreading due to molecular attraction and indicates that the solid material is hydrophilic.

Most thermoplastic bulk materials are hydrophobic [104]. The contact angle of water on COC is 89°, that of water on untreated PDMS is 98°, and that of water on PC is around 70°. It is difficult to fill the liquid for hydrophobic channels. Hydrophobicity is not very favorable for protein analysis due to protein absorption by hydrophobic interaction. Moreover, hydrophilicity will be beneficial to improve the bonding strength of polymers. Therefore, the hydrophilic surface is most desirable in most microfluidic devices.

Surface treatment is often required to change the hydrophobic nature of a polymer to hydrophilicity. Such treatments include by oxidation (such as UV, UV/ozone [106], and oxygen plasma [107]) and photografting by other hydrophilic polymer layer (such as linear polymer UV grafting [104]).

3.1.3 Chemical Resistance and Solubility

Many organic solvents, acids and bases are involved in bioanalytical chemistry. Therefore, one requirement for suitable polymer substrate for microfluidics is chemical resistance.

A chemical will be a solvent for a polymer material if the molecules of the two materials are compatible, i.e., they can co-exist on the molecular scale and there is no tendency to separate. Solubility parameter δ, an experimentally determined property, is a measure of the energy required to separate the molecules of a liquid [108].

Table 3-2 Solubility parameters of some polymers and some common solvents [108]

Polymer	δ		Solvent	δ	
	$Mpa^{1/2}$	cal/cm^3		$Mpa^{1/2}$	cal/cm^3
Polytetrafluoroethylene (Teflon)	12.6	6.2	Acetone	20.4	10.0
Polyvinylidene Fluoride (PVDF)	13~16		Methanol	29.6	14.5
Polypropylene	16.3	8.0	Ethanol	26.0	12.7
Polyethylene	16.3	8.0	Methyl acetate	16.3	8.0
Polystyrene	18.7	9.2	Ethylene dichloride	20.0	9.8
Poly Vinyl Alcohol	19.2	9.4	n-Hexane	14.9	7.3
Poly Vinyl Chloride	19.4	9.5	Cyclohexane	20.2	9.9
Polycarbonate	19.4	9.5	Acetic Acid	25.7	12.6
PolyethyleneTerephthalate (Polyester)	21.8	10.7	Water	47.7	23.4
Polyacrylonitri1e	28.7	14.1	Isopropanol	23.4	11.5
Cellulose	21.6	10.55			
PolyHexamethyleneAdipamide (Nylon 6/6)	27.8	14.1			

Compatibility between polymers and solvents can only occur when polymer and solvent have similar solubility parameters (in practice within about 2 $Mpa^{1/2}$ or 1 cal/cm^3) [108],

which indicate the solvent is able to attack the polymer. Non-comparability between polymer and solvents means that the solvent cannot attack the polymer. Table 3-2 lists solubility parameters of some polymers and some common solvents. For example, the values in Table 3-2 [108] show that PC is soluble in acetone, ethylene dichloride, or methyl acetate, but not in methanol, n-hexane or cyclohexane. The chemical properties and solubility of COC are close to those of other members of the polyolefin family, including PE or PP. Hence COC only dissolves in solvents such as toluene and hexane that are less likely to be used in standard microfluidic applications. Therefore, COC exhibits better chemical resistance than PC.

3.1.4 Costs

Microfluidics usually have a large footprint compared with IC, typically several cm^2, therefore, the cost of bulk materials is also an important consideration when choosing the substrates. The price of quartz is on the order of 80~90 cents/cm^2. The price of Borofloat glass (e.g., Corning Pyrex) is on the order of 10~20 cents/cm^2. Boro-silica glass (e.g., Scott 270) is on the order of 5~15 cents/cm^2. Among polymers, PMMA is on the order of 0.2~2 cents/cm^2, PC is on the order of 0.1~0.3 cents/cm^2. Since COC is a new material, mainly manufactured by Topas ® and Zenor ®, the price of a COC sheet is more expensive than the COC pellets. PDMS is cheaper since Sylgard ® 184 kit can make numerous pieces.

Microfabrication involving lithography and wet/dry etching also increase the expense while thermoplastic microfabrication technique can facilitate batch manufacture and lower the fabrication cost.

3.1.5 Summary

Although PDMS exhibits many advantages in optical properties, cost, and chemical resistance, the poor hardness (or elastics) and resistance to pressure (for reversible sealing, ~5 psi; for irreversible sealing, <15 psi) are not desirable, especially for filling with high viscosity solutions. Therefore, in this project, PDMS was not considered as a good candidate. Among the other three thermoplastic candidates, PC is very favorable due to its low cost and mature fabrication technique; it was first considered but was rejected due to its optical characterizations. Because of its very good chemical and optical property, COC was used in this project to achieve photoiniated polymerization within the microchannels.

3.2 General Fabrication Process Flow

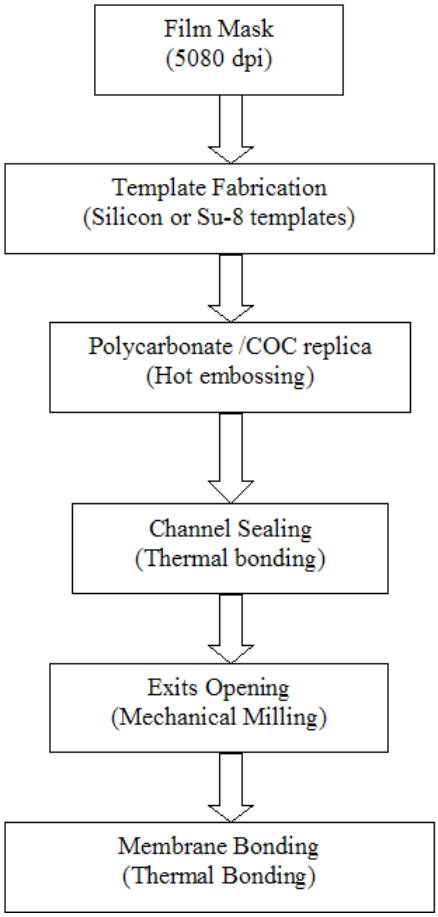

Figure 3-2 General Fabrication Process Flow

The general fabrication processes flow chart for microfluidic devices in this project is shown in Figure 3-2.

First, high-resolution (5080 dpi) film mask transfers the designed structure patterns from AutoCad. The inverse master fabrication utilizes standard lithography and wet chemical etching for silicon templates and Su-8 lithography for Su-8 templates. PC or COC replica is generated upon the master by hot embossing and then the resulted channels are sealed by another piece of PC or COC as cover plate via thermal bonding. Mechanical milling

opens the exits of microchip and a porous thin PTFE membrane is then secured to the exits surface of microchip by thermal bonding.

3.3 PC and COC Microfabrication

3.3.1 Template Fabrication

Several templates fabrication methods, including silicon bulk etch, LIGA, electroplating, deep reactive ion etching (DRIE) and Su-8, have been reported in the literature. LIGA (specified as X-ray LIGA) and electroplating can be used for high aspect ratio structures with straight sidewalls. Their drawbacks though, are slow fabrication time due to electroplating and lack of expensive synchrotron source for LIGA. DRIE also creates straight sidewall structures but this process is complicated compared with silicon bulk etching, which is the conventional method for template fabrication. The lifetime of silicon inverse templates is usually long (>25 imprints) but breakage due to thermal expansion coefficient mismatching between the master and the polymer can be problematic. Room temperature imprinting was explored to elongate the lifetime of the templates but the pattern transferring was not perfect [109]. Another limitation of silicon bulk etched templates is that the microchannels are always trapezoidal in cross-sectional area due to the anisotropically etched behavior of silicon. This structure feature is undesirable in many cases.

Recently, utilizing patterned Su-8 as template has been demonstrated with variety of results in many groups. The advantages of Su-8 template over the silicon bulk etched template are simple and fast fabrication and favorable structure features (i.e., vertical

sidewalls and smooth surface finish). However, delaminating of Su-8 from silicon substrate due to thermal expansion mismatches limited the lifetime of Su-8 templates. Esch [110] reported positive hot embossing results with very low Su-8 thickness (<17 microns) and less than 10 imprints per templates.

In this project, silicon bulk etched templates and Su-8 templates on bare silicon substrate were both investigated.

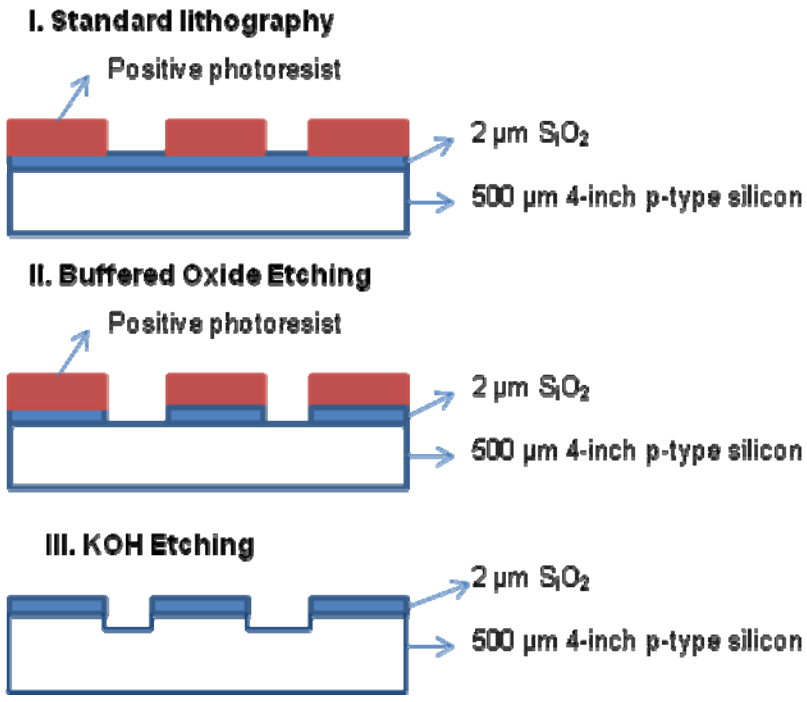

Figure 3-3 Fabrication processes for silicon templates

The silicon bulk etched templates fabrication involved standard lithography and potassium hydroxide etching as shown in Figure 3-3. The template substrate consists of a 4-inch–diameter <100> oriented p-type silicon wafer with 2 microns thermally grown silicon dioxide (WaferNet, San Jose, CA). Standard lithography was performed using a

transparent positive film mask with the resolution 5080 dpi and a contact mask aligner (Karl Suss MA6 Mask Aligner, Suss Microtec Inc). The wafer was then baked into a 5:1 buffered hydrofluoric acid solution to remove the exposed silicon dioxide. The remained silicon dioxide pattern was used as a hard mask for the following potassium hydroxide etching. The mold feature in silicon bulk etched template is trapezoidal in sectional area as shown in Figure 3-4.

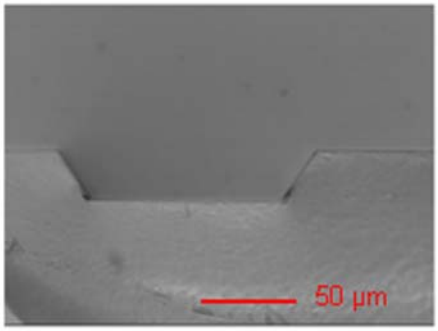

Figure 3-4 PDMS replica shows trapezoidal section of silicon template by KOH etching

Fabrication of Su-8 templates on bare silicon substrate utilized lithography according to Su-8 manufacturer's specifications (Microchem, Newton, MA) as shown in Figure 3-5. Su-8 resist was spin-coated on a clean and dehydrated bare silicon wafer (Nova Electronic Materials, Carrollton, TX) by a SCS G3P-8 spin coat system (Specialty Coating System, Indianapolis, IN) with selecting the appropriate Su-8 resist type and spin condition to achieve the desired film thickness. A Tamarack PRX-1000 UV source (Tamarack Scientific Co. Inc, Corona, CA) was utilized to initiate Su-8 cross-linking. Exposure time was experimentally determined to obtain the best sidewall profiles with different film thickness. Su-8 development, using Su-8 developer PGMEA (Microchem,

Newton, MA), was typically under 3 minutes. Figure 3-6 showed the straight sectional profiles of PDMS replica upon Su-8 template.

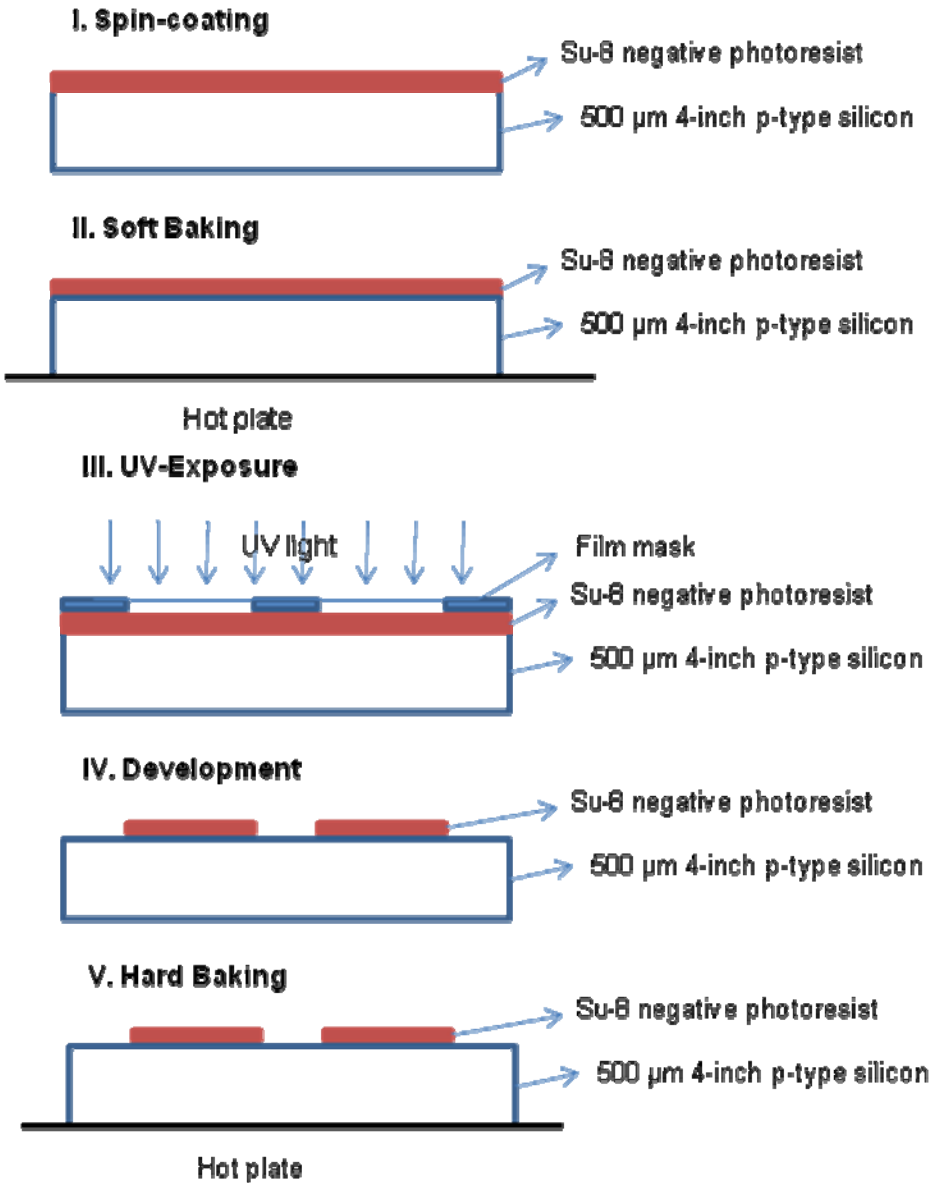

Figure 3-5 Fabrication processes for Su-8 templates

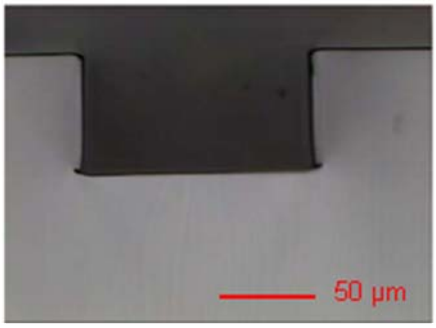

Figure 3-6 PDMS replica shows the straight cross-section of SU-8 template

3.3.2 Hot Embossing

Becker et al suggest some guidelines for hot embossing conditions for polymer with micro-sized features [103]. The thermal cycle (ΔT, defined as the temperature range between embossing and de-embossing) should be 25~40 °C to minimize thermally induced stresses. Applying sufficient pressure for embossing ensures even replication and helps the polymer to flow around the template to obtain complete pattern transferring., Excess pressure, however, leads to more lateral deformation of the replica, resulting in unwanted shear action, This shear force can even squash the master--especially for Su-8 masters. Manually removing polymer imprint from the mold caused a prying force that may result in the deformation of the imprints and damage the template structure. Therefore, automatic vertical de-molding is favorable for mold removal.

A Carver AutoFour /15 Press (Carver, Wabash, IN) was used to create PC and COC replicas from the negative templates. The carver press consists of a stationary upper plate and a hydraulically driven bottom plate which both are temperature-controlled via heating and water /air-cooling.

An embossing fixture was constructed for automatic de-molding taking advantage of the press's inherent vertical motion. The fixture consists of an upper plate, onto which a thick glass plate was affixed to provide a smooth imprinting surface, and a bottom plate that holds the template. Both of two plates are amounted on the press. The template was glued on a 1/8" thick steel plate by thermal epoxy. Local temperatures of both plates are monitored via embedded thermalcouples (Omega Engineering, Stamford, CT). When the plates are separated, the upper and the lower fixture plates move in conjunction with the press plates, respectively. The PC replica adheres to the glass plate attached to the upper platen due to van der walls force between the PC molecules close to the glass surface and the glass surface molecules. The template is held on the lower fixture, thus mold removal occurs automatically. The imprint can then be removed from the upper plate with minimal effort when the plates are cooled down to a temperature below the glass transition temperature of PC. This shear action is due to the thermal stress developed by the thermal expansion coefficient mismatches during the cooling.

Hot embossing for PC replica by inverse templates is a simple process. A 3.5-inch-diameter clean PC sheet with 1.6mm in thickness was degassed in a vacuum oven at 100 °C for at least two hours to evaporate the air trapped in the sheets prior to imprinting. The press was preheated to a set temperature above the glass transition temperature prior to the insertion of blank PC sheet. After inserting PC sheet, a pressure about 250 psi was applied by the press for about 10 minutes at an imprinting temperature (above the glass transition temperature of PC, typically, 330 °F). Then the press plates were cooled down to a de-molding temperature still applying the same pressure before opening. The PC

replica adheres to the top glass plate with vertical movement of top plate at de-molding temperature and is easily separated from the glass plate when the press is cooled down to a temperature below the glass transition temperature.

The experimental results showed that pressing at higher temperature still well below the melt temperature results in better pattern transferring because the PC flows around the corners of the templates well, which results in better edge replication and minimizes the bubble formation, and forming even surface. In addition, elongating the holding time at press temperature helps to obtain complete pattern transferring but this factor is not as important as press temperature.

Usually, the silicon bulk etched templates can last for more than 30 imprints with good pattern transferring utilizing specification here. A template feature up to 50 microns in depth with high-density microchannel structures (i.e., 128 channels with 100 microns in width and 120 microns in space) can be imprinted. The frictional stress in this case was about 10 times larger than that of a simple structure (i.e., several channels with 100 microns in width in a whole wafer area). Hence, the template was easily damaged in mold removal without the utilization of the embossing fixture. The present automatic mold removal technique was able to achieve 5~7 imprints with complete pattern transferring. A simple structure of Su-8 template nearly 100 microns deep also can achieve more than 14 imprints with good pattern transferring using this technique.

After microchannels were created, the polycarbonate replica was sealed via thermal bonding by another bare PC sheet with pre-drilled holes as reservoirs. Two sheets were aligned and sandwiched by the glass, then inserted into the press at the bonding

temperature (lower than the glass transition temperature, typically, 280 °F) while applying bonding pressure for about 10 minutes. The closed microchannels may collapse. In that case, bonding parameters (bonding pressure, temperature and holding time) should be adjusted to obtain the maximum bonding strength.

COC hot embossing is very similar to PC hot embossing with parameters adjusted according to their different glass transition temperatures.

3.3.3 Exit Formation

For electrospray tips, the channels should be open to create exits for electrospray. The repeated moving of mills by CNC milling machine (Micromill 2000 HD/LE, Microproto Systems, Chanlder, AZ) opened the channel exits. The size and uniformity of openings were two keys to obtaining good parallel performance in the following sealing.

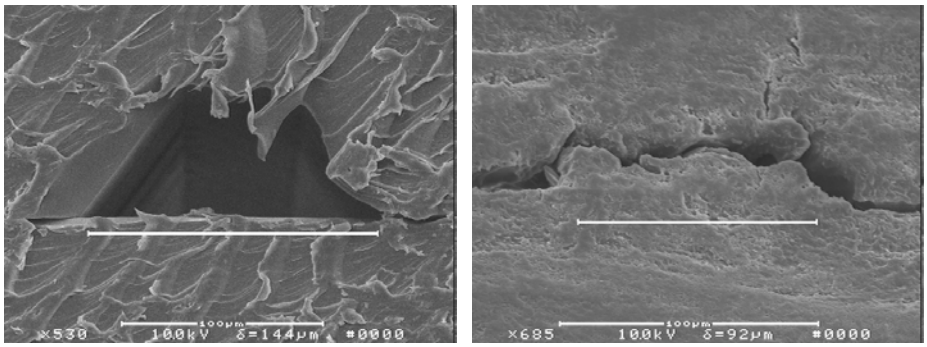

(a) (b)

Figure 3-7 Different opening shapes of channel exits in the same chip by milling
(a) Open-channel exit (b) Closed-channel exit

The final surface roughness in CNC operation results from the combination of two effects: the geometry of tool and feed rate, and the irregularities in the cutting operation

[111]. It is experimentally proven that using the end mill at higher feed rates generated higher surface roughness.

Although the surface roughness was optimized through parameters control in milling operation, the uniformity of each channel exit remained problematic as shown in Figure 3-7. The different opening of channel exits in the same chip results in different flow resistance so that the voltage/ flow rate varied greatly channel-to-channel.

A high precision, low-speed sectioning saw (Burhler Isomet Low speed Saw, Burhler Ltd, Lake Bluff, IL) was then used to open the channel exits due to its advantages, such as minimal deformation to cutting surface and smoother surface texture.

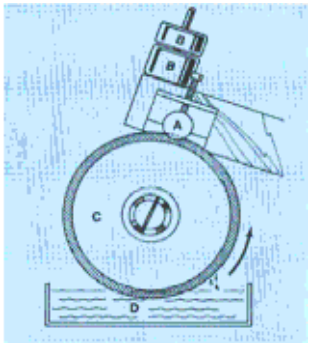

Figure 3-8 Basic principle of sectioning operation of Isomet Low speed Saw

The basic principle of the low speed saw sectioning is illustrated in Figure 3-8. A sample (A) is held in a suitable chuck and is introduced through gravity by a known load (specifically, 25 gram weight as increase) (B), to a rotating wafer blade (C), which is coated with a film of lubricant picked up during its rotation through the cooling tank (D). Usually moderate speed is effective for cutting and minimizes the damage. The smaller rotational speed, the better surface finish can be achieved. Figure 3-9 shows a typical exit opening.

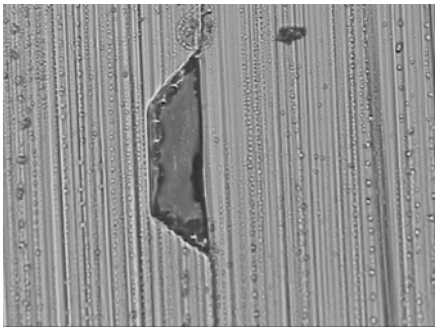

Figure 3-9 Surface finish and exit opening of moderate speed

However, when this low-speed sectioning saw was applied for COC (a polymer with low glass transition temperature, about 105 °C), the debris from the cut materials was melted and covered the channel exits. In this specific case, adjusting the spindle speed cannot result in desirable opening.

Another novel idea was designed to obtain the uniform channel opening. The detail will be described in the later chapter.

3.4 Conclusion

After considering polymer properties such as optical properties, physical properties, surface chemistry as well as cost, PC and COC were chosen as the polymer substrates for this project.

General fabrication process of the polymer microfabrication was schematically demonstrated and followed by the detailed process steps such as template fabrication, hot embossing and sealing, and microchannel exit opening.

This technique of polymer microfabrication was proven to be effective, ultra-rapid and mature fabrication technique that can be easily applied for microfluidics based on PC and COC, and even to a boarder range of thermoplastic materials such as PMMA and PS.

Chapter 4 Microfluidics Interfacing to Mass Spectrometry

4.1 Introduction

ESI, utilizing a strong local electric field to transfer ions from solution to the gas phase in a fine spray at atmospheric pressure, is a promising approach for interfacing microfluidics to mass spectroscopy, either by direct ESI-MS interfacing, or by ESI deposition of analytes onto a MALDI target for further MALDI-MS analysis.

Various approaches for fabricating ESI interfaces into microfluidic systems have been reported by a number of groups and summarized in 1.1.1. There were two trends to improve the stability of the electrospray process. One was to use shaped spray tips at the channel exits [20, 24-25] to significantly reduce the exit spreading. However, this always involved complicated processes, either mechanical machining of the substrate or the use of additional lithographically patterned material layers in the microfluidic system.

More straightforward approach is to open the flat surface at the microchannels in an effort to increase the hydrophobicity of the channel exit, either by application of a surface coating [21], or by using polymer substrates with high native hydrophobicity [119];

however, they still suffered from the difficulty to establish the stable electrospray performance.

Here, a novel and simple electrospray tip was reported to increase the hydrophobicity of the channel exit by attaching a thin layer of PTFE porous membrane.

4.2 Fabrication of Single-Channel Electrosprayer

4.2.1 Membranes Selection

In the technology of membrane ES tip a porous membrane is bounded to the flat orifice of a microchannel. The porous structure acts as a dense array of nanoscale ES tips and establishes stable electrospray by preventing the fluid from expanding along the flat surface due to the high hydrophobicity of the membrane.

To prevent the liquid from spreading for electrospray and to enable loading of the membrane with enzyme such as Trypsin for protein digestion, hydrophobicity is the first requirement of membrane selection. Most hydrophilic membranes generally have a contact angle that is less than 50°. Raw PC film has a contact angle of approximately 70°, which is neither hydrophilic nor hydrophobic. Untreated PTFE has a contact angle of approximately 105~110° and treated PTFE membrane has a higher hydrophobicity.

Small thickness also is required to minimize band broadening. High porosity of membrane will reduce pressure requirements and high tortuosity is required to provide increased surface area for loading enzymes. In addition, the membranes must have good solvent resistance for biochemical analysis.

4.2.2 Membrane Bonding Methods

Depending on the devices material and the material of the membrane itself, porous membranes can be sealed to plastic devices using several different techniques, such as ultrasonic welding, radio-frequency (RF) sealing, thermal bonding, and adhesive bonding, as summarized in Table 4-1.

Table 4-1 Several common membrane bonding methods

Methods	**Principle**	**Application Area**
Ultrasonic welding	*Assembly of thermoplastic materials through the use of heat generated from high-frequency mechanical motion by ultrasonics*	*Plastic material having high surface tension*
Radio frequency (RF) welding	*Assembly of thermoplastic materials through the use of high frequency radio energy to produce molecular agitation in thermoplastic materials*	*Plastic materials having the correct dielectric properties*
Solvent bonding	*Softening of the bonding area of the plastic substrate with a solvent formulation, assembly the mating surface together under slight pressure, and allowing sufficient time for the solvent to dissipate from the joint area*	*e.g., the solubility parameters are similar for plastic-1, plastic-2 and the solvent*
Thermal bonding	*Heating of the thermoplastic material to its glass transition temperature via convention, press the parts together under pressure and the softened polymer surface re-flows and form a strong bond due to Van del Waals forces between molecules of each part*	*Popular for thermoplastic materials*
Adhesive bonding	*Use of adhesive*	*Widely used*

4.2.3 Some Porous Membranes

- PTFE membrane

PTFE membranes (GE PTFE (Teflon®), show in Figure 4-1 [112], have very strong hydrophobicity. PTFE membrane was considered as the first choice utilizing its hydrophobicity and porosity.

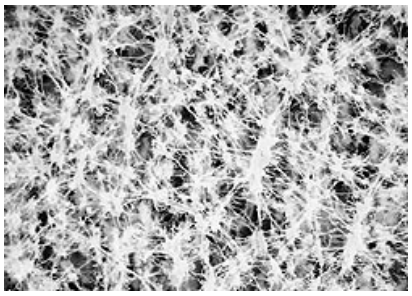

Figure 4-1 SEM image of PTFE membrane [112]

According to data in Table 3-2, the solubility parameters of PTFE and PC, 6.3 and 9.7 cal/cm^3, respectively, are very different and thus there is no suitable solvent compatible with both of them. Due to low surface tension, the frictional coefficient of PTFE is very low and the generated heat is limited. Hence it is difficult to bond PTFE to PC via ultrasonic welding or RF welding.

In the thermal bonding of PTFE membrane to PC chip, the PC microchip is heated to a temperature above its glass transition temperature (typically 150 °C), The PC microchip is then pressed to the PTFE membrane, allowing the melted polycarbonate molecules re-flow and form a bond between PC and PTFE molecules. The mechanical strength of thermal bonding is not very strong but still works under low flow rates or low pressure. The heat-generated degradation of PTFE membrane was a concern since the pore sizes and pore distribution of PTFE membranes were changed as observed. This random change of pore structures also increases the complexity of multi-channel ESI tips.

- Anopore inorganic membrane

Anopore inorganic membrane (Anodics, Whatman) is composed of a high purity alumina matrix, shown in Figure 4-2 [113]. The membrane is manufactured electrochemically,. The benefit sof this membrane include no change of pore structure under pressure or heat

due to its non-deformable honeycomb pore structure. The problem with this membrane is its hydrophilicity. The liquid spreads on the surface of anodics membrane and it is very difficult to establish a stable electrospray.

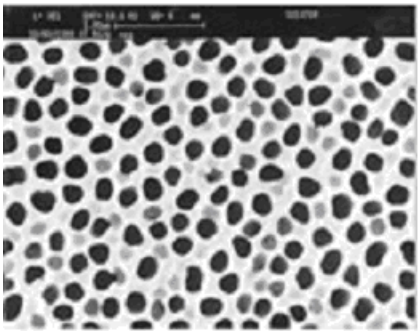

Figure 4-2 SEM image of Anopore membrane [113]

- Glass fiber filters

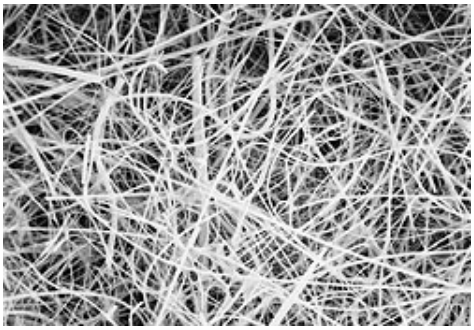

Figure 4-3 SEM image of glass fiber filter [114]

Glass fiber filters are usually used as filters in many areas. Figure 4-3 demonstrated the SEM of glass fiber filters (GE glass fiber binderless filters) [114]. From experiment, the liquid expanded across the whole membrane area and did not form beads, indicating that the hydrophobicity of glass fiber filters is so poor that it cannot be used to establish stable electrospray.

- PVDF membrane

PVDF membrane has very good hydrophobicity, higher than polycarbonate. Figure 4-4 shows SEM of PVDF membrane (Durapore PVDF membrane, Millipore) [115].

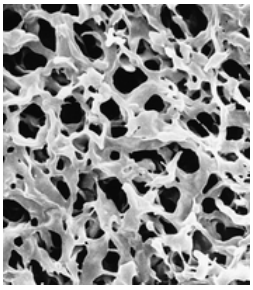

Figure 4-4 SEM image of PVDF membrane (Millipore, Durapore PVDF membrane) [115]

The thickness of tested PVDF membrane is about 150 μm. The working temperature of PVDF is about 85 °C which is lower than the glass transition temperature of PC (typically 105 °C). Experimentally proven, thermal bonding did not get good mechanical strength due to high thickness. Solvent bonding using Ethylene dichloride was explored but failed.

- PC membrane

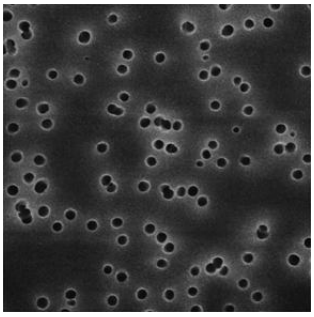

Figure 4-5 SEM image of PC membrane [116]

PC membrane is produced through a two-step manufacturing process, called a track-etched process [116] and the resulting membrane is a thin, translucent and microporous

PC film with a smooth, flat surface, with cylindrical pores of uniform size and length, as shown in Figure 4-5.

Ethylene dichloride was used as solvent to bond polycarbonate membrane to PC microchip. The microchip was first exposed to solvent for the optimum time (typically, several minutes at room temperature) and care was taken to avoid extra solvent evaporation and over-melting the surface of microchip resulting in channel exit blocking. The microchip then was pressed to the porous membrane for 10 seconds with a slight force.

Electrospray was established by using PC membrane bonded to PC chip. The performance of the electrospray, however, was not very stable and less repeatable chip-to-chip. Because of so-so hydrophobicity of PC, the liquid easier tends to spread along the exit before the onset of the electrospray and requires higher electric field to maintain compared with the PC chip using the highly hydrophobic PTFE membrane.

Finally, porous PEFT membrane was chosen to use in this project via thermal bonding method.

4.2.4 Fabrication of Single -Channel Electrosprayer

The repeated high-speed shoulder movement of end mill opened the exits of microchip with a finished surface by using a CNC milling machine (Micromill 2000 HD/LE, Microproto Systems, Chanlder, AZ), as described in section 3.3.3. Figure 3-7(a) showed SEM of a typical channel exit after milling. The channel width is about 120 microns and the formed channel depth is about 30 microns. Mechanical cutting produced the channel

exit surface with average roughness of 12 microns as measured by a stylus profilemeter (XP2, Ambios Technology, Santa Cruz, CA).

A 50 μm thick PTFE hydrophobic membrane (GE Osmonics Labstore, Minnetonka, MN) with the average pore size of 0.22 microns and porosity of 70% was used to dramatically reduce the flow rate to form a stable Taylor cone under some electric field [117]. Figure 4-1 showed SEM image of the membrane before bonding. Single-channel ESI tip was demonstrated with good electrospray performance due to high hydrophobicity of PTFE in this project [117].

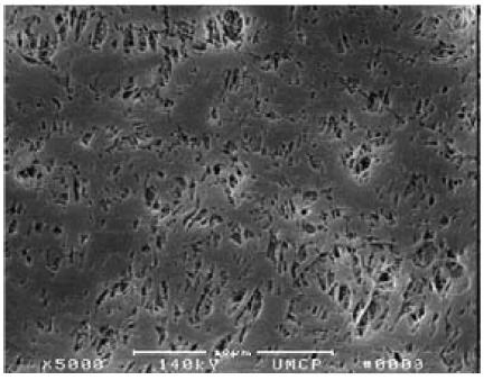

Figure 4-6 SEM image of the PTFE membrane after bonding with chip [117]

The PTFE membrane was thermally bonded to the microchannel in PC chip described in section 4.2.3. This resulted in PC bonding to the adjacent membrane surface without substantial deformation of the channel exit. Figure 4-6 shows an SEM image of the PTFE membrane after bonding with the PC chip. The average pore size and surface pore distribution were modified during thermal bonding due to bonding force and high temperature, with moderate reduction in porosity observed.

4.3 Characterization of Single-Channel Electrosprayer

4.3.1 Instrumentation

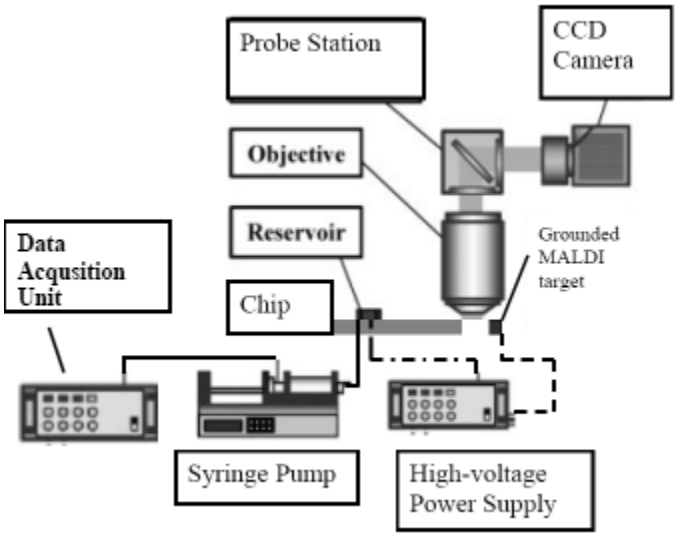

Figure 4-7 Schematic of ES tip experimental setup

The schematic of ES tip experimental setup is depicted in Figure 4-7. A solution containing 50% water, 49% methanol, and 1% acetic acid (pH ~ 3.6) was delivered at a constant flow rate by a syringe pump (PHD2000, Harvard) to fill the microchannel through capillary connectors (Nanoports, Upchuch). The optical visualization of electrospray was performed using an experimental setup assembled on a probe station (Cascade REL4800, Cascade Microtech, Beaverton, OR) through a microscope (FS-70, Mitutoyo, Japan) with objectives ranging from 2 ~ 100 X and images were captured by a CCD video camera. A high voltage power supply (CZE1000R, Spellman High Voltage Electronics, Plainview, NY) provided the required electrospray voltage through a platinum electrode interfaced via a T-junction. Total ion current generated from the spray

between the tip and a grounded aluminum plate at a fixed distance was obtained from a multimeter (Agilent 34410A, Palo Alto, CA) by measuring the voltage across a 100 kΩ resistor. The precise distance between the grounded aluminum plate and the tip was implemented by a micropositioner and determined through a reticle in the microscope eyepiece calibrated by a stage micrometer. A microswitch force sensor from Honeywell was attached to the syringe to detect the pressure change and a data acquisition unit (Agilent 34970A) collected all the data during filling and electrospraying.

4.3.2 Characterization of Single-channel Electrosprayer

For chips bonded with PTFE membrane, liquid exiting the channel formed small rounded droplets without liquid expansion observed. The potential was slowly raised from zero. The first effect was that the liquid meniscus adopted an equilibrium ellipsoidal shape, the eccentricity of which increased with voltage. At a well-defined voltage, V_t, defined as 'threshold voltage', the meniscus accelerated towards a sharp, and emitted a droplet from the tip, then relaxed back to a low eccentricity ellipsoid. At higher voltage, the process repeated at low frequency. The frequency of this process increased with voltage. At higher frequency, the appearance was one of two superimposed menisci, one cusp-like and one approximately hemispherical. At some higher and reasonable well-defined voltage, V_s, defined as 'stable electrospray voltage', the meniscus suddenly became conical and appeared stationary. A stable total current indicated the stable electrospray stated. A filament issued from the apex of this cone, referred to as the 'Taylor Cone', and subsequently formed a plume. This was typical for many large flow rates, but for some small flow rates the plume was difficult to observe under the microscope. Further

increase in potential caused an increase in current and a decrease in size of the Taylor Cone. Eventually, a potential, V_d, defined as 'discharge voltage', was reached for which no steady-state mode existed and a discharge occurred. The current abruptly became unstable and reached above 1mA—a value indicative of the discharge. There is a reasonable range above the stable electrospray voltage and below the onset discharge voltage.

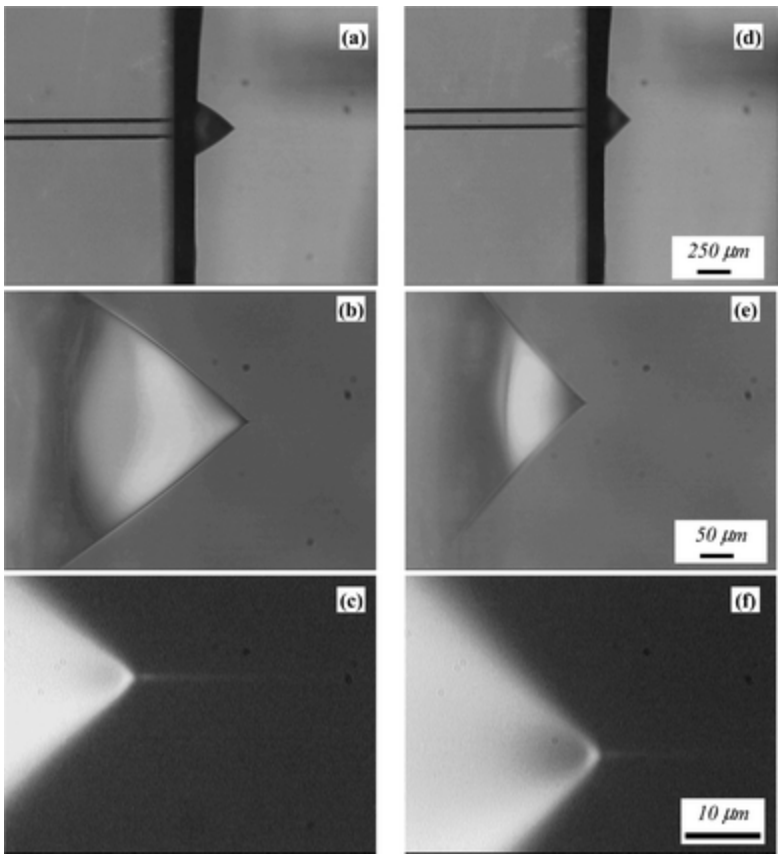

Figure 4-8 Photomicrographs of stable Taylor cones established at microchannel exit for a flow rate of 120nL/min and chip-to-counterelectrode spacing of 2mm. The applied voltage for images (a)-(c) is 3800V, and for images (d)-(f) is 4000V.

Figure 4-8 shows a typical photomicrograph of stable Taylor cone established at a microchannel (channel width is 100 microns) exit for a flow rate of 120 nL/min and chip

–to-counter-electrode spacing of 2mm and the applied voltage of 3800V for images (a)-(c) and 4000V for images (d)-(f) [117].

The electrospray process can be followed by measuring the electrical current between the positive electrode and the ground plate and by observing the spray through a microscope. Current/voltage (I/V) characteristics were measured for fabricated ES tips as a function of applied flow rate.

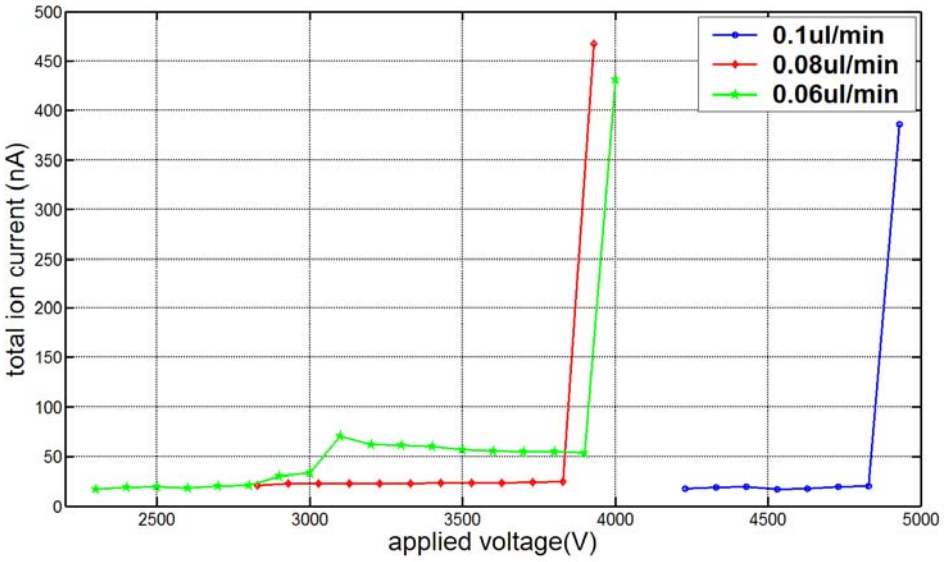

Figure 4-9 Current-voltage curve obtained for electrospraying through a single channel

Figure 4-9 shows the current-voltage curves for electrospraying through a single channel (100 microns in width and 40 microns in depth) with different flow rates under the chip-to-counter-electrode spacing of 2 mm. There is, in all cases, a wide range of voltages where a stable spray was observed without a discharge. The sudden rising in current indicates a discharge occurred. As shown in Figure 4-9, the threshold voltage increases

as the flow rate increases. For example, the threshold voltage in this specific case at 0.06 μL/min was 2300V while the threshold voltage at 0.1 μL/min was 4230V.

Figure 4-10 Increase in current caused a decrease in size of Taylor Cone for the same flow rate. (a) A typical electrospraying with applied voltage of 3600V (b) a typical electrospraying with applied voltage of 3970V, the other conditions include chip-to-counter electrode spacing of 2 mm and the flow rate of 120 nL/min

Further increase in voltage results in a decrease in size of Taylor Cone for the same flow rate since increase in electric field caused an increase in jet velocity; droplets will leave the Taylor cone more rapidly. Figure 4-10 demonstrates that an increase in voltage causes a decrease in the size of the Taylor Cone.

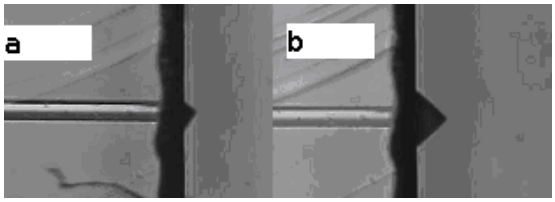

Figure 4-11 Different sizes of Taylor cone with different flow rates for the same applied voltage. (a) A typical electrospraying with flow rate of 80 nL/min ;(b) a typical electrospraying with flow rate of 120 nL/min, the other conditions include chip-to-counter-electrode spacing of 2mm and the applied voltage of 3600V.

Different flow rates indicate different pressure from the syringe pump. Apparently, the larger the flow rate, the larger the wetted area and, therefore, the size of the Taylor cone

increases with the flow rate. Figure 4-11 demonstrates different sizes of the Taylor cone with different flow rates for the same applied voltage.

4.4 Mass Spectrometry Analysis by Single-Channel Electrosprayer

4.4.1 Experimental Instrumentation

A schematic of the experimental apparatus is shown in Figure 4-12 [118]. The microfluidic chip was fixed on an insulated plate mounted on a 3-axis transnational stage for alignment of the emitter tips to a stainless steel MALDI target. The x-y-z stage allows for precise adjustment, accurate to 10 μm, between the spray tip and grounded MALDI target. Experimental setting was the same as described in 4.3.1. A potential ranging from 2~3 KV was applied to the analyte solution with a stable total ion current between 42~55 nA for all tests.

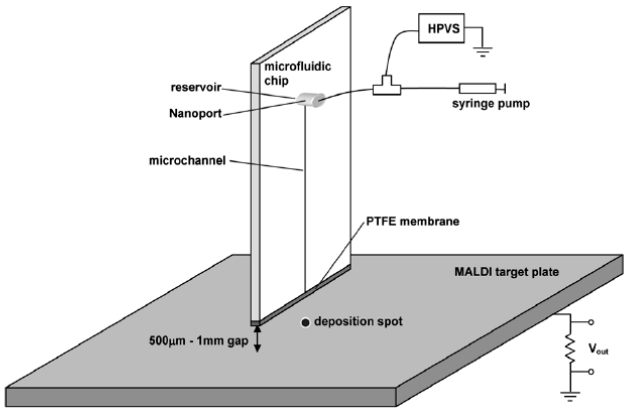

Figure 4-12 Experimental apparatus for electrospray deposition [118]

All analyses were performed using a buffer solution containing 50% water, 49% methanol and 1% acetic acid. After the analytes were electrospray-deposited on the stainless steel MALDI target, matrix solution was added following sample deposition using a custom capillary spotting tool according to a two- layer preparation method. Matrix solution was delivered to the deposited spots at a flow rate of 70nL/min. The deposition time was chosen to maintain the analyte: matrix ratio of 1:1 (v/v).

MALDI mass spectrometry measurements were performed with a Bruker Autoflex MALDI-TOF-MS equipped with a 337nm nitrogen laser. Each mass spectrum was operated in the linear mode and produced by averaging 30 laser shots.

4.4.2 Deposited Film Morphology

Using peptide angiotensin I (MW 1.29 KDa), the film morphology was studied by different matrix solutions. Matrix solution was prepared with α-cyano-4-hydroxycinnamic acid (CHCA, MW 192.0) 10 μg/μL in an organic solvent solution with an acidic compound. Variations in organic solvent components (acetonitrile or methanol), solvent content (70% or 50%) and acidic component (acetic acid or trifluoroacetic acid) were explored. Different matrix solutions generate different crystal morphologies. Matrix solutions with higher organic solvent content resulted in greater heterogeneous films, presumably due to enhanced resolution and resulting segregation of deposited peptides. Compared to methanol as the solvent, acetonitrile generally resulted in more homogeneous films. The best matrix solution was 50% acetonitrile, 40% water and 10% acetic acid. This provided consistently uniform films with nearly constant film

morphology across the deposited spot. Furthermore, this solvent produced the smallest deposited spot diameters with no observed spreading of analyte from the initial deposited diameter, suggesting that this matrix produces the highest on-target concentration of analyte.

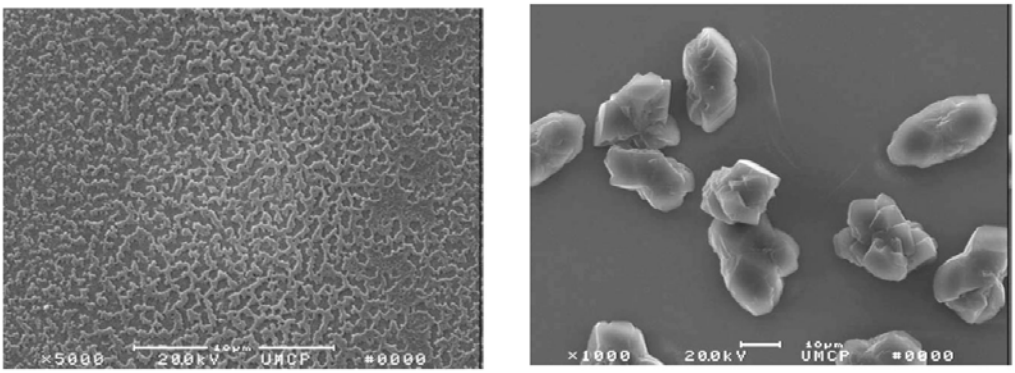

(a) (b)

Figure 4-13 SEM images of angiotensin following addition of CHCA in 50% acentronitrile, 40% water and 10% acetic acid for (a) electrospray deposition, and (b) mechanical spotting of sample

The deposited film morphology was observed using scanning electron microscopy. Electron micrographs reveal a significant difference in crystallization between the electrosprayed sample and mechanically spotted sample in Figure 4-13. The spotted sample was prepared by depositing 10.5 pmol of sample using the capillary spotting method, followed by spotting of an equal volume of matrix solution using the same method. Compared to the electrospray-deposited peptides, which exhibit excellent uniformity and an average crystal size of several μm, the spotted sample shows larger individual crystals, about 25 μm, with significant variation in crystal distribution across the deposition spot. No significant segregation was observed during the addition of matrix solution to the electrospray-deposited analyte. A possible explanation for this observation is that crystallization of the evenly deposited analyte films occurs without

substantial resolution in the matrix solution, thereby preventing any diffusion and segregation of the mixture components as observed in traditional dried-droplet sample preparation.

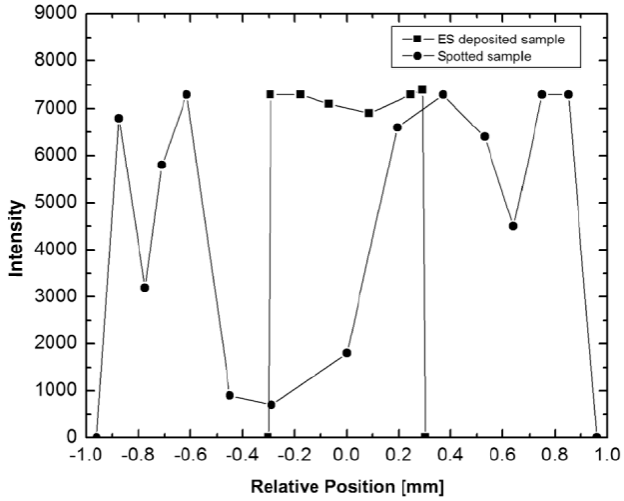

Figure 4-14 MALDI peak intensity profiles across 5 pmol angiotensin spots deposited by electrospray and mechanically-spotted method

A comparison of signal reproducibility was examined by plotting ion signal intensity against laser position, with the results shown in Figure 4-14. Each spot was prepared with a total of 5 pmol of angiotensin followed by the addition of 2 μL matrix solution. At this high loading level, the electrosprayed sample exhibits nearly constant analyte ion signal intensity across the deposition spot, while the spotted sample shows up to a tenfold variation in signal intensity. Sample-to-sample reproducibility was monitored by measuring the variations in the analyte ion peak intensity on five different deposition spots. The relative standard deviation for the electrosprayed sample was 1.4%, significantly lower than 49% for the spotted sample. This figure also demonstrates the

sizes of the deposited areas by different preparation methods. The size of the deposited area by mechanically spotted method was evaluated to be 2mm and the size of the deposited area by electrospray method was about 600 μm. The reduced size of the deposited area also increased the intensity of sample ion signals, improving the reproducibility of shot-to-shot.

4.4.3 Peptide Loading

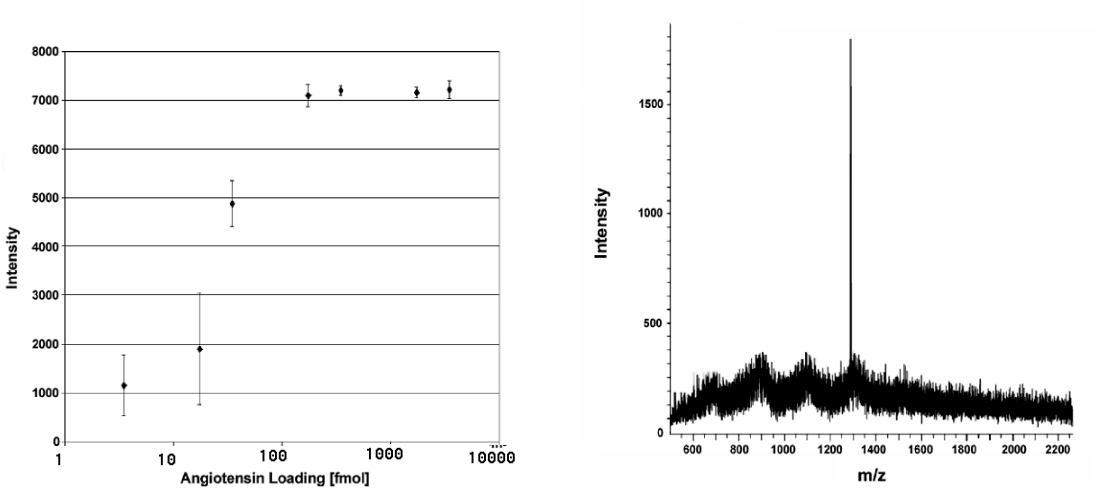

Figure 4-15 (a) MALDI-MS peak intensities measured for varying amounts of deposited angiotensin and (b) measured MALDI-MS spectrum for 3.5 fmol deposition

To evaluate the effects of local peptide concentration on ion signal intensity, the total amount of angiotensin deposited by electrospray deposition from the microfluidic chip was varied, followed by MALDI-MS analysis. Angiotensin was diluted to concentrations from 50 pmol/μL down to 0.05 pmol/μL, and deposited at a flow rate of 70 nL/min for 1min. The corresponding amount of angiotensin deposited on the target ranges from 3.5 pmol down to 3.5 fmol. As shown in Figure 4-15 (a), ion intensity remains relatively constant down to a concentration of 2.5 pmol/μL (total peptide loading of 175 fmol),

beyond which the average signal begins to drop. For the 3.5 fmol spectrum (Figure 4-15(b)), the average signal-to-noise was between 4~5, putting this measurement at the limit of detection.

Similarly, a dilution study was also performed using the mechanical spotting method, with angiotensin concentration ranging from 50pmol/μL to 0.05pmol/μL. No ion signal for angiotensin could be measured following repeated laser probing of the sample for depositions of 35 fmol and below, indicating at least a 10X higher detection limit compared to electrospray deposition.

When sample loading was reduced, increasing variability in signal intensity was observed, due to the formation of discontinuous sample films on the target surface. From Figure 4-15 (a), 175 fmol can be considered as the lowest loading for which constant intensity was measured and then the number of the angiotensin molecules is $1.05 \times 10^{11} molecules$. Given the effective molecular diameter of angiotensin around 1.2 nm, and assuming this diameter expands to twice this value when impacting the target plate, then the deposited area covered by angiotensin can be calculated as $0.24 mm^2$, which was very close to the area of the deposited spot size about 0.28 mm^2. This implies that 175 fmol loading generates a nearly continuous monolayer on the target surface, while lower loading level will produce some regions without sample, and the corresponding MALDI-MS spectra with increasing variations in measured intensity.

Thus, the electrospray deposition method enabled the detection limit of angiotensin at least ten times lower than that using the mechanically spotted method.

4.4.4 Chip-to-target Spacing Effect

Demonstrated in Figure 4-14, the electrospray-deposited sample was constrained to a diameter of 600 μm for the 1mm spacing. Since a smaller spot size implies increased analyte concentration, and thus improved signal intensity for low-abundance analytes, this represents a significant benefit for the electrospray deposition approach.

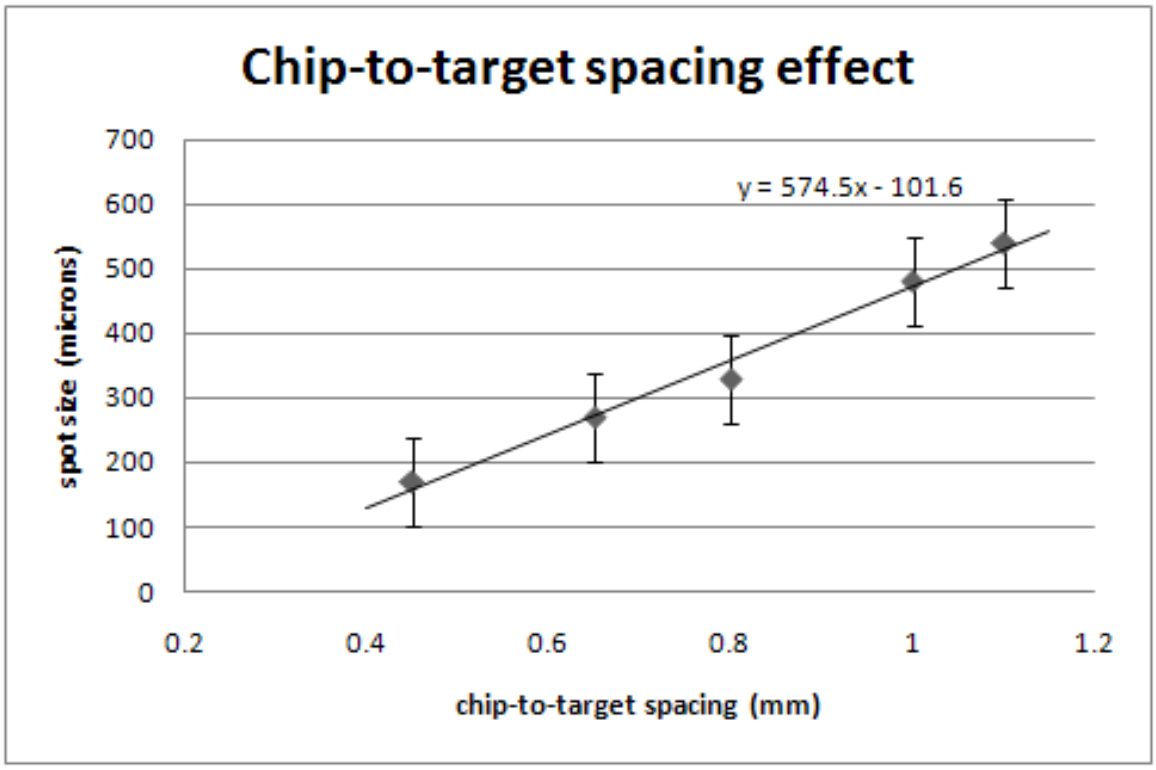

Figure 4-16 Relationship between chip-to-target spacing and resulting angiotensin spot size on the MALDI target

Chip-to-target spacing is expected to affect the deposited spot size on the MALDI target. Spot size measurements were performed by evaluating angitensin ion signal intensity along the diameter of each spot, and calculating the diameter limits when the MALDI-MS signal dropped to four times the noise level. As expected, smaller chip-to-target spacing was found to generate a smaller deposition spot size. The relationship between

spacing and spot diameter is nearly linear over the tested range as shown in Figure 4-16, from a diameter of 545 μm at 1.1 mm spacing to 170 μm at 0.45 mm spacing.

Lower detection limit from the microchip format should be feasible by reducing the chip-to-target in order to increase on-target concentration of deposited analyte.

4.5 Fabrication of Multi-channel Electrosprayer

4.5.1 Multi-channel Electrosprayer with Separated Inlets

As shown in Figure 4-16, if a chip-to-target spacing of 0.45 mm is used, a deposition spot diameter of 170 μm can be achieved. This suggests the potential for simultaneously depositing analytes from multiple closely spaced electrosprayers without contamination between adjacent spots.

To explore this concept, an electrospray chip containing three parallel microchannels was fabricated. Each channel is 100 μm wide at the top, 50 μm wide at the bottom and 35 μm deep. Peptide solutions of 50pmol/μL bradykinin (MW 904.Da), angiotensin (MW 1925.Da), and fibrinopeptide (MW 1570.68Da) were introduced into specific channels. An average flow rate of 70 nL/min was applied for 3 min with a chip-to-target spacing of 1mm. A 200 nL droplet of matrix solution was then added to each spot individually using the capillary spotter to prevent diffusion of peptides between spots.

Individual flow rates for each channel were adjusted to initiate stable electrospray. Up to 20% variation in flow rate was required to maintain stable electrospray from three channels simultaneously. This variation in flow rate is due to difference in the effective

flow resistances imposed by the bonded PTFE film that can be exhibit different amounts of pore collapse during the bonding process. Different shapes of channel exits also partially caused the variation in flow resistances.

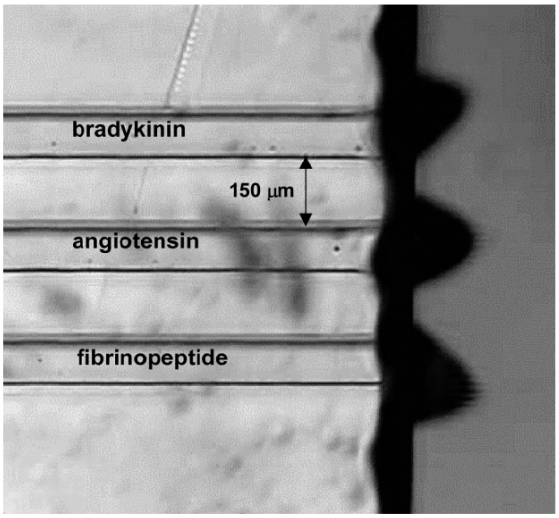

Figure 4-17 Optical micrograph showing simultaneous ESI from three parallel 100 um wide microchannels spaced 150 um apart

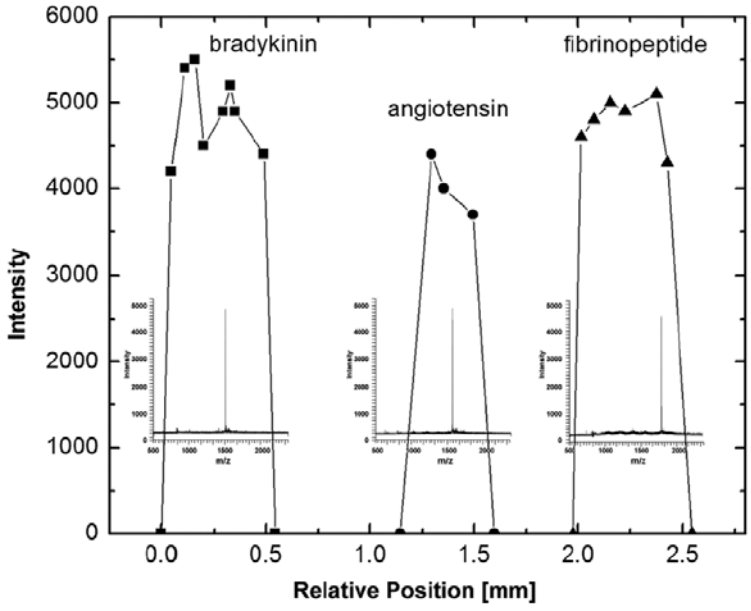

Figure 4-18 Ion signal intensities measured across peptide spots from the multichannel electrosprayer array

Figure 4-17 shows the optical micrograph of simultaneous electrospray from three channels. Due to the small spacing of 150 μm, electrostatic interaction between the fluids eluted from each electrospray tip result in a slight distortion.

MALDI-MS analysis was performed by sampling along a line through the centers of the deposited spots. The resulting measurements of ion intensity were shown in Figure 4-18. The mass spectra across each spot reveal no observable contamination between adjacent peptides, indicating that no significant cross talk occurs during deposition of matrix crystallization. In the regions between adjacent spots, no signal above noise was detected for any of the deposited peptides.

4.5.2 Multi-channel Electrosprayer without Embedded Capillaries

As described in the above 3-channel electrosprayer array, three pump systems were used to adjust each flow rate individually. Many high voltage power supplies and syringe pumps would be required if this was applied in multiplexed analysis. The glass multi-channel CE-MS chip by Xue et.al [21] also used ‘one-by-one’ mode via switching the syringe connection and the electric connection from one channel to another, which is not ‘parallel analysis.’ To reduce the numbers of high voltage supplies and syringe pumps, a parallel connection for multi-channel tip including the smallest number of high voltage supply and syringe pumps is desired.

2-channel ESI tip was used to do initial multi-channel testing. These two channels shared one reservoir, one syringe connection (including 500 μL syringe and syringe pump) and the same electric connection through the T-junction. Typical testing chip geometry uses a

channel width of 120 microns, channel depth of 30 microns and channel-to-channel spacing of 500 microns. Figure 4-19 shows a typical image of two Taylor cones established in the exits of a 2-channel tip with different cone sizes under the condition: applied voltage of 3330V, chip-to-counter-electrode spacing of 2mm and flow rate of 100 nL/min. The different sizes of Taylor cones indicated the different volumes of liquid through the membrane due to different flow resistances between channels.

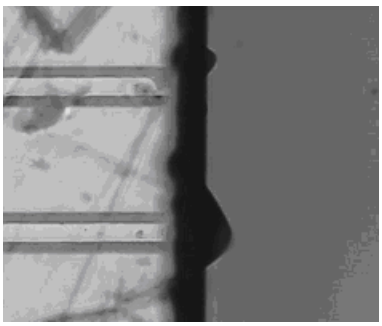

Figure 4-19 A typical image of two Taylor cones formed in 2-channel tip with different sizes under the condition: applied voltage of 3330V, chip-to-counter-electrode spacing of 2 mm and flow rate of 100 nL/min

The flow resistance of each channel produced differences including different sizes of Taylor cone and different pressure required (or flow rate). The different flow resistance of each channel is either caused by non-conformity due to fabrication processes such as collapse during thermal bonding, or is generated by non-conformity due to membrane thermal bonding.

4.5.3 Embedded Capillary Method

As described in section 4.2.4, the previous polycarbonate electrospray chips were prepared by the repeated motion of a milling machine or low speed saw. It was observed

that the adjacent channel exits have different flow resistances due to the debris that covered the exits during the cutting process.

A new method, the embedded capillary method, was explored. A microchannel about 100 μm in depth was hot embossed upon the Su-8 template in COC substrate. Then a section of 5mm long silica capillary (OD: 100 μm, ID: 40μm) was carefully cleaved to have a flat cross-section and embedded into the ends of each channel. The whole sandwiches were bonded together in a hot presser according to the similar thermoplastic bonding protocol, with increased pressure. The channel exits were opened by the low speed saw. Due to the different materials between the COC and the silica capillary, the debris due to thermal melting during the cutting was dramatically decreased. All the channel exits appeared as round openings due to the constraints of the capillaries, as shown in Figure 4-20 (a). A rectangle capillary shape could be considered to decrease the gap between microchannel and capillary.

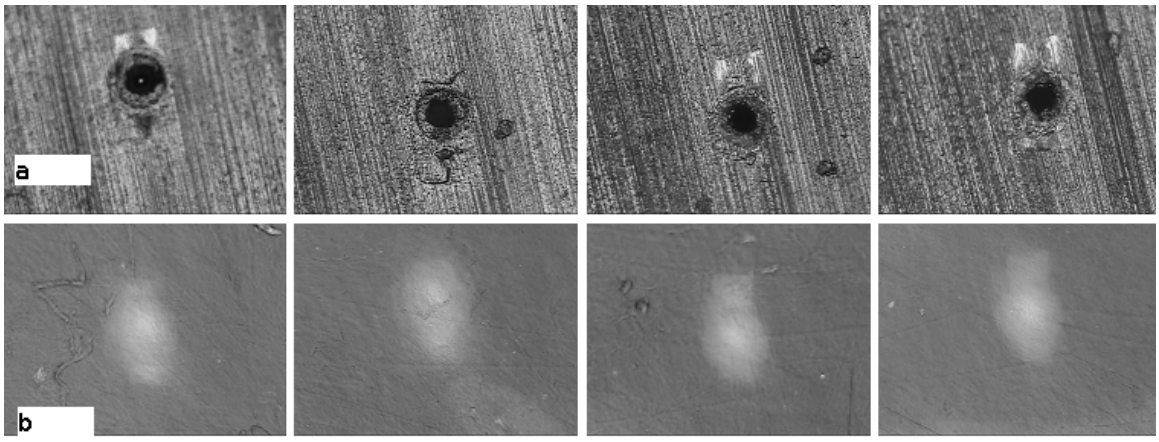

Figure 4-20 Open channel exits after sawing (before membrane bonding) (a) and membrane surface after bonding (b), the white areas are corresponding to channel exits, other dark area are transparent in view.

To bond the membrane with the chip, first attach the membrane to the channel exit surface on a flat glass slide at a temperature above the glass transition temperature of the substrate, then roll the exit surface on a heated steel ball till most areas appeared transparent, shown in Figure 4-20 (b).

4.5.4 Multi-channel Electrosprayer with Embedded Capillaries

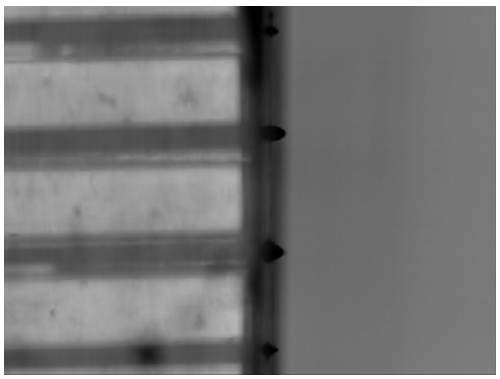

Figure 4-21 A typical 4-channel Taylor Cones showed under 5800V, 0.13 ul/min, and 2mm chip-to-counter electrode distance.

The flow rate had to be carefully chosen in this case. Higher flow rates caused leakage from the edges of the membrane. The rolling back and forward causes the change of the pore structure but not complete collapse, and results in the increase of water-entry pressure of membrane and breaks the bonding of the membrane and the chip, causing a leak.

The difference in sizes of each Taylor cone can be explained by the difference in the flow resistances of the channels due to fabrication, embedded capillary and bonded membrane. In Figure 4-21, the channel width is about 120 um. Taylor cones are positioned in the opening of the embedded capillaries.

4.6 Conclusion

In this chapter, a novel electrospray tip based on a polymer chip was fabricated utilizing the addition of a highly hydrophobic porous membrane on the orifice of the microchannel exit. The characteristic of electrospray performance in a single-channel electrospray tip was measured. Also, the application of the novel electrospray tip to deposit the protein/peptide sample on a stainless steel plate followed by MALDI-MS has shown to improve the MALDI-MS performance with improved signal-to-noise ratio, detection limit and repeatability.

Using a similar principle, a multi-channel electrospray tips array was explored to work either on ‘one-to-one’ mode or parallel analysis mode. To achieve the same flow resistances for each channel, a novel method, referred to as embedded capillary method, was reported and has shown potential for parallel analysis application.

Chapter 5 Microchannel Gel Electrophoresis Coupled with Mass Spectrometry

5.1 Introduction

CE is one of the most popular separation techniques in proteomics and peptidomic investigation due to its high separation efficiency, high resolution and small sample volume consumption. One of its drawbacks, though, is its low sample loading capacity. Therefore, this technique and its connection to a sensitive mass spectrometry, is a suitable to be an alternative to two-dimensional gel electrophoresis.

As summarized in 2.1.3, replaceable polymeric separation matrix is such a solution that can be conveniently pumped out of a capillary after each run and replaced with a fresh portion of the same matrix [120]. Cross-linked gel, e.g. PA, also can be in-situ photoiniated polymerized in a desired area by controlling the light exposure. This chapter explores the implementation of GE in polymer microfluidics, either using replaceable gel or highly cross-linked gel. Substantial reports have shown the success of PEO, a typical linear polymer. Hence the replaceable PEO was fist applied in this project.

5.2 Design

5.2.1 Microchip Layout

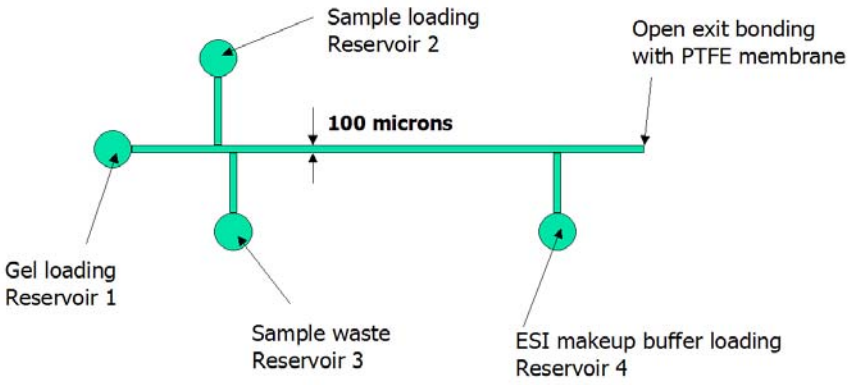

Figure 5-1 Schematic of a microchip layout

GE and the following electrospray ionization can be performed in a microchip including 5 reservoirs (gel loading, gel waste, sample loading, sample waste and ESI makeup) and 5 distinct channel sections (channel head, cross-injector, separation channel, detecting window and ESI channel) as shown in Figure 5-1. Typically, the microchip was 100 μm in width and 50 μm in depth. The channel was filled with a polymeric sieving solution prior to sample loading and electrophoretic injection. The gel electrophoresis involves two steps to load protein molecules into the separation channel. First, a mixture of samples (i.e., proteins or peptides) is drawn into the channel by a potential gradient that is imposed between the sample loading and the waste reservoirs of the cross-injector. This process is referred to as sample loading and results in a uniformly distributed sample plug within the cross-injector. The second step is called as electrophoretic separation. A run voltage is imposed between gel loading and ESI makeup reservoirs in order to initiate protein molecules migration toward the cathode. Sample loading and electrophoretic

separation of samples/mixture were observed within the cross-injector portion of microchip using a Fluorescence microscope.

5.2.2 Electrokinetics in Microchannels

Buffer solutions used in on-chip applications usually have high ionic concentration, e.g., 10^{-2} M, therefore the electrical double layer is very thin and can be considered a negligible thickness. In this way, the liquid in the microchannel can be considered electrically neutral, or $\rho_e = 0$. The applied potential, ϕ, in the buffer solution can be described by Poission equation [121],

$$\nabla^2 \phi = -\frac{\rho_e}{\varepsilon_0 \varepsilon} = 0 \tag{5-1}$$

The basic equations describing the flow field are the continuity equation,

$$\vec{\nabla} \cdot \vec{V}_e = 0 \tag{5-2}$$

and the momentum equation,

$$\rho[\frac{\partial \vec{V}_e}{\partial t} + (\vec{V}_e \cdot \vec{\nabla})\vec{V}_e] = -\vec{\nabla}P + \mu\nabla^2\vec{V}_e + \rho_e\vec{\nabla}\phi \tag{5-3}$$

where $\vec{V}_e$ is the velocity vector, ρ is the density of the liquid, P is the pressure in the microchannels, μ is the viscosity of the liquid and ρ_e is the net charge density in the solution. Because $\rho_e = 0$, the third item in the driving force of the flow is ignored.

Considering that the velocity component in z-direction is very small compared to the velocity component in x-direction and y-direction (u and v), the analysis can be considered as a two-dimensional problem [122].

The distribution of the sample concentration can be described by the conservation law of mass, assuming no the electroosmotic flow [123],

$$\frac{\partial C_i}{\partial t} + \nabla \cdot (-D_i \nabla C_i - z_i u_i F C_i \nabla \phi + C_i \vec{V}_e) = 0 \qquad (5\text{-}4)$$

where C_i represents the concentration of the ion i (mol/m^3), D_i is its diffusivity (m^{2}s^{-1}), u_i is its mobility (mol m^{2}s^{-1}V^{-1}A^{-1}), F denotes Farday's constant (mol^{-1}).

The detailed numerical analysis simulation results will be discussed alongside the experimental data in the following sections.

5.3 Microchannel GE by PEO

5.3.1 Instrumentation

A schematic of MGE-ESI chip visualization system is shown in Figure 5-2. The system consists of a high-sensitivity charge-coupled device camera from Andor Technology (Belfast, Northern Ireland), a Nikon fluorescence microscope (Melville, NY) fitted with 2X, 4X, and 10X objectives, a high-voltage power supply from Spellman and syringe pumps from Harvard Apparatus.

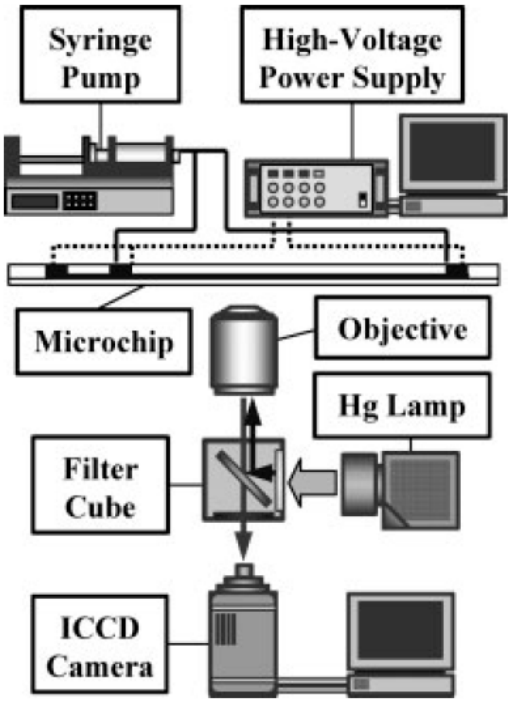

Figure 5-2 Schematic of MGE-ESI chip experimental setup showing imaging equipment, syringe pump used for press-injection control, and high voltage power supply

5.3.2 Protein Sample Preparation

Before a sample can be loaded onto a gel for analysis, it must be properly prepared. Depending on the gel type, preparation may involve denaturing the proteins, reducing any disulfide bonds, adjusting the ionic strength and removing interfering contaminants. Here sample preparation processes include staining of proteins, denaturing of protein, reduction of protein concentration and formation of protein-SDS complexes with negative charges. In brief, the covalently linked polypeptide chains of native proteins are folded in three dimensions in a pattern that is characteristic for each type of protein. When a protein is denatured, the characteristic three-dimensional arrangement of its polypeptide chain is disrupted and it unfolds into random structures, without damage to

the covalent backbone structure. The denaturing agent can be SDS or urea. After denaturing, when SDS is dissolved into protein solution, most proteins will bind to SDS at a constant ratio, i.e., 1.4g SDS per gram protein, and form rod-shaped SDS-protein complexes with a net negative charge.

Prelabelled fluorescent protein conjugates (such as albumin from bovine serum (BSA) BODIPY FL conjugate, MW 66000 Daltons; excitation: 550 nm; absorption: 630 nm) were purchased from Molecular Probes (Eugene, OR). The model protein with a final concentration of 1mg/mL was completely denatured and reduced in a 10mM Tris-(hydroxymethyl) aminomathane (Tris) with pH at 8.0 containing 8M urea at room temperature overnight, then 2% SDS was added to form protein-SDS complexes.

5.3.3 Gel Interface

PEO powder (MW 60 kDa) was gradually added to running buffer containing 10 mM Tris and 0.05% SDS with constant stirring to produce a homogeneous suspension to make a 1.5% PEO gel. Rhodamine B (excitation: 510nm, absorption: 550nm) was added into PEO gel to visualize gel motion in the channel under fluorescence microscope.

Because the resistance of porous membrane is much larger than the resistance of a 100μm wide 50 μm-deep microchannel, and the PEO gel is high viscous fluid, the basic steps to form a gel interface are depicted schematically in Figure 5-3. These steps can be summarized as follows:

1. PC microchannel surface treatment: fresh BSA solution with a concentration of 5mg/mL in 10 mM Tris, as a dynamic coating, was introduced into the entire

chip. The regulation of electroosmotic flow and the prevention of analyte adsorption are essential for the rapid, efficient separation of protein within microchannels. The adsorption of protein on the wall of microchannel results in sample loss, and even formation of clusters on the surface of the channel wall. The adsorption of BSA onto the plastic channel walls eliminates the electroosmotic flow and reduces the absorption of sample, reported in [124].

2. Introduction of a high-viscosity separation gel in the separation channel: a solution of 1.5% PEO in 10 mM Tris and 0.05% SDS as separation medium was introduced from gel loading reservoir A. Keeping injection of ESI running buffer from reservoir E, restricted the gel not beyond D, as shown in Figure 5-3 (2).

3. Next, as shown in Figure 5-3, the injections of the gel syringe pump and ESI syringe pump were interrupted while the syringe connection was maintained to avoid inner pressure change; from sample loading reservoir B, another solution i.e., sample or low conductivity solution was introduce to flush the extra gel out of the cross-injector. The gel-free interface was dynamically established, though, open to ambient pressure.

The gel-free scheme relied on the stability of gel solution and the environmental pressure. Therefore, another scheme, in which the injector was filled with gel without the additional cleanup step, was also employed in this project.

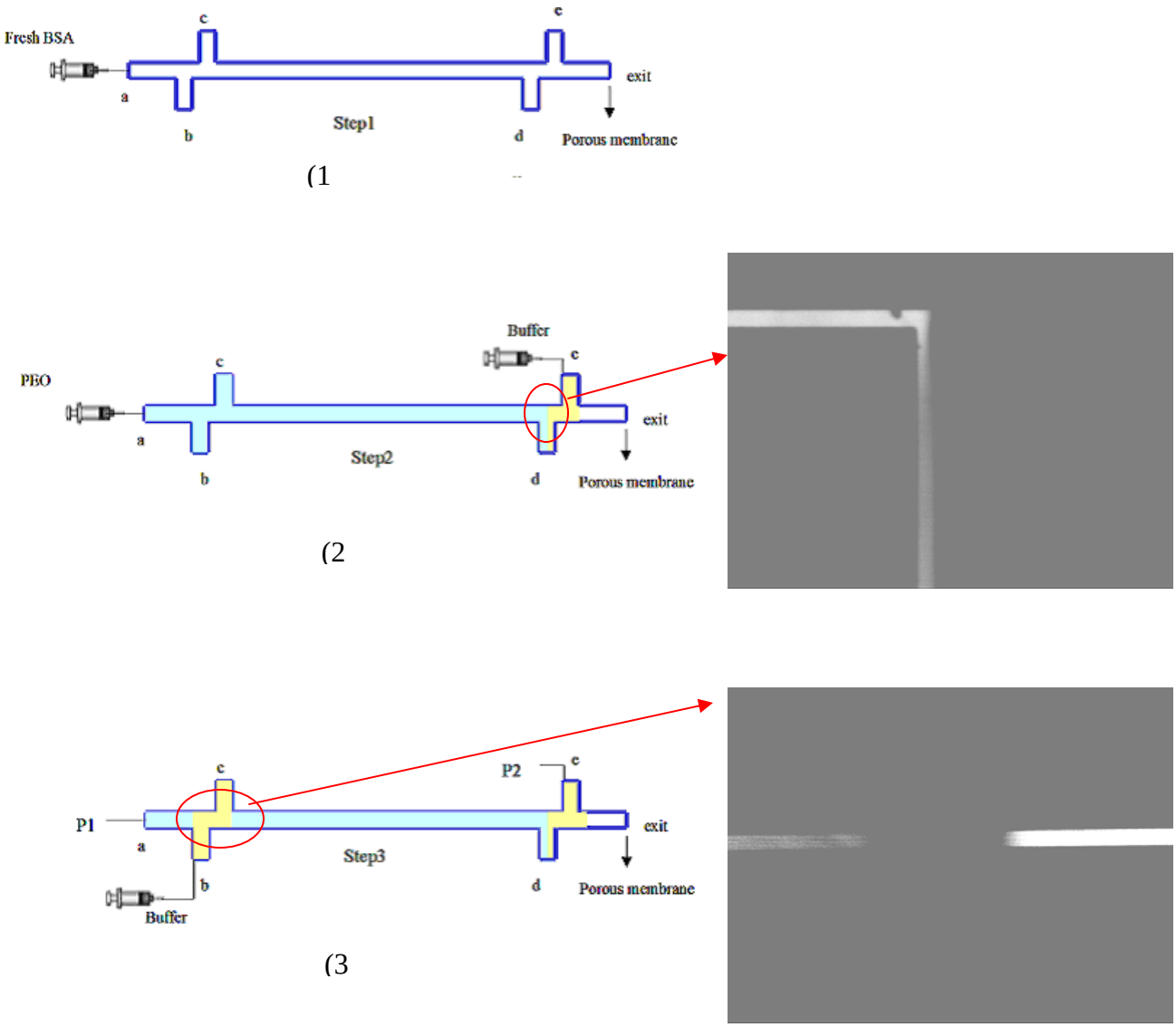

Figure 5-3 Gel-free Injector interface (Left) Procedure (Right) Images

5.3.4 Sample Injection

The chip was operated under a ‘sample-loading’ mode and a ‘separation’ mode. High voltage was provided by a high voltage supply from Spellman. In the sample-loading mode, a mixture of protein-fluorescein conjugates was prepared and introduced into the cross-injector to form a defined sample plug. Different sample injection methods (i.e.,

hydrodynamic or electrophoretic injection) were investigated to control sample plug leakage due to both hydrodynamic and diffusion effects

Hydrodynamic Injection

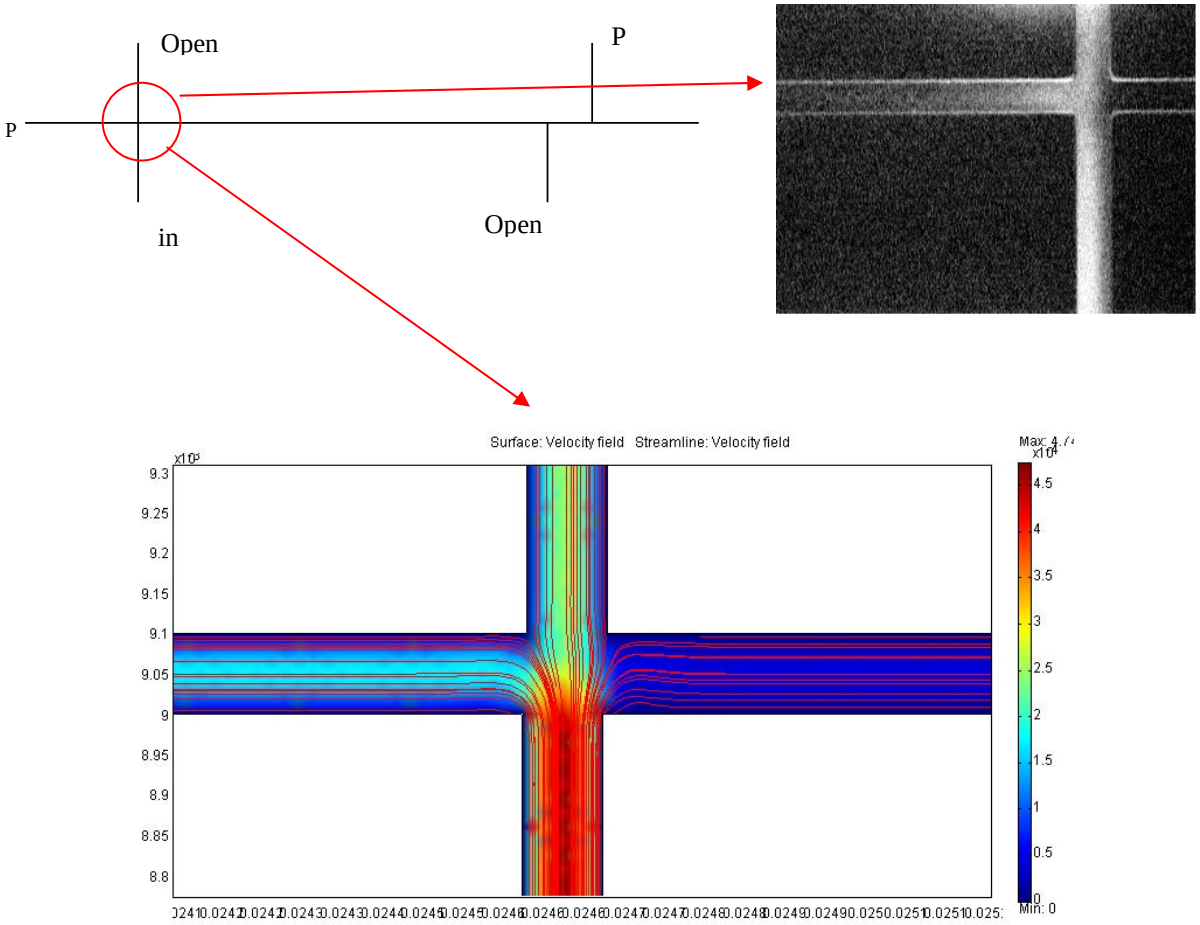

Figure 5-4 Hydrodyanamic sample loading (a) Schematic of simulation model (b) sample plug defined by hydrodynamic injection in a typical microchip (b) Numerical Simulation of velocity profile in cross-injector

In hydrodynamic injection, sample was injected from the sample loading reservoir B. The sample waste reservoir C remained open while the extra gel was flushed out from the

cross-injector. The great benefit of this method is that it forms a gel-free cross-injector so that preconcentration of sample at the interface (or stacking) is possible. This method also has disadvantages: it requires a long filling time (or flushing time), and a large sample volume. Because the Knudsen number in this case is very small (~2×10^{-5} for water), non-slip boundary condition is valid [142, 143]. From the numerical simulation, the flows divide into three directions with different velocities profiles. Most flows into the reservoir A due to lower flow resistance at this reservoir. Therefore, the sample plug length was not well-defined in this case, as shown in Figure 5-4.

Electrophoretic Injection

Electrophoretic injection was adapted to reduce the band broadening due to long sample plug. In electrophoretic injection, gel filled the separation channel as well as in the sample loading channel and the sample waste channel. No gel-free cross-injector was formed. Two types of sample introduction by electrophoretic injection were investigated.

For 'floating' sample loading, a potential was applied to the sample waste reservoir with the sample loading reservoir grounded and with the gel loading reservoir and ESI reservoir floating. As shown in Figure 5-5, the numerical simulation result showed the current density contours that indicated the concentration of sample in cross-junction was not focused. When the flow of mobile phase in the separation channel is not controlled, the analyte is free to move into the channel through eddy flow, resulting in a more diffuse injection plug.

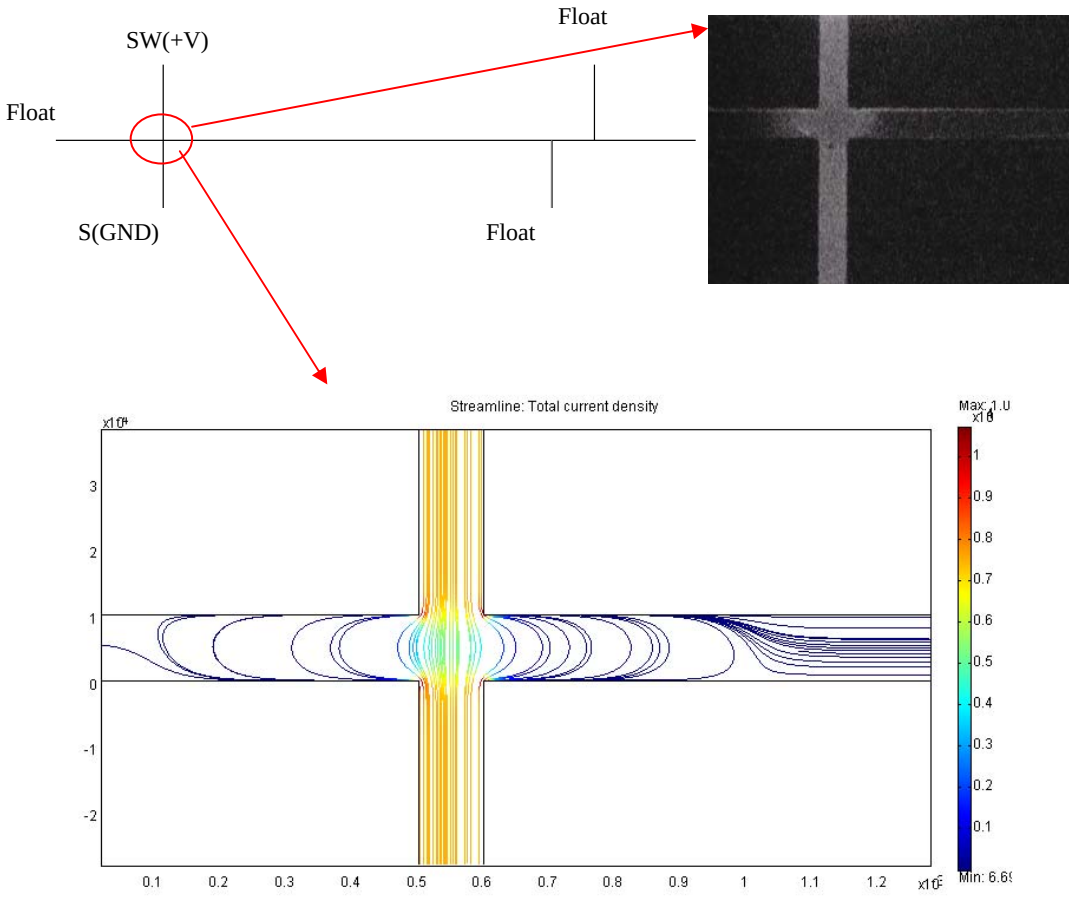

Figure 5-5 'Floating' sample loading (a) schematic of simulation model (b) a steady state of sample plug by 'floating' sample loading (c) Numerical simulation of current intensity profile in cross-junction

For a 'pinched' sample loading [125], potential was applied to the sample waste reservoir and the sample loading reservoir. The gel loading reservoir and ESI reservoir both were grounded to control the injection sample plug. Figure 5-6 (b) shows the 'pinched' sample loading prior to being switched to separation mode. Consequently, the analyte in the injection cross has a trapezoidal shape and is constricted and diluted in the analyte waste

channel (up) by this flow pattern. Compared to floating sample loading, pinched sample loading is superior in two areas: temporal stability and plug length. When two or more analytes with vastly different nobilities are to be analyzed, a sample loading with temporal stability ensures that equal volumes of the faster and slower moving analytes are introduced into the separation channel. A smaller plug length leads to a higher efficiency and, consequently, reduction of band broadening and dilution of analytes.

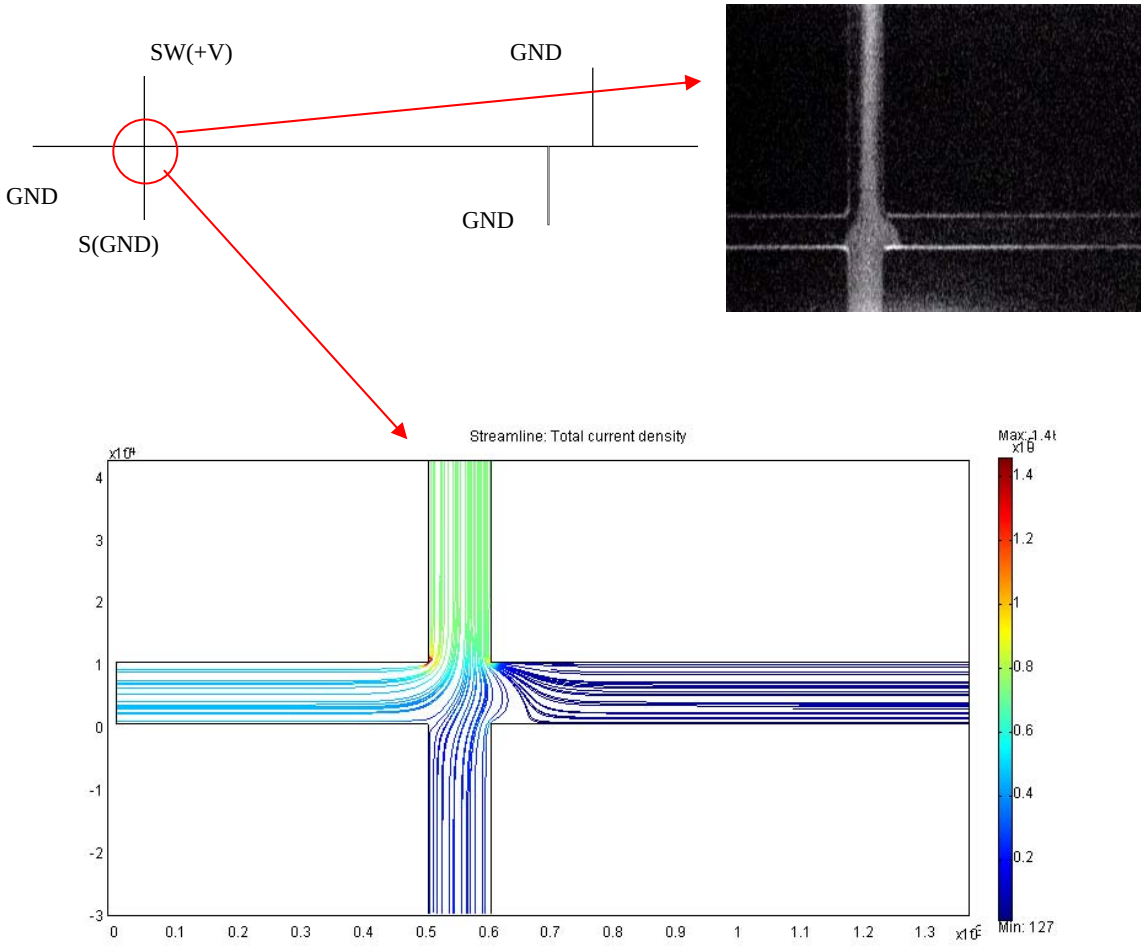

Figure 5-6 'Pinched' sample loading (a) schematic of simulation model (b) sample plug defined by 'pinched' sample loading (c) Numerical simulation of current density profile in the cross-junction

Injector Configuration

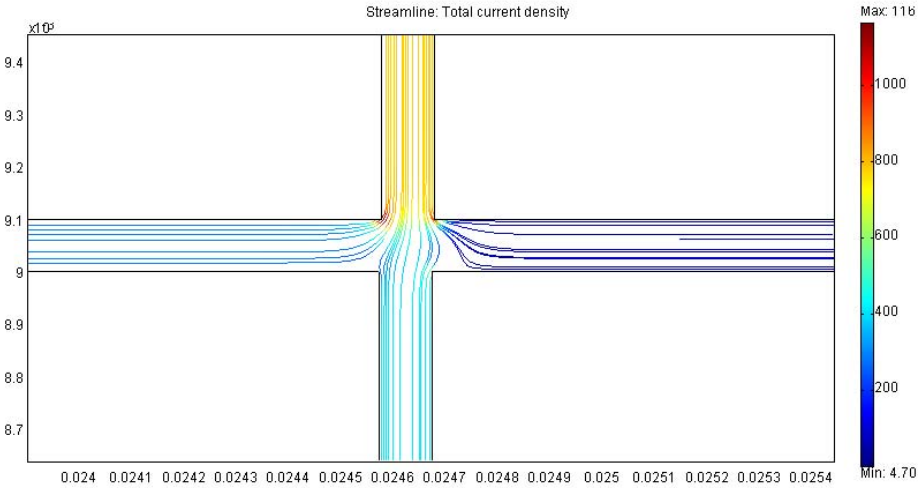

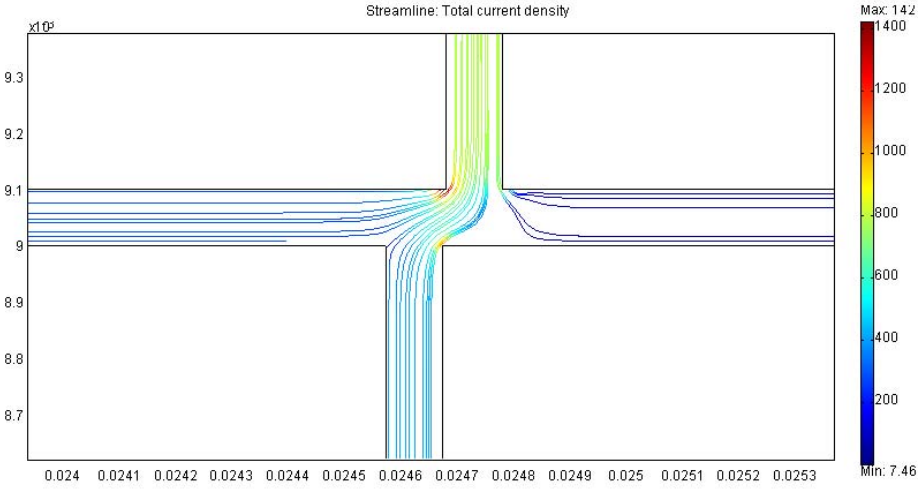

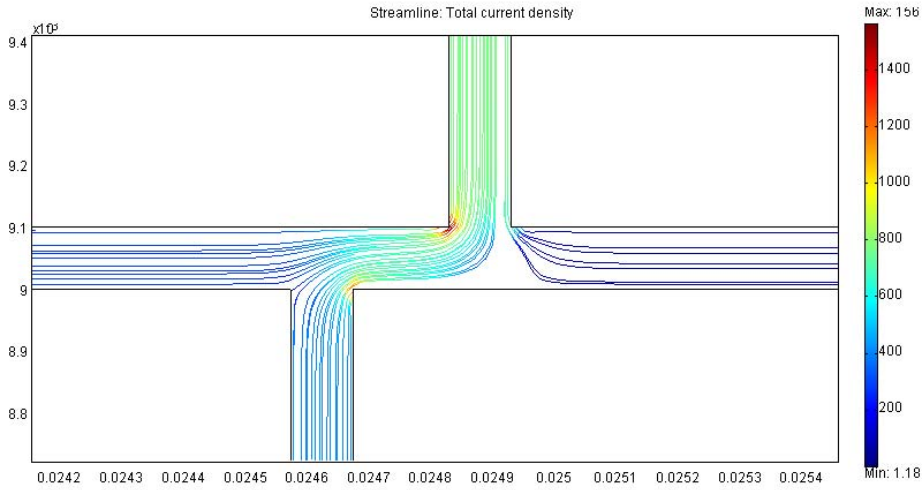

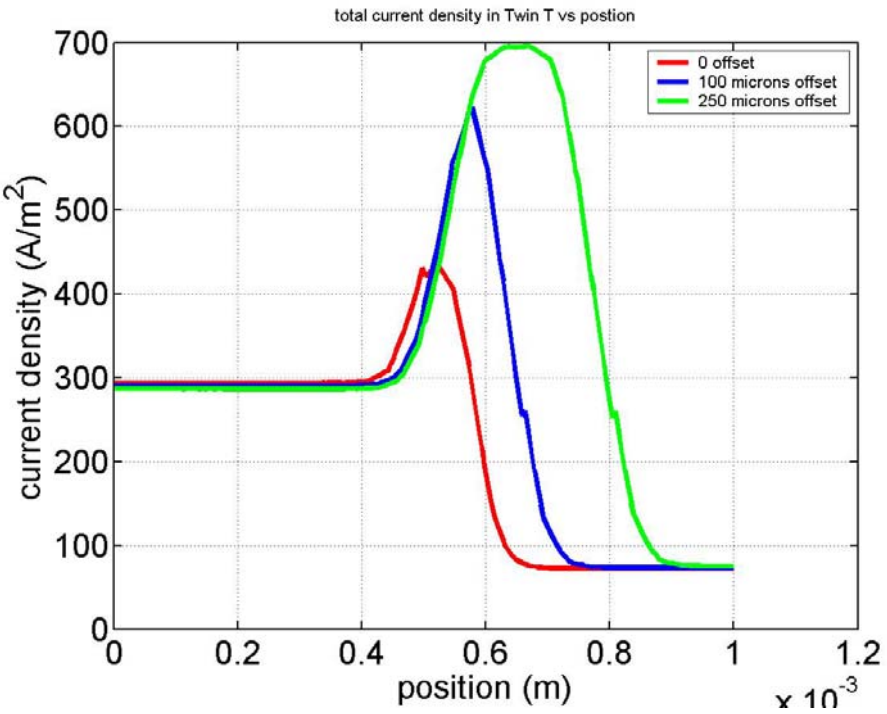

Figure 5-7 Numerical simulation of current density profile in different offset double-T injector Configuration (a) 0 microns (b) 100 microns (c) 250 microns (d) line-cut in the center of separation channel in double-T junction

Common on-chip injector configurations include the cross, the tee and the offset double-tee. In the offset double-T configuration [126, 129], the sample and dispensing channel run together for the short distance between T-intersections resulting in an effectively larger injector length, similar to the configuration in Figure 5-3. It was found that larger injector lengths increased signal at the expense of resolution [126, 129]. The flowing of buffer and sample adjacently in the injector channel causes increased diffusion and results in diluted dispensed sample. As shown in Figure 5-7, the numerical simulation results showed the 250 microns injector gave increase in signal peak. Further investigation showed a major loss of sample during the onset of the separation step due to pullback flow induced in the offset channels. Therefore, cross-tee configuration was mainly explored in the following experiments.

5.3.4 Separation

Protein molecules are loaded into the microchannel, then a run voltage is applied between the anode and the cathode so that the protein molecules migrate towards the anode with different velocities according to their different sizes. Proteins with less molecular weight travel more quickly through the gel than those with greater mass because of the sieving effect of the gel matrix. Protein molecular weights can be estimated by running standard proteins of known molecular weights in a separate lane of the same gel. This process is known as gel separation.

Figure 5-8 shows a sequence of the movement of single model protein. Typically, a positive voltage corresponding to the electric field strength of 130 V/cm was applied

between the gel loading reservoir and the ESI buffer loading reservoir while the sample loading and the sample waste reservoirs remained floating. The tailing of sample in the initial separation was obvious: the sample continuously migrates toward the anode from the sample loading channel and sample waster channel.

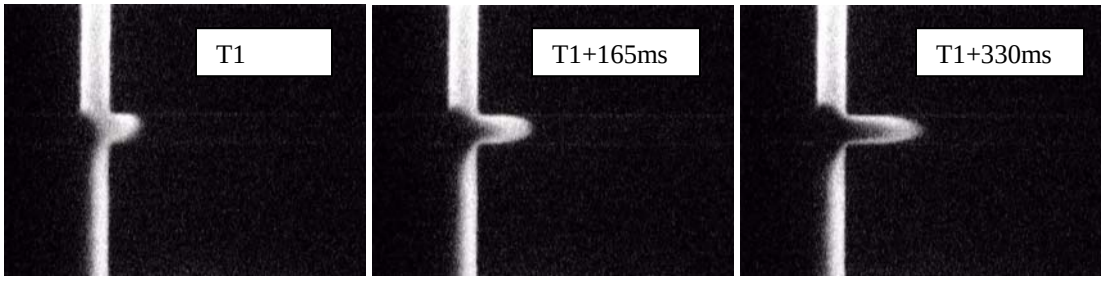

Figure 5-8 (a)-(c) Movement of single protein by applying a positive voltage between E and A (corresponding to 130V/cm electric field strength) while keeping sample, sample waste reservoirs floating.

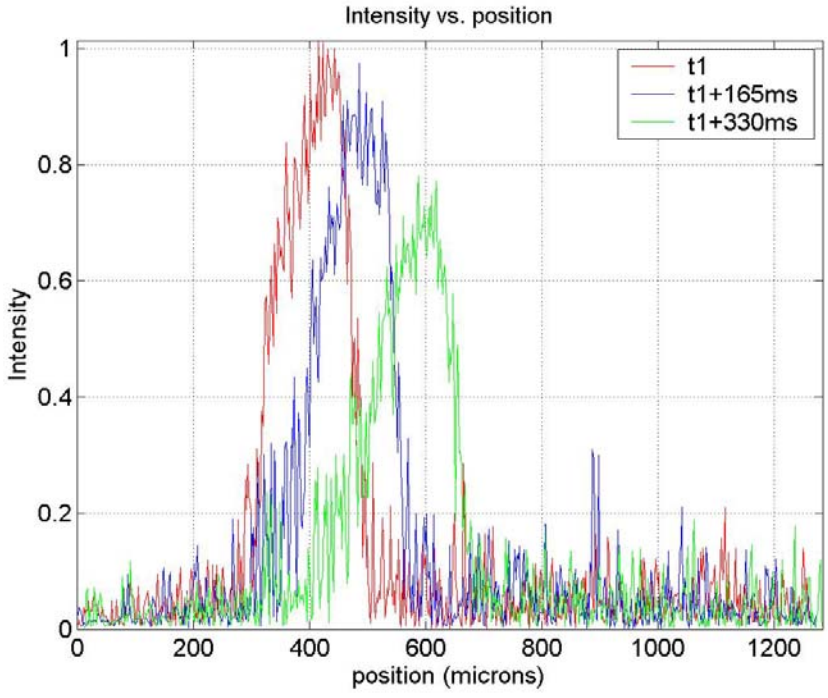

Figure 5-9 Intensity profile of Figure 5-8

However, the experimental results indicated significant loss of sample at the peak concentration only a few channel widths downstream of the intersection, as shown in Figure 5-9 .

In addition, the velocity/concentration profile of the sample showed parabolic instead of bulk – a phenomenon called Taylor dispersion [127]. This is due to a slight velocity bias caused by pressure forces originating in the reservoirs. These pressure effects are investigated next. From Eq. 5-3, the sample's velocity is a summation of electrophoretic velocity of the sample and hydrodynamic velocity due to this slight pressure. A flow resistance model based on the microfluidics geometry helps to well understand the sensitivity of velocity to pressure disturbances, a pressure difference to each reservoir.

A particularly useful equation for calculating the pressure drop through a long channel is [128]

$$\Delta p = QR_f \tag{5-5}$$

where Q is the flow rate and R_f is the flow resistance.

Usually, the concept of the hydraulic diameter can be used to assess flows through irregular shapes such as the trapezoidal cross section created by anisotropic wet etch in silicon.

$$D_h = \frac{4A}{P_{wet}} \tag{5-6}$$

where P_{wet} is wetted perimeter referring to the perimeter of the channel that is in direct contact with the flow and A is the cross sectional area referring to the area through which the flow is occurring.

$$R_f = \frac{\eta L}{8\pi D_h^4} \tag{5-7}$$

where η is the viscosity of the fluid, L is the length of the channel, and D_h is the hydraulic diameter [128].

Considering a typical value of liquid surface position difference of 1mm, standard buffer solution based on water ($\eta = 8.9 \times 10^{-3} kgm^{-1}s^{-1}$), and a channel length of 5.6cm, for a channel with 100 μm in width and 50μm in depth, we have an average velocity of 27 μm/s and a maximum velocity of about 40~54 μm/s. If the channel depth is reduced to 20 μm, then the sensitivity of velocity to pressure can be reduced to 15% of that in a 50 μm channel. Siphoning is a very serious concern in this geometry configuration and it must be taken into account.

Two distinct physical phenomena, stacking and destacking, may occur in the initial separation. Ideally, during the initial stage of separation, the protein molecules migrate rapidly within the sample plug of the cross-injector with lower conductivity, but they experience an abrupt drop in velocity when they reach the high-conductivity gel. This results in the pre-concentration of the sample plug. This phenomenon is called field-amplified sample stacking (FASS) [130-132].

In contrast, the analytes migrate slowly through the sample matrix until they reach the background gel and accelerate due to the increase in electric field. This leads to band broadening and a decrease in signal-to-noise ratio. This process is called ’destacking’ and the sample appears diluted. Destacking is another important cause of band broadening.

To obtain sample stacking, protein sample should be prepared by low concentration of SDS to form protein-SDS complexes, and an interface of two different analytes with different conductivities should be formed. Figure 5-10 shows the contour of electric field in cross-injector with different ratio of conductivity of sample to running buffer. As shown in Figure 5-10 (b), sample slows down where the electric field is weaker (in the separation region) so that stacking/concentration occurs at the interface of these two solutions with different conductivities.

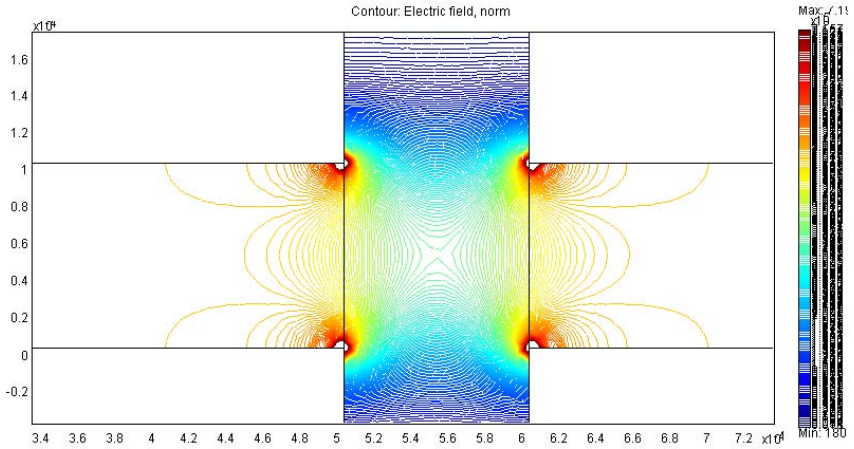

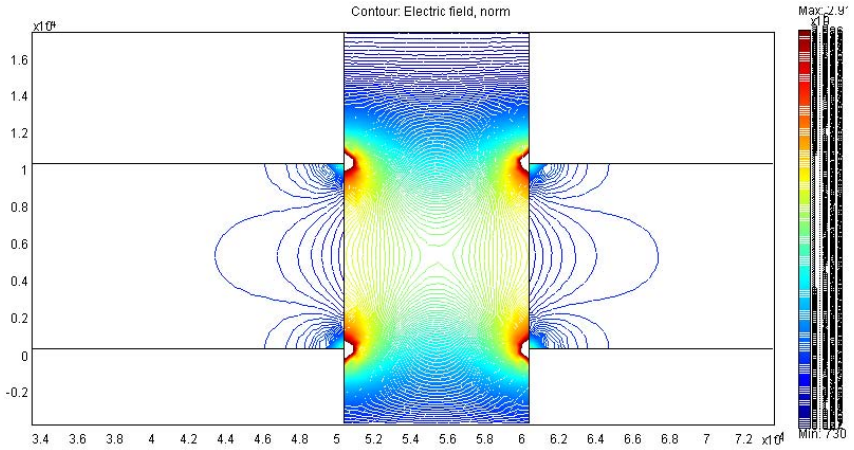

Figure 5-10 Contour of Electric field in cross-injector (a) ratio of conductivity of sample and running buffer =1 (b) ratio of conductivity of sample and running buffer=5

Stacking occurs at the interface between two solutions of different conductivities where the gel-free injector is formed by flushing running buffer. The gel-free cross-injector scheme was helpful to establish field-amplified stacking and to concentrate the sample using the established interface between two solutions with different conductivities. However, due to its dynamics, it was difficult to precisely control the sample plug length using hydrodynamic injection to introduce sample into cross-injector while flushing out the extra gel. Electrophoretic injection makes it easier to obtain the controllable sample plug without obvious stacking. Such is the tradeoff between hydrodynamic and electrophoretic injection in the present design.

In previous experiments, the movement of protein showed dilution in the concentration of sample and parabolic velocity profile during initial. This resulted in band broadening and

low signal intensity, even loss of the detection capacity. PEO gel is a high-viscosity fluid, but it still is a fluid. Any hydrodynamic forces (such as pressure from syringe pumps, or siphoning in 20 microns deep channel) can affect the location of PEO gel. Solidification of gel is needed to fix the gel in the separation channel whatever the hydrodynamic forces are. Additionally, the solid gel dramatically increased the flow resistance and the electric resistance. Therefore, highly cross-linked polyacrylamide gel was explored in the following section to obtain the good stability of separation medium.

5.4 Microchannel Gel Electrophoresis by Polyacrylamide

5.4.1 In-situ Polyacrylamide Polymerization in PDMS Microchannel

5.4.1.1 Chip Fabrication

To explore gel formation principle and protocol, a simple structure was fabricated on PDMS. PDMS has been utilized in the ‘rapid prototyping’ design for microfluidics using its advantages: easy fabrication and short turnaround time. The fabrication process of PDMS chip was published everywhere [132]. A negative mold was fabricated by SU-8 lithography or by silicon bulked wet etching, as described in 3.3.1. PDMS prepolymer (Sylgard 184, Dow Corning, Midland, MI) was mixed thoroughly with its cross-linking catalyst at 10:1 (w/w) and degassed by vacuum. The prepolymer mixture was cast against the silicon mold and allowed to cure at 70°C for 1 hour. After curing, the PDMS replica

was peeled from the mold and holes were punched into the polymer to create access ports as reservoirs.

The PDMS replica was then sealed with a clean borosilica glass. The unmated PDMS and the glass cover plate both were placed in oxygen plasma for 55s (50W at 60mTorr). When joined together, the oxygen plasma-treated parts were sealed irreversibly. The oxygen-treated PDMS has hydrophilic properties that degrade over time in air. Therefore, after sealing, the PDMS chip was immediately filled with water/buffer solution to ensure its lasting hydrophilicity.

5.4.1.2 Surface modification of PDMS

As summarized in section 3.1.2, most polymers are hydrophobic. The weaknesses of hydrophobic polymers in bioanalysis application are as follows: the difficulty to fill aqueous solutions into a hydrophobic microfluidic networking, the tendency to absorb molecules onto the surface of the hydrophobic polymer, and the unstable and uncontrollable EOF [135]. The monolith tends to bond poorly to the wall of the plastic chips, and the voids may even develop at the interface of monolith and walls. Therefore, the channel must be modified prior to the in-situ preparation of monolith [134]. A variety of solutions to this incompatibility, primarily surface treatments, have been demonstrated. For example, oxygen plasma treatment, silanization, adsorbed coating, dynamic coating (protein or lipid coating) etc were reported in the literature [134-135]. Surface treatment is also necessary to suppress the undesirable phenomenon of EOF.

A two-step surface modification procedure was developed to increase the stability of the monoliths in polymer channels in this study. An altered procedure from [136] is described as following: first, UV/oxygen treatment is used to oxide the polymer surface. Second, a well-known primer silane reagent 3-(trimethoxysilyl)propyl methacrylate is used to react with surface-generated oxide spices, thus facilitating the methacrylate groups to copolymerize with linear polyacrylamide. This step is called 'conditioning step'.

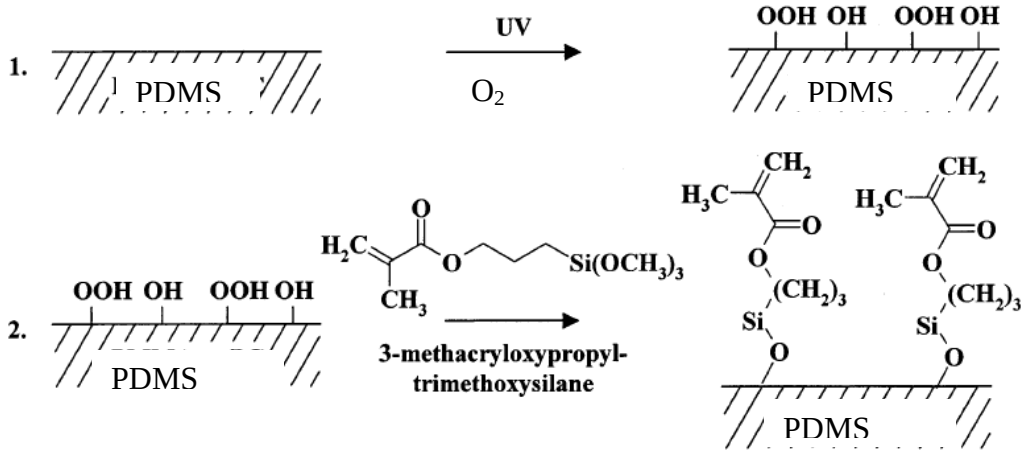

Figure 5-11 Schematic Diagram of chemical modification on PDMS surface

The conditioning solution was prepared by 2:3:5 (v/v/v) of 3-tri3-(trimethoxysilyl) propyl methacrylate, acetic acid and water. After initial vigorous mixing during the addition of water, the mixture was subjected to 10-minute sonication followed by 5-minute of degassing. After the PDMS channel was bonded to the borosilica glass slide, the conditioning solution was flushed through the channels for 30 minutes. After this step, the channels were flushed clean by water for 10minutes.

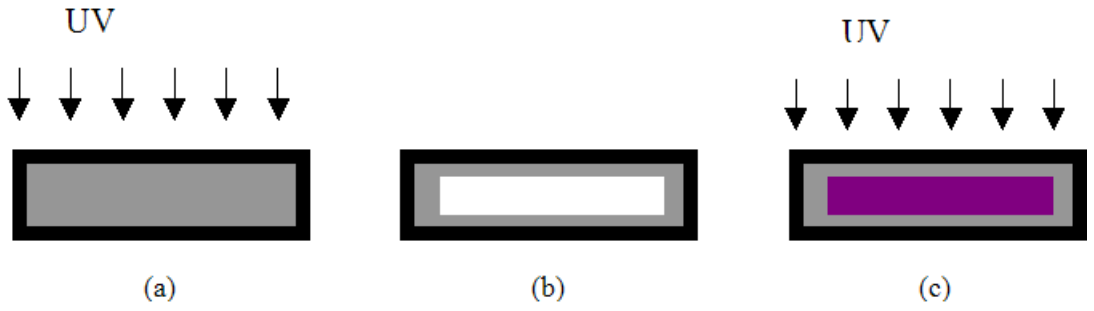

Figure 5-12 Schematic of two-step monolith polymerization. (a) acylamide was filled in the channel with UV exposure to form a thin layer of linear polyacrylamide; (b) the unpolymerized acrylamide was flushed out of the channel; (c) acrylamide/bisacrylamide solution was filled in the channel and UV selectively exposes the desired area to cross-link polymerization.

After the conditioning step, the suppression of electroosmotic flow was still weak. Therefore, a two-step monolith manufacturing procedure was applied [134] [137]. First, UV-initiated grafting with LPA is used to coat the channel surface with a thin layer of polymer that has a multitude of pendent double bonds. These bonds are then used in the next step for covalent attachment of the PA monolith to the wall.

As shown in Figure 5-12 (a), a solution of 5% (w/v) acrylamide containing 5mg/mL water-soluble photoiniator 2, 2'-azobis (2-methylpropionamide) dihydrochloride (V-50) was flushed through the channels, followed by 10-minute exposure to a 100W mercury lamp to initiate polymerization of a LPA coating on the wall surfaces. The unpolymerized solution was flushed out of the channels, shown in Figure 5-12 (b). Then a solution of 20% acrylamide/bisacrylamide including 0.2% (w/v) water-soluble photoiniator 2,2'-azobis[2-methyl-N-(2-hydroxyethyl) propionamide] (VA-086) was introduced into the channels. At last, selective exposure to UV formed a narrow gel band, shown in Figure 5-12 (c).

5.4.1.3 Gel Quality Control

As shown in Figure 5-13, the interface of gel and the aqueous solution was quite different from the gel inside the gel range. The interface seemed 'glue-like' such that during the concentration testing, protein sticks to the interface. There are a few reports on the gel interface control [138]. As discussed in [138], the interface shape underscores the good control of gel. The resolution of the photo-patterned polymer in the channels is determined by the photolithographic resolution and the diffusion of radical from exposed area to unexposed area. The photolithographic resolution was limited by the wavelength of light and the thickness of the cover plate, as described in [138]:

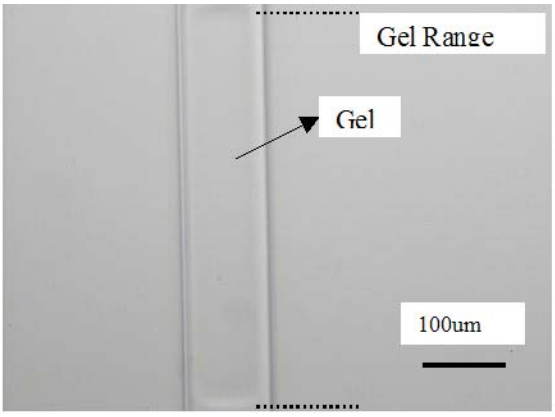

Figure 5-13 A gel formed in the PDMS channel

$$b_{\min} = \frac{3}{2}\sqrt{\lambda(s + z/2)} \qquad (5\text{-}8)$$

where λ is the wavelength of the light, b_{min} is the resolution, s is the distance between the mask and the polymer surface, z is the thickness of the cover plate. The gel in PDMS microchannel was prepared using the projection lithography with a 170um borofloat glass. Therefore, the resolution in this case is not an important in the generation of this glue-like interface.

Another possible reason for the interface is the diffusion of free radicals migrating from the exposed area to the unexposed area. As shown in Figure 5-14, using different objective to input the same energy into the system, different exposure time caused the different degree of diffusion of free radicals, thus resulting in different gel plug length. The later (Figure 5-14 (b)) is about 4 times as long as the former gel plug length (Figure 5-14 (a)). Also the blooming due to the partially polymerized polymer was increased with the exposure time. From this comparison, increase in the light intensity with short exposure time limits the diffusion of free radicals.

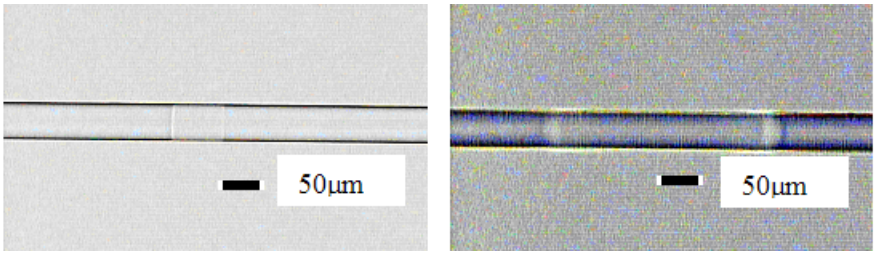

(a) (b)

Figure 5-14 (a) PAAm gel formation in 50 um channel with 40 X objective (NA 0.6) for exposure for 10s; (b) PAAm gel formation in 50 um channel with 10X objective (NA 0.3) for exposure for 160s (both images are contrast-adjusted)

Atmospheric oxygen inhibits radical-initiated polymerization. These radicals must first react with the oxygen dissolved in the sample to reduce its concentration low enough (~10^{-5}M) to allow the monomer to compete successfully with oxygen for the scavenging of the initiating radicals [139]. The effect of this is particularly pronounced in the present case because of the slow production of free radicals upon the photochemical decomposition of the photoiniators. Also, PDMS is an air permeable material through which oxygen can easily diffuse, resulting in the failure of gel formation. One strategy can be used to minimize the inhibitory effect of the atmospheric oxygen: High intensity

of light can be used to speed up the iniators photolysis. This will increase the production of free radicals, and reduce the exposure time limiting the diffusion of free radicals and oxygen. Also, soaking PDMS in the water or aqueous solution helps to reduce oxygen scavenging.

Another method of improving photopolymerization is to increase the rate of free radical generation by using fast decomposited photoiniators. VA-086 is an azo-group initiator with the disadvantages such as low absorption and associated low polymerization rate [139]. Other photoiniators such as hydroxyphenyl ketone were reported to be applied to UV curing of acrylate systems with short curing times [139].

5.4.2 Cross-linked Polyacrylamide in COC Microchip

5.4.2.1 Chip Fabrication

As summarized in 3.1.5, COC has become an attractive candidate for polymer-based microfludics due to its excellent optical properties and its good chemicals resistance. Also, COC can easily be fabricated by hot embossing and injection molding.

COC chip fabrication is a simple process. A negative Su-8 was fabricated on a bare silicon wafer by Su-8 lithography with different thickness between 20um and 100um. To increase the adhesion of Su-8 to the silicon wafer, an extra 3-hour baking at 200°C was applied. A piece of 3.5”x3.5”x2mm COC (Zenor® 1020R) was sandwiched between a clean 5” glass and 4” Su-8 mold. The sandwich was inserted into a pre-heated hot press at a temperature 20 °C above the glass transition temperature of COC (Zenor® 1020R, i.e,

Tg, 105 °C). A pressure was applied during the hot embossing. After the press was cooled down below the glass transition temperature, the replica was separated from the Su-8 mold and allowed to cool down to room temperature. The pattern was 1:1 transferred to the replica. After that, another piece of blank COC plate with pre-drilled holes was aligned with the replica and sandwiched between two clean glass plates. The sandwich was inserted into the pre-heated hot press with pressure, whose temperature was set to just above the glass transition temperature of COC. High pressure was applied to achieve the desired bonding strength.

5.4.2.2 Cross-linked Polyacrylamide Fabrication

The primarily function of polyacrylamide fabricated in COC chips is to separate proteins with different mass/size according to a size-excluded mechanism. Therefore, a different concentration of acrylamide/bisacrylamide was used to for the separation gel, usually 8%. Polymerizations both with and without photografting step were explored. The photografting procedure started with the introduction of a mixture of 1:1 ethylene dimethacrylate (EDMA) and Methyl Methacrylate (MMA) into the channel by the syringe pump at 0.2 μL/min for 30minutes to avoid trapping bubbles inside. The whole chip was then exposed under 28 mW/cm^2 for desired time, typically 3 minutes. Finally the un-polymerized solution was replaced by methanol.

The mixture of 8% (%T) acrylamide/bisacrylamide containing 10mg/mL V-085 was slowly injected into the chips by syringe pump at 0.2 μL/min for 30min. For visualization, Blue G-250 (Coomassie Brilliant) was added into pre-gel solution. A film

mask was firmly attached to the chip. The chip was then exposed under 28 mW/cm^2 using contact lithography for optimized time, typically for 5~15 minutes, depending on the concentration of the photoiniators. The chip was stabilized for another 15 minutes to let the remaining free radicals finish polymerization. This process was finished by flushing water through the chip for 12 hours to remove all the unpolymerized solution.

In the absence of prior surface treatment (photografting), after flushing for 2 hours, the channel seemed clear. It was believed that most of the monolith was pumped out of the channel. It seemed that the monolith was loose within the channel and the pressure from flushing pump finally removed the entire monolith out of the channel.

Using grafting with EDMA and MMA for 3 minutes, a section of gel remained in the center of channel after flushing for 16 hours (shown in Figure 5-15 (Left)). This indicates the PAAm gel has covalently bonded to LPA layer, strengthening the bonding between the PAAm and the chip walls.

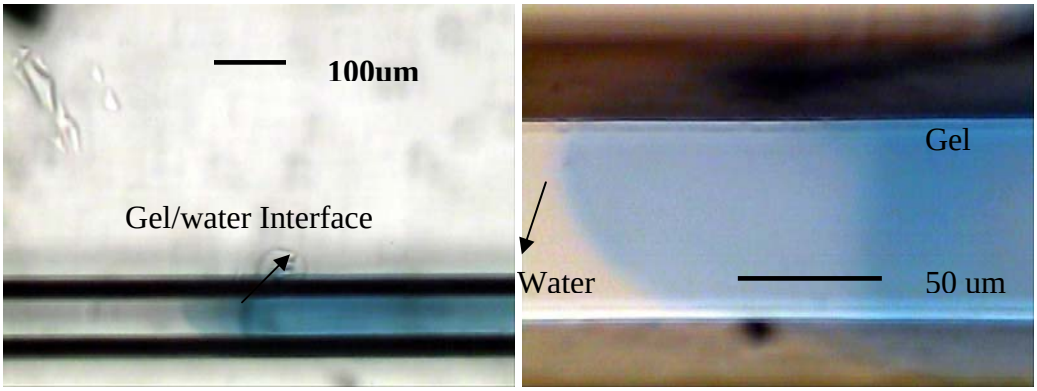

Figure 5-15 PAAm gel/water Interface in microchannel (Left) and its closed-look (Right)

Figure 5-15 (right) is the closed-look of the PAAm gel/water interface. It shows that more than 100 μm 'blurring' of gel plug is observed. As discussed in 5.4.1.3, the

resolution of the gel is determined by the resolution of the contact lithography. The thickness of the top plate was as thick as 2mm, leading to a theoretical resolution limit of 30~40 μm. It indicated that the resolution of the contact lithography is not the impact factor to determine the resolution of the gel. Other factors, i.e., diffusion of free radicals in the interface, may play more important role in affecting the gel resolution.

5.4.2.3 Further Discussion of Gel Fabrication

Knowledge about how to improve the gel quality within a microchannel was generally developed through the experiments in 5.4.1 and 5.4.2. Several strategies to improve the gel quality are summarized as follows:

- Increase the exposure intensity and decrease the exposure time.

The first benefit of increasing the exposure intensity and decreasing exposure time is to reduce the diffusion of free radicals. The diffusion will be worse with time: $L = \sqrt{2Dt}$ (here D is diffusivity, t is time, and L is diffusion length). This diffusion causes the low resolution shown in Figure 5-15.

A UV band filter was necessary since, in most case, UV lamp has a wide range spectrum. For example, SunRay400SM UV lamp has the spectral distribution as demonstrated in Figure 5-16. It includes several peaks around 300nm, 360nm, 450nm, 550nm etc. A narrow band filter with a peak around 345nm~375nm can exclude the undesired UV components.

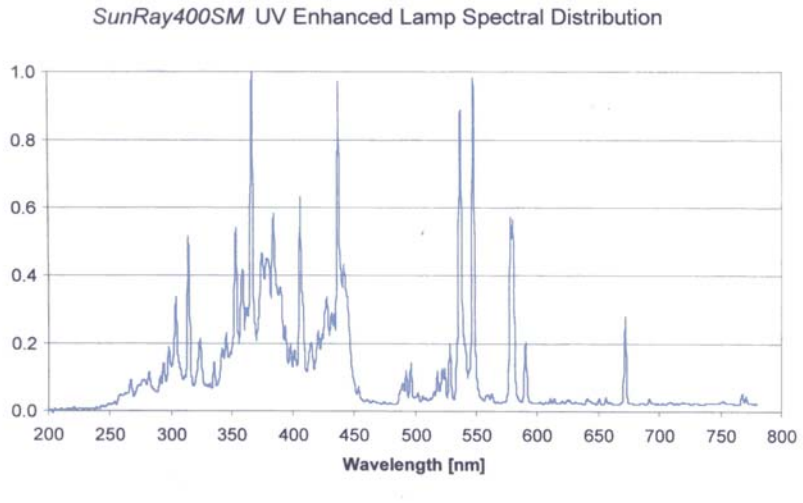

Figure 5-16 SunRay400Sm UV enhanced Lamp spectral distribution

A better solution to get a sharp interface of gel-water is to use a laser light source or projection lithography. High magnification of lens can provide enough intensity with the tradeoff of small depth of focus (DOF).

- Thinner cover plate

Here a 2mm thick COC plate was applied. As calculated in 5.3.3.2, the resolution was limited by thick cover plate. Also, thicker polymer absorbs more thermal energy and, due to low thermal conductivity, the thermal effect is considerable.

- Chemicals

Photoiniators play very important role in the polymerization. Increasing the concentration of photoiniators will be helpful to increase the polymerization ratio. The higher the polymerization ratio, the lower the diffusion of free radicals or oxygen due to limited exposure time. Hydroquinone is a radical scavenger of free radicals. It can be added to

prevent premature polymerization of the monomer that may occur due to exposure to ambient light or elevated temperature.

5.5 Conclusions and Future Works

This chapter first demonstrated the concept of microchannel gel electrophoresis by replaceable separation medium (e.g., PEO gel) in a microfluidic chip, including instrumentation and protocol. Several issues (such as sample loading, stacking/destacking etc) were discussed in detailed. Due to hydrodynamic force, the stability of PEO gel was so poor that the separation of protein was not dependent on the electric field only, resulting in a boarder band and faster dilution of protein during the separation step.

To increase the stability of the separation medium, highly cross-linked PAAm gel was explored in the microchannels via in-situ photoiniated polymerization. PAAm gel was fabricated in PDMS via two-step surface treatment and two-step polymerization procedure to increase the covalent bonding of the monolith to the sidewalls of the polymer. Also, the gel performance was verified through DNA concentration and elution against the gel. Then, the PAAm manufacturing technique was transferred into the microfluidics based on COC. In addition, several strategies to improve the gel quality were discussed in detailed.

Protein separation in PAAm gel is not yet tested. The future works include the gel quality control in COC chip, the demonstration of protein separation in 8% (%T) PAAm gel and the following ESI deposition onto the target as designed.

Chapter 6 Gas-Phase Electrophoretic Protein/Peptide Concentration for MALDI-MS

6.1 Introduction

Air-dried method is one of the oldest and simplest sample preparation methods for MALDI. A sample deposited by air-dried method typically measures 5~15 mm^2 in size. Only a tiny portion of this (0.002~0.004mm^2) is irradiated by laser for ion generation because the laser spot size is around 200μm [140]. In addition to this discrepancy, the heterogeneity of sample prepared by air-dried method is a concern. It has been shown that the problem of heterogeneity can be overcome or reduced if the sample diameter is reduced to below 250 μm. In that case, a large portion of the deposited sample can be laser-irritated simultaneously since the laser spot diameter is usually 200 μm, improving sensitivity and rending signal suppression less frequent. Therefore, one strategy for improving signal reproducibility is to decrease sample size.

As described in Chapter 4, a polymer microfluidic chip with PTFE membrane has been demonstrated with good performance. The size of the deposition was observed to have a linear relationship with the chip-to-ground spacing for gaps larger than 450 μm [141].

Further efforts to reduce the size of the deposited sample by reducing the chip tip-to-electrode spacing below 450 μm was explored, resulting in limited success due to the instability of electrospray performance, as shown in Figure 6-1. It indicates simply reducing the spacing to a very short distance did not offer good stability and repeatability of electrospray performance because a considerable amount of debris in the ES solution remained onto the target due to short evaporation time.

(a) 1 min elapse *(b) 2 min elapse* *(c) 3 min elapse*

Figure 6-1 Taylor Cones Observed for 300 μm spacing with time elapsed, 2.1KV applied

Another method to concentrate the density of the sample on the target, electric field focusing method, was explored in this project.

6.2 Theoretic Design

6.2.1 Background

Under static condition, the potential, *V*, can be described by

$$E = -\nabla V \qquad (6\text{-}1)$$

Using this equation combining with the constitutive equation $D = \varepsilon E$ to rewrite Gauss's Law, $-\nabla D = \rho$, then Poisson's Equation is written as

$$-\nabla(\varepsilon_0\varepsilon_r V) = \rho \qquad (6\text{-}2)$$

where $\varepsilon_0, \varepsilon_r$ are the permittivity of vacuum and the relative permittivity, V is the electric potential, and ρ is the surface charge density. This equation can be solved by FEMLAB combined with the boundary conditions.

When a positive potential is applied to a point-like structure with a very small size compared with the ground electrode, the electric field appears as a Gaussian distribution, as shown in Figure 6-2. Due to the electrophoretic motion of the molecules under the electric field, the deposited area is larger than the point source size.

To increase the local density of molecules on the ground electrode, the deposited area should be reduced. Here, a cross field was proposed to focus the electric field into a small range to deposit the sample in a more refined area.

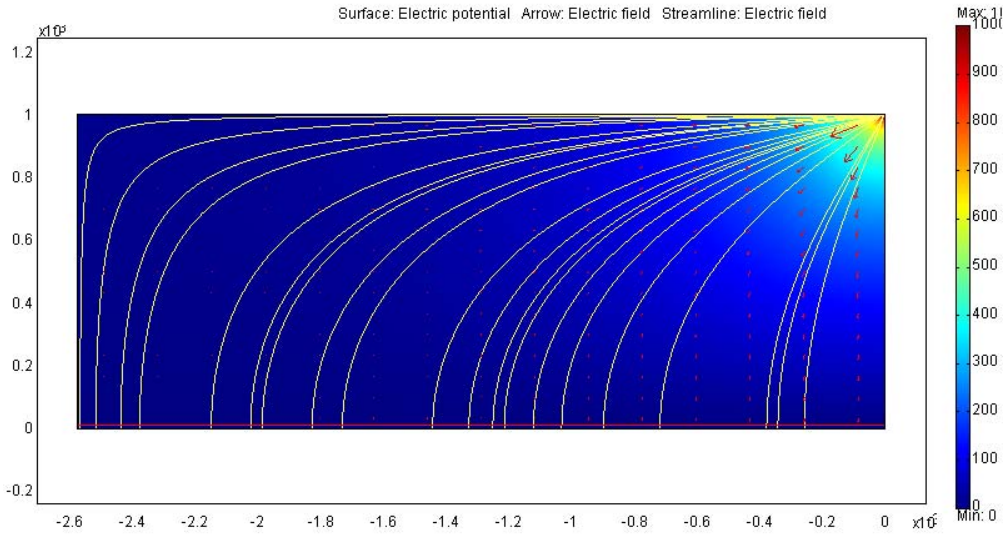

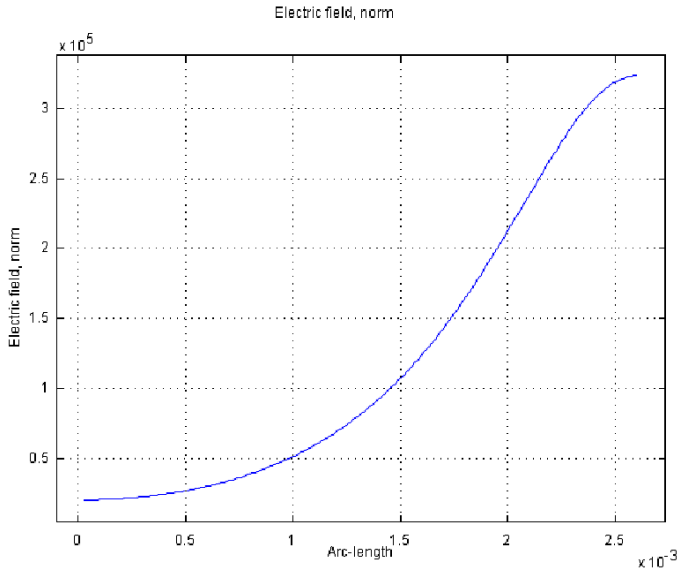

Figure 6-2 Electric field distribution for a large ground electrode plate without focusing

6.2.2 Horizontal Cross Field Focusing Model

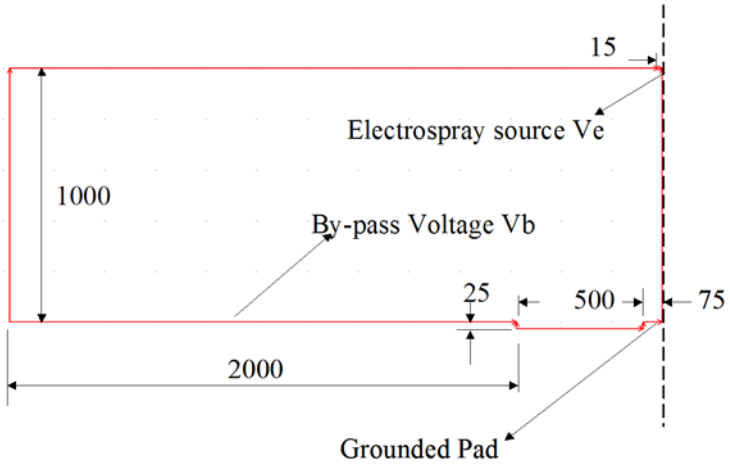

Figure 6-3 Schematic of horizontal cross field focusing model (unit: micron)

The model shown in Figure 6-3, referred to as a horizontal cross field focusing model, indicates that the cross field was generated by the potential applied to the by-pass area, which was located at the same level as the grounded target. The electrospray source is located in the center with applied voltage *Ve*. The distance between electrospray source and the ground target is 1mm.The ground pad in the target is 150 μm in diameter. The gap between the pad and the by-pass area is 500 μm. Assume the by-pass area is larger than 1mm.

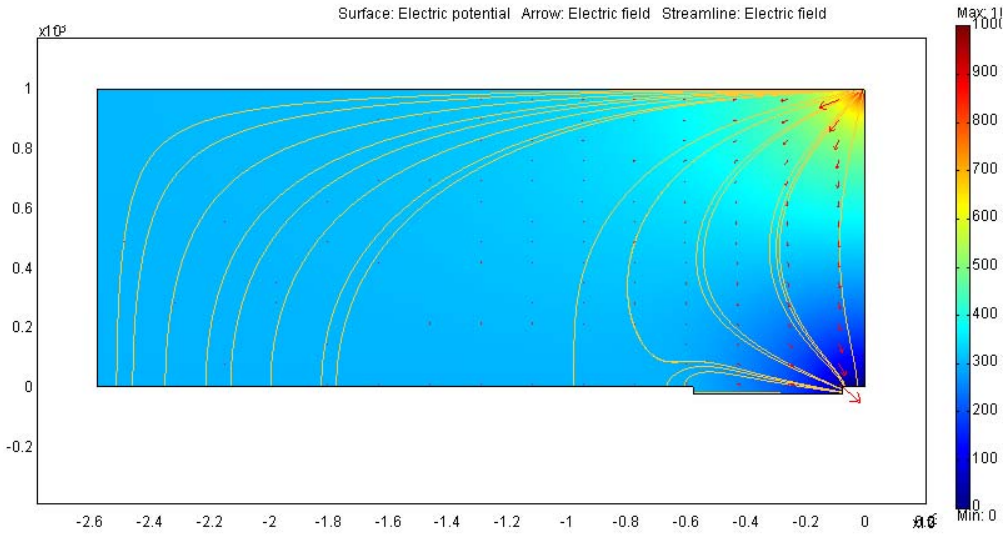
Surface: Electric potential Arrow: Electric field Streamline: Electric field
x10³
1
0.8
0.6
0.4
0.2
0
-0.2
-2.6 -2.4 -2.2 -2 -1.8 -1.6 -1.4 -1.2 -1 -0.8 -0.6 -0.4 -0.2 0
Max: 1
1000
900
800
700
600
500
400
300
200
100
0
Min: 0

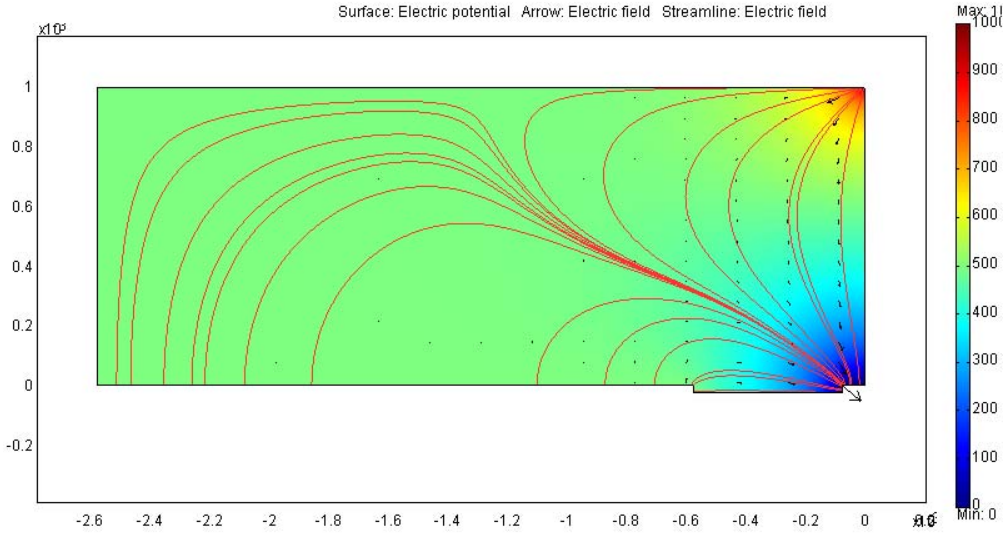
Surface: Electric potential Arrow: Electric field Streamline: Electric field
x10³
1
0.8
0.6
0.4
0.2
0
-0.2
-2.6 -2.4 -2.2 -2 -1.8 -1.6 -1.4 -1.2 -1 -0.8 -0.6 -0.4 -0.2 0
Max: 1
1000
900
800
700
600
500
400
300
200
100
0
Min: 0

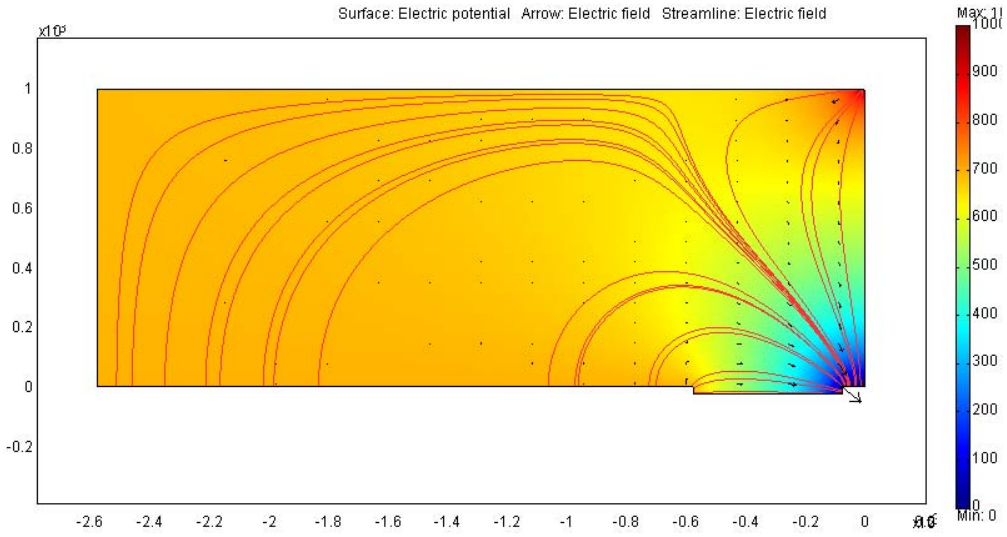

Figure 6-4 Simulation results for different by-pass voltage (from top to bottom, 300V, 500V, 700V respectively) at a constant electrospray voltage of 1000V

Figure 6-4 shows the simulation results for different by-pass voltages at a constant electrospray voltage of 1000V. The arrow size and the direction in the figure represent the electric field intensity and the direction of electric field. The surface plot shows the distribution of electric potential. With an increase in the by-pass voltage (as shown in Figure 6-4), the electric filed from the electrospray source to the center pad was further confined by the electric field from the by-pass area to the center pad, indicating that the ions will be deposited in a smaller area.

Figure 6-5 demonstrates the relationship between x-component electric field and the position to the center of the pad with different by-pass voltages. All the data were collected at the surface level above the target plate 10 μm. The position 2.575mm is the

center of the target plate. Starting with a by-pass voltage around 300V, the x-component electric field was directed to the target, indicating that the cross field had taken effect on the focusing of the electric field. With the higher by-pass voltage, the higher x-component electric field was directed to the target plate. This indicates more ions will be attracted to the target plate due to electrostatic force.

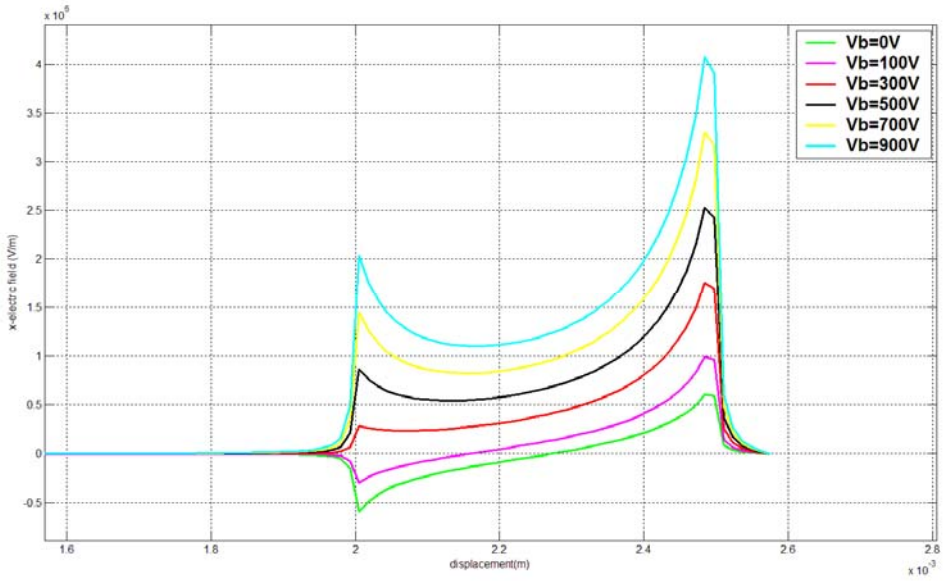

Figure 6-5 X-component electric field vs. displacement in different by-pass voltage cases

However, due to small spacing between the by-pass area and the central target plate, air breakdown may occur if by-pass voltage is too high. The electric potential between the by-pass area and the central target should be lower than the breakdown voltage, i.e., 1500V at 500μm gap because the air dielectric constant is $3\times10^{6}V/m$. Surface electromigration, a directed motion of atoms at solid surfaces, grain boundaries and interfaces, will also be one possible source of failure due to an electric current in the bulk

of the material. Electromigration is exacerbated by high current density and Joule heating of the conductor, eventually leading to failure of electrical components. Considering the above reasons, the by-pass voltage was limited to 30~40% of the electrospray voltage, with the trade-off of low focusing effect.

During the alignment of the electrospray tip with the target plate (around 150 μm in size), misalignment, which means the electrospray source is not centered on the top of target plate, may occur. Figure 6-6 shows simulation results exploring the effects of misalignment. The electric field distribution changed when the source position was far away from the center of the target plate. Also, as demonstrated in Figure 6-7, the center of the normal electric filed generally moved with the moved source. The corresponding motion of the electric field is not significant, so many misalignments smaller than 300 μm could be ignored.

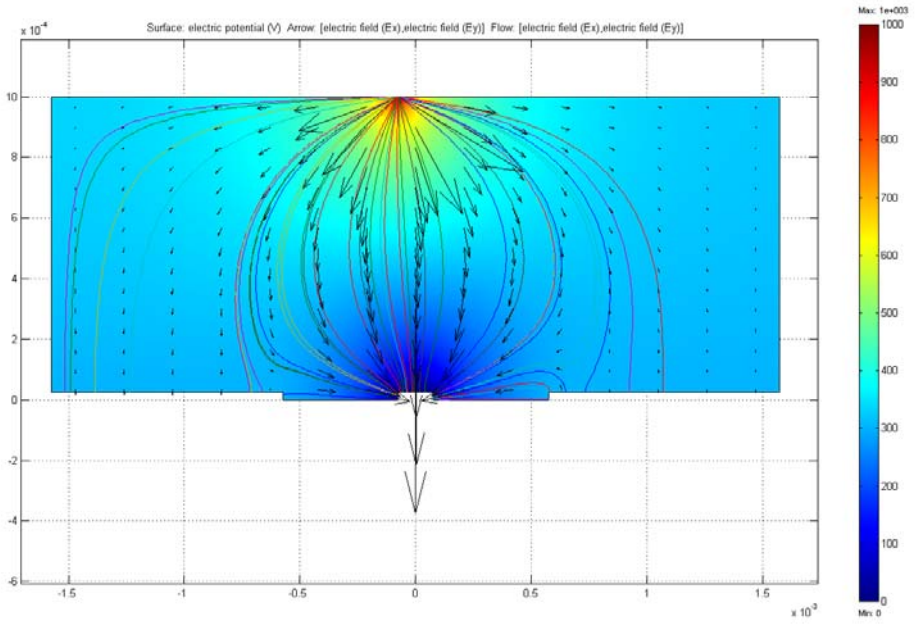

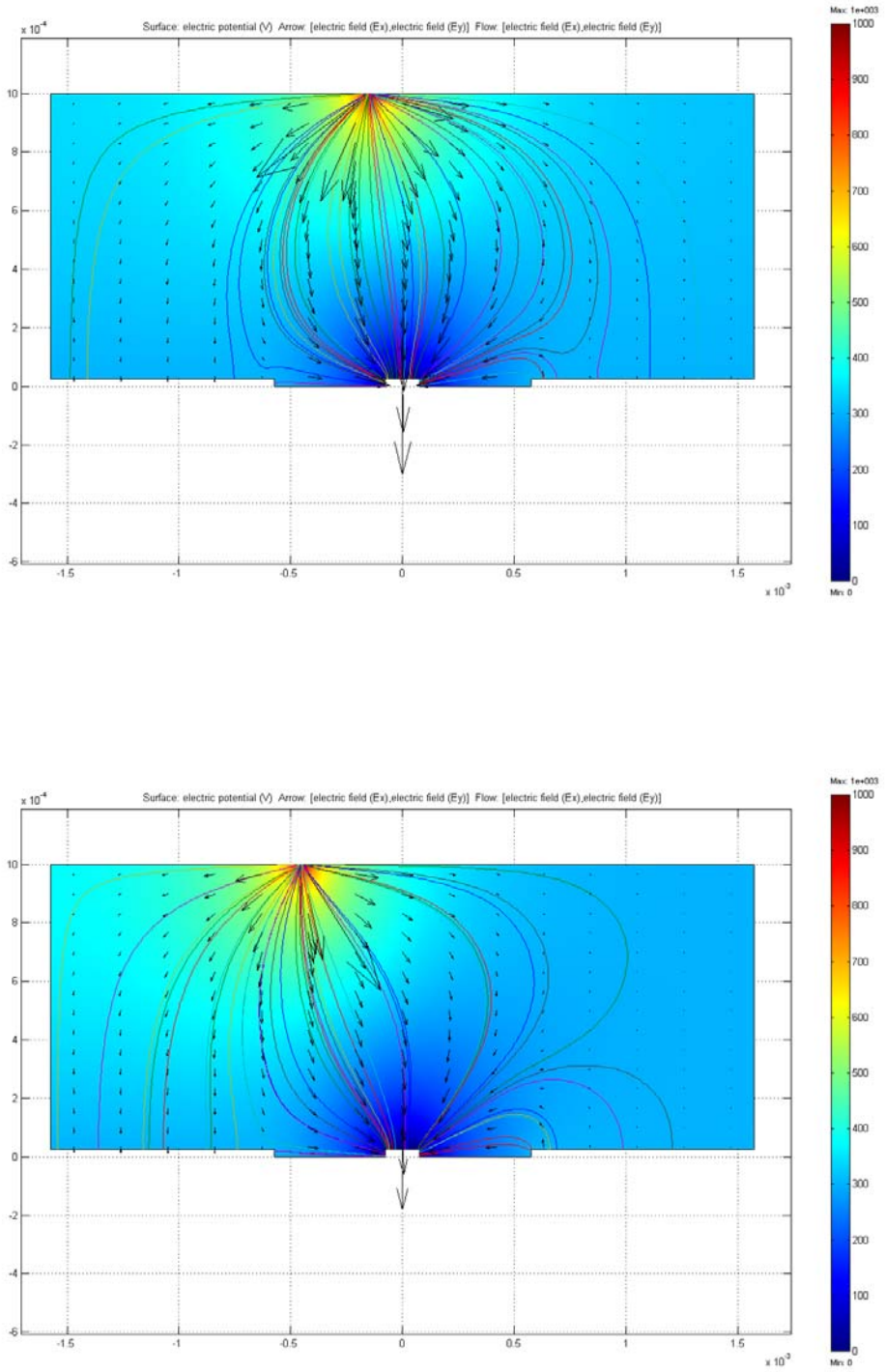

Figure 6-6 Misalignment effect. From top to bottom, (a) The source is positioned around 75um far away the center of the target plate. (b) The source is positioned around 150um far away the center of the target plate. (c) The source is positioned around 450um far away the center of the target plate, while the by-pass voltage is 300V and the electrospray source is 1000V.

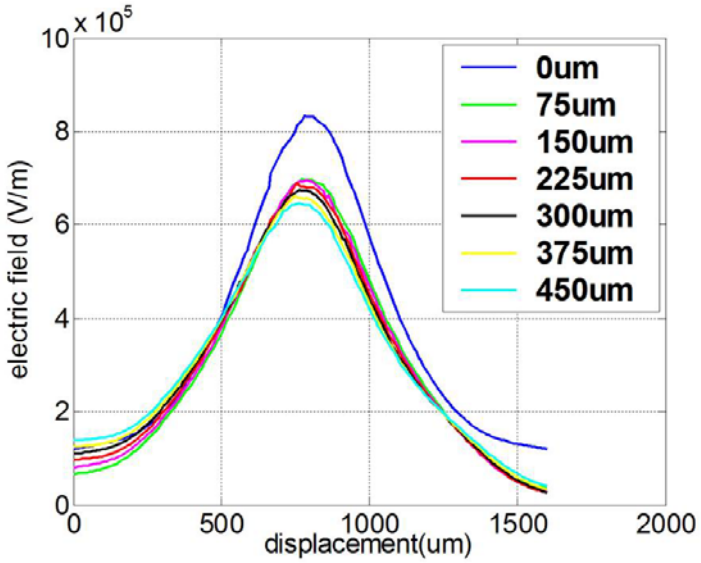

Figure 6-7 Peak of the normal electric field vs. the distance of electrospray source to the center

6.3 Mass Spectrometry Analysis by Line-structured Concentrator

6.3.1 MALDI Sample Preparation

1mg of peptide Angiotensin I (MW 1296.5) was prepared in a buffer solution containing 50% water, 49% methanol and 1% formic acid at a concentration of 10pmol/μL. The sample was stored in the freezer. The initial Angiotensin I solution of 10pmol/μL can be diluted to the desired concentration by adding more buffer solution. 10mg CHCA powder was added into 1mL matrix buffer (50% Acetonitrile, 40% water, 10% acetic acid) to achieve 10mg/mL concentration, vortexed for 1 min, and followed by ultrasonication for 20 mins untill the powder was fully dissolved. The 10mg/mL matrix solution can be diluted to a desired concentration by adding more matrix buffer. The same volume of

sample and matrix was mixed and vortexed for 1min, keeping the constant ratio of sample amount to matrix amount.

6.3.2 MALDI Analysis on Standard Stainless Plate

A high performance mass spectrometry MALDI AXIMA CFR™ plus (Shimadzu Biotech) was used for mass spectrometry analysis. The sensitivity of this instrument is about 10 fmol in reflectron mode (insulin B chain).

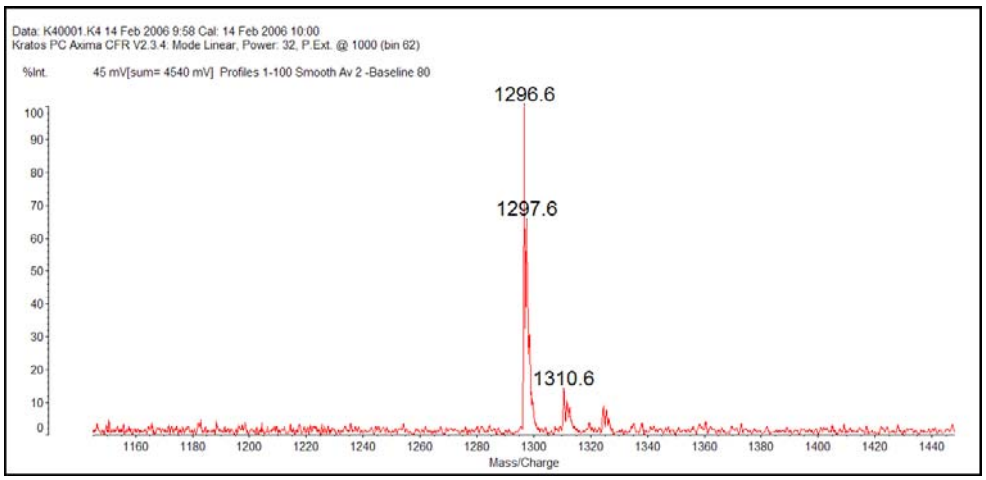

(a)

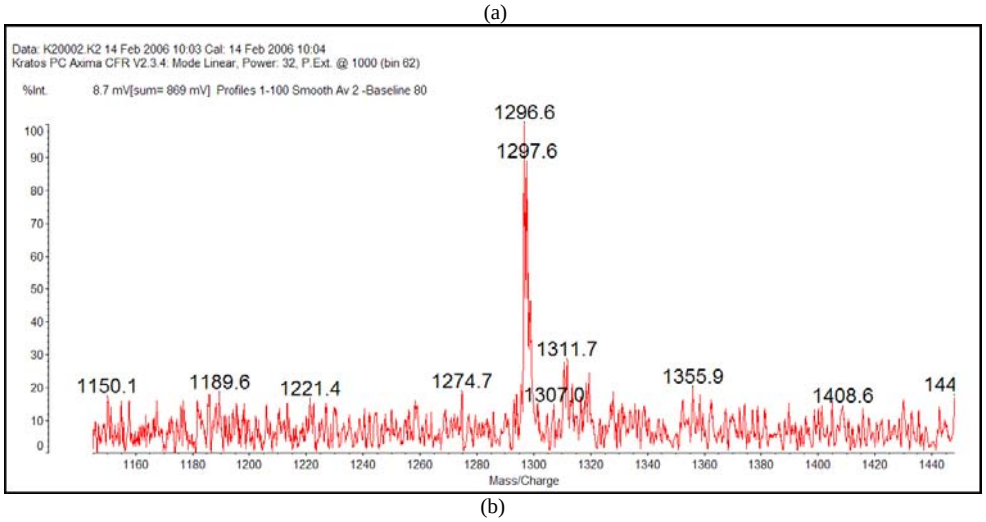

(b)

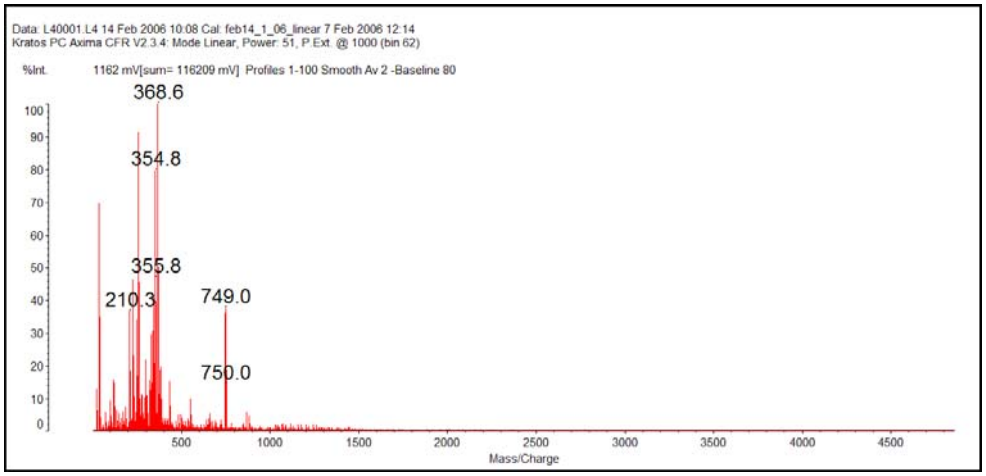

(c)

Figure 6-8 MS analysis by electrospraying on stainless steel plate with varying sample amounts (a) sample amount=100fmol; (b) sample amount=10fmol; (c) sample amount=1fmol

The MS analysis of the sample deposited by electrospray method on the standard steel plate was explored first. The steel plate was electrically ground and the same sample was deposited on the pre-cleaned target plate. The deposited amount was calculated as the product of the flow rate and the deposition time. Figure 6-8 shows the MS analysis data by electrospraying the sample on the stainless steel plate with varying sample amounts. As shown in Figure 6-8 (c), a great deal of noise background was observed when the sample amount was 1 fmol; therefore, the detection limit of electrospraying on the stainless steel plate without any focusing effect was about 10 fmol.

6.3.3 MS Analysis on Line-structured Concentrator

The fabrication of the line-structured concentrator started from a single-layer PCB board, with 25 μm thick copper on the top. The patterns were generated by a high-precision

CNC milling. The final dimension of a typical line is 150 μm in width and 500 μm in space to by-pass area.

The concentrator was fixed on a house-made 45° x, y, z-translation stage. A 5cm tapped capillary tip (ID: 100μm, OD: 360μm, New Objective, MA) was connected to a T-junction with a platinum electrode as the electric contact. This electrospray source was also mounted on another homemade 135° three-dimensional translation stage. The distance between the electrospray source and the prestructured target plate can be adjusted by these two translation stages.

Non-concentrated method and concentrated method were both explored on the same target plate. For the non-concentrated method, the by-pass area was grounded as target. For the concentrated method, a by-pass voltage (~560V) was applied to the by-pass area and the line with deposited sample was grounded when the electrospray voltage was around 1700~2100V on the electrospray source. The deposition showed a small line on the copper line 150μm in width, and 1/64" ~ 1/32" in length depending on the specific deposited matrix amount. No apparent matrix (or color) showed in any other area except the grounded line. The deposition time is timed starting from when a stable current is monitored. Total deposited amount is calculated as the product of the set flow rate and the deposited time.

As demonstrated in Figure 6-9, the red curve was the MS signal profile of non-concentrated method in 1 fmol and indicated using this method 1fmol cannot be detected. However, the blue drawing in Figure 6-9 was the MS signal profile of concentrated

method in 1 fmol. Although the signal-to-noise ratio was high, the concentrated method still can detect this low amount.

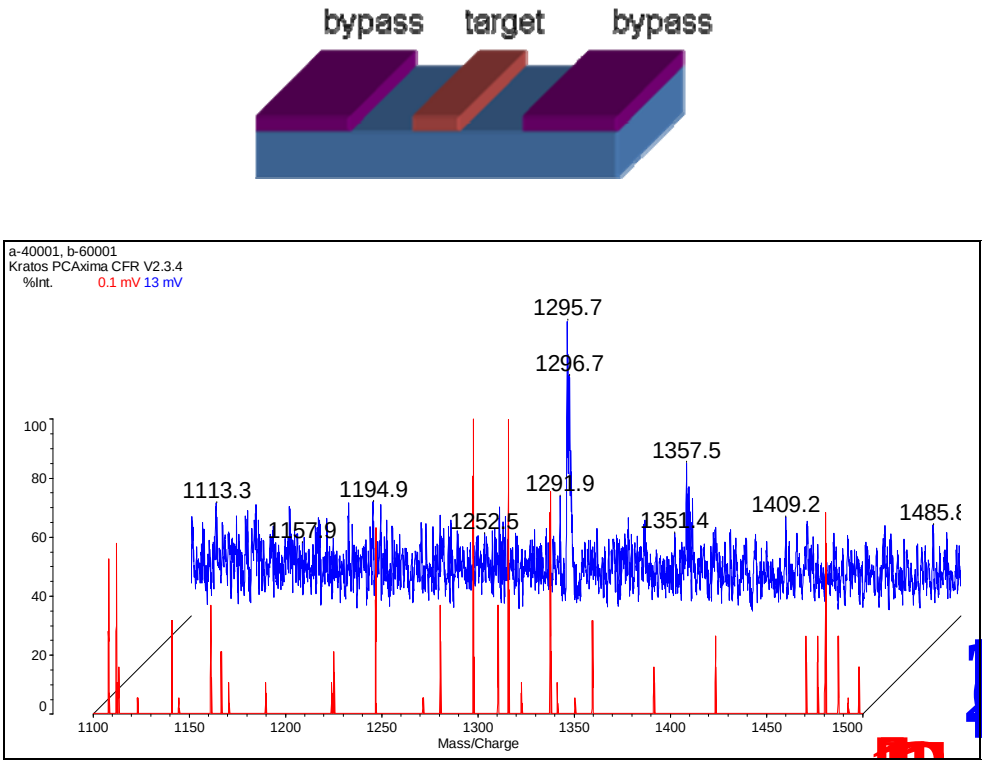

Figure 6-9 Concentrated method improved the detect sensitivity compared with non-concentrated method.

6.4 Mass Spectrometry Analysis on Point-structured Concentrator

6.4.1 Fabrication of Point-Structured Concentrator

The line-structured concentrator only provided one-dimensional concentration, resulting in the sample deposited in a narrow but long (around 500μm) linear area. To improve the concentration effect, a round pad (or called as point-structured) concentrator was fabricated to achieve two-dimensional concentration.

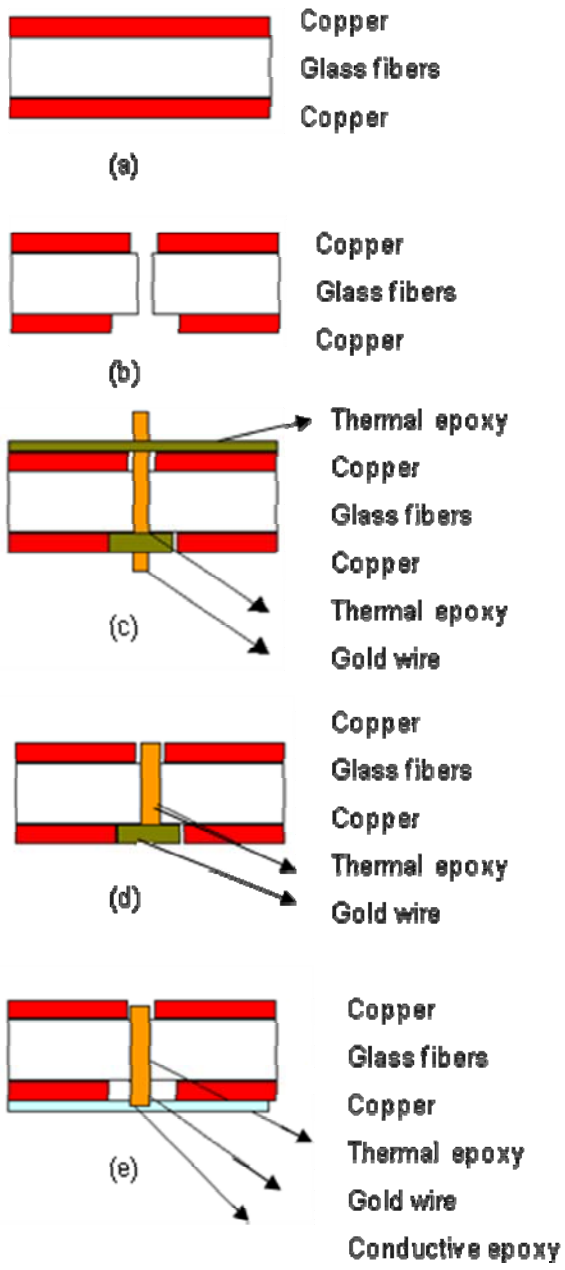

Figure 6-10 Schematic of fabrication process of point-structured concentrator

The fabrication of the point-structured concentrator started with a 1.7mm thick double-side PCB board, shown in Figure 6-10 (a). A series of Φ2mm holes 100μm in thickness was drilled with a CNC milling machine from its backside with 5mm spacing. On the

front side, a series of Φ1mm holes 100μm in thickness was drilled with the alignment to the backside holes. Then a series of Φ200μm through-holes were centered in the Φ1mm holes, shown in Figure 6-10 (b). After drilling these holes, a section of gold wire that was coated by PTFE (i.d. 75μm, o.d. 200μm) was inserted into each drill-through hole. The wires were fixed in position by thermal epoxy after cured at 85 °C for 2 hours (Figure 6-10 (c)). Both sides of copper surface were mechanically polished to expose the gold wire, as demonstrated in Figure 6-10 (d). The final step was to coat the backside with a thin layer of electrically conductive epoxy followed by curing at 80°C for 2 hours (Figure 6-10 (e)).

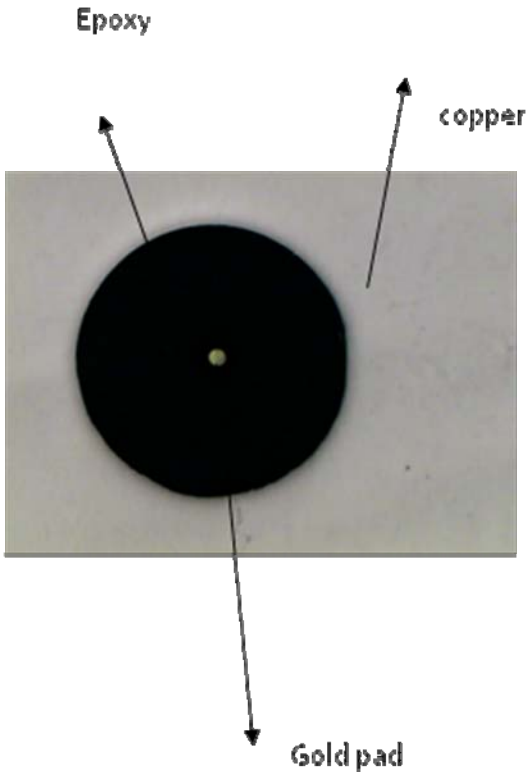

Figure 6-11 Microphotograph of a typical point-structured concentrator

The typical topography of a concentrator is demonstrated in Figure 6-11. In the center, the shining circle is the gold wire. The dark is thermal epoxy coating and the outside range was copper. The diameter of the dark epoxy was about 1mm and the resulted space between the gold wire and the copper was nearly 500 μm.

6.4.2 Mass Spectrometry Analysis by Point-structured Concentrator

The experiment setup is similar to that described in section 6.3.3. After optical and electrical examination, the desired amount of the sample was deposited on the selected point/pad by applying by-pass voltage and electrospray voltage on the by-pass area and the electrospray source, respectively. The typical electrospray voltage was around 1500~2000V and the by-pass voltage was around 600~700V. The typical measured current was in the range of 20~100 nA.

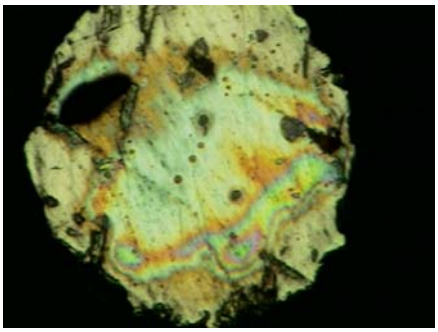

Figure 6-12 Microphotograph of a typical pad with deposited sample

Also, from microscope observation, there was sample deposited on the pad after electrospray, shown in Figure 6-12. In this figure, some dark area showed the scratching due to mechanical polishing.

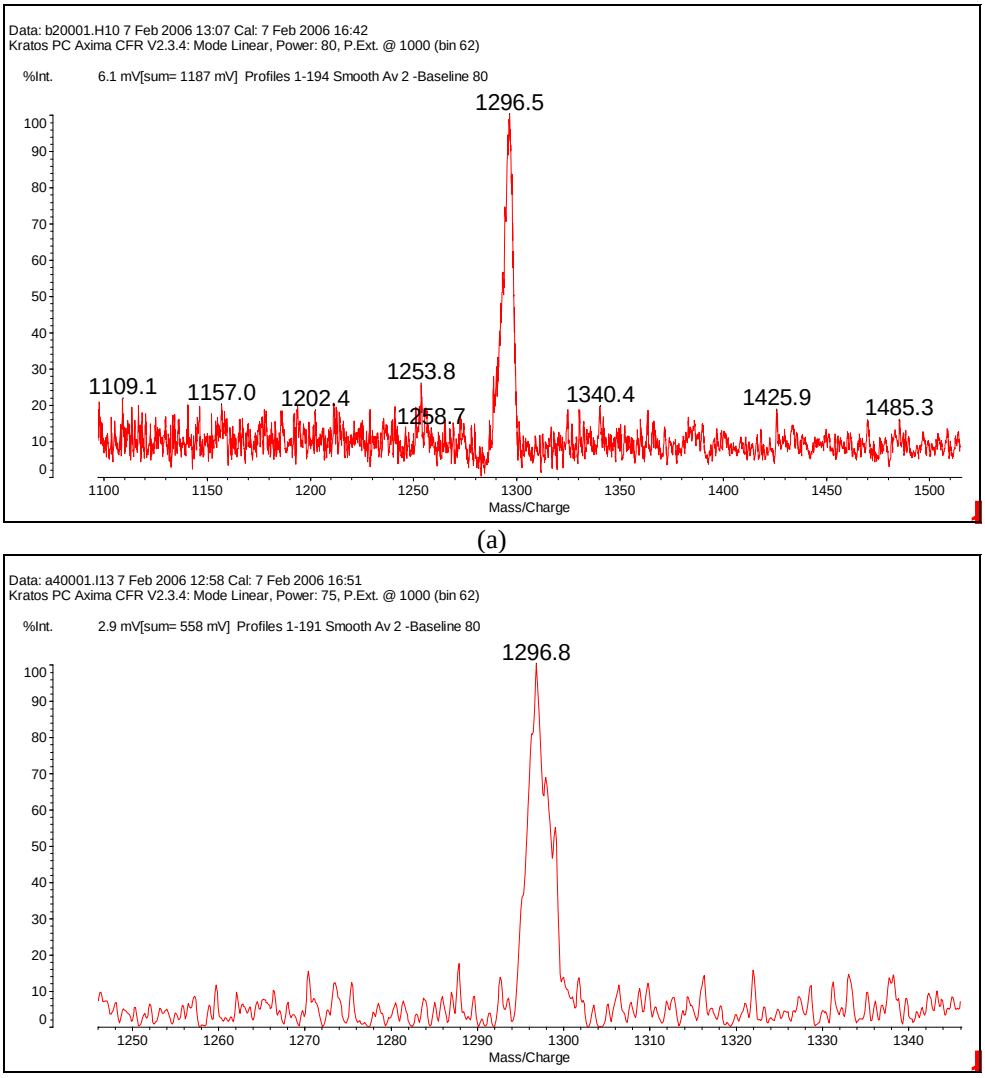

Figure 6-13 MS analysis of low-abundance sample prepared by point-structured method (a) 100amol; (b) 50 amol.

For low-abundance sample, the signal-to-noise ratio decreases as the concentration decreases, as shown in Figure 6-13. There are two possible factors that affected the concentration effect. First, the optical scheme in MALDI MS works for the standard steel plate, but it does not fit for the concentrator. The tilted surface of the gold pad caused the difference in light intensity. This tilt problem is likely due to surface polishing. As shown

in Figure 6-14, 2X objective embedded camera in MALDI MS made the light spot alignment with the gold pad very difficult. Some solutions to this problem include, using another method to get a flat surface; or changing the optical path in MALDI. Further research will explore a new fabrication method.

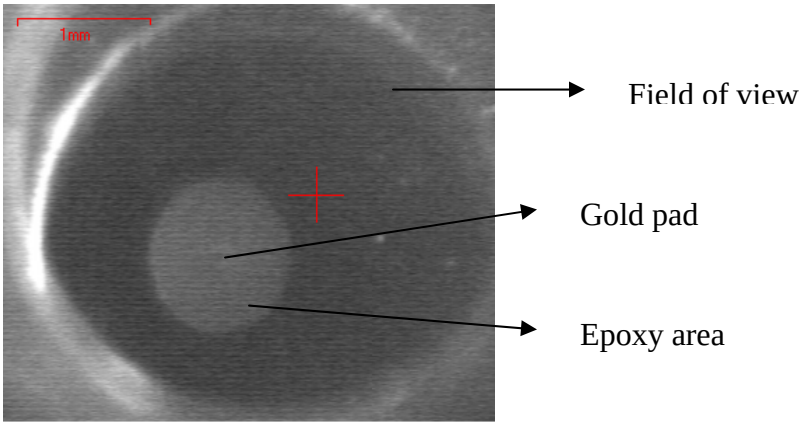

Figure 6-14 Microphotograph taken by the embedded camera in MALDI-MS

Another problem came from the misalignment of the electrospray source and the gold pad. As demonstrated in the FEMLAB simulation, with low concentration, the monolayer size will be small, thus the misalignment effect will be worse than that case in line-structure. Also, due to the electric field in the epoxy area, some sample could be deposited on the epoxy area, further reducing the amount deposited on the gold pad. A more precise experimental setup is required to obtain the entire sample located on the gold pad to increase the effective sample amount.

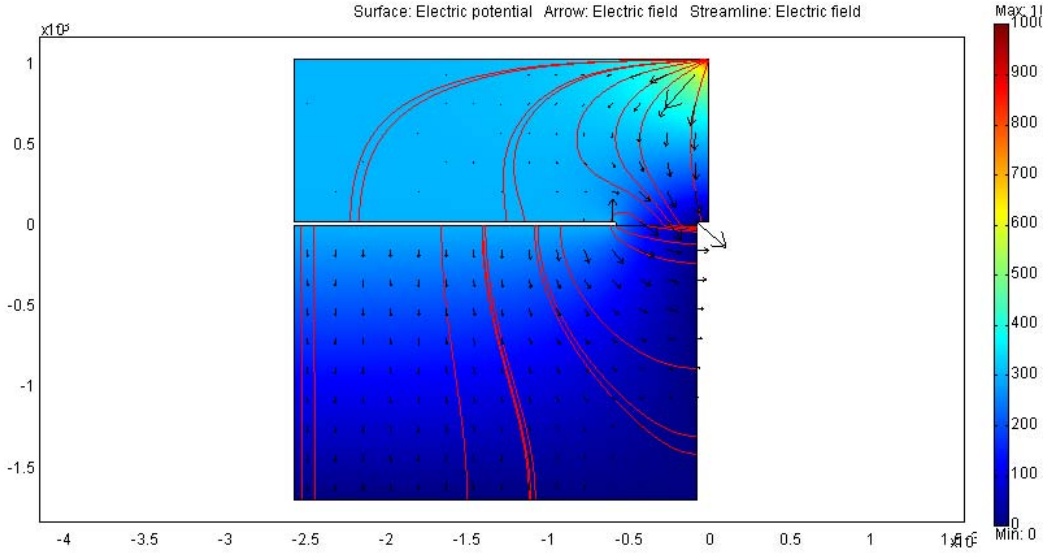
Surface: Electric potential Arrow: Electric field Streamline: Electric field
x10^5
1
0.5
0
-0.5
-1
-1.5
-4
-3.5
-3
-2.5
-2
-1.5
-1
-0.5
0
0.5
1
Max: 1
900
800
700
600
500
400
300
200
100
0
Min: 0

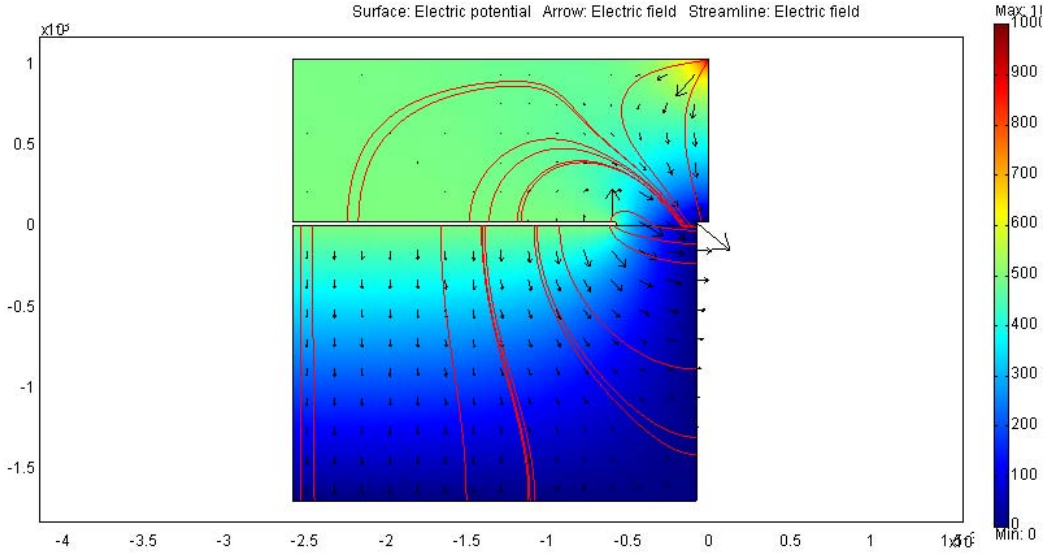
Surface: Electric potential Arrow: Electric field Streamline: Electric field
x10^5
1
0.5
0
-0.5
-1
-1.5
-4
-3.5
-3
-2.5
-2
-1.5
-1
-0.5
0
0.5
1
Max: 1
900
800
700
600
500
400
300
200
100
0
Min: 0

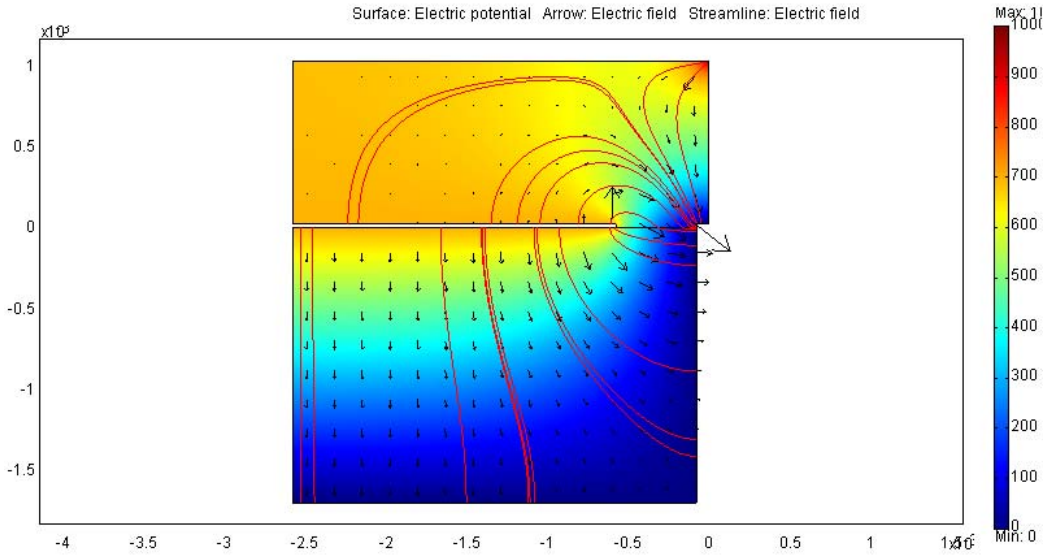

Figure 6-15 Varying by-pass voltage effect on the point-structured concentrator. From top to bottom, the by-pass voltages are 300V, 500V, and 700V respectively while the electrospray voltage is 1000V.

Considering that the point-structured was fabricated on a double-side PCB board and the thickness of glass clothes inside was only 1.7mm, the modified model was simulated as the results shown in Figure 6-15. There is certain electric field leaking into the PCB so that the focusing effect was weakened. It appeared that the by-pass voltage should be increased compared with the line-structure to achieve the same concentration in one-dimension.

6.5 Middle Cross Field Focusing Model

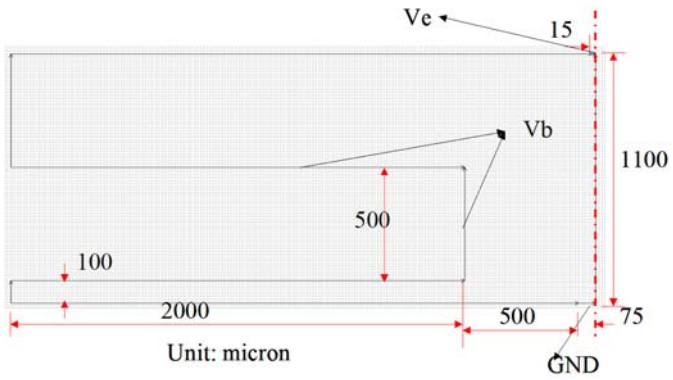

Figure 6-16 Middle Cross Field Focusing Model

To improve the efficiency of the focusing effect, another method, the middle cross field focusing method, was demonstrated by numerical simulations. Unlike the horizontal cross field focusing model, this model describes a configuration that the by-pass area is located between the electrospray source and the grounded target pad, as shown in Figure 6-16. A 500μm thick conductive metal sat on the top of the target surface with a high dielectric constant material as its base. Varying by-pass voltages were applied to this configuration.

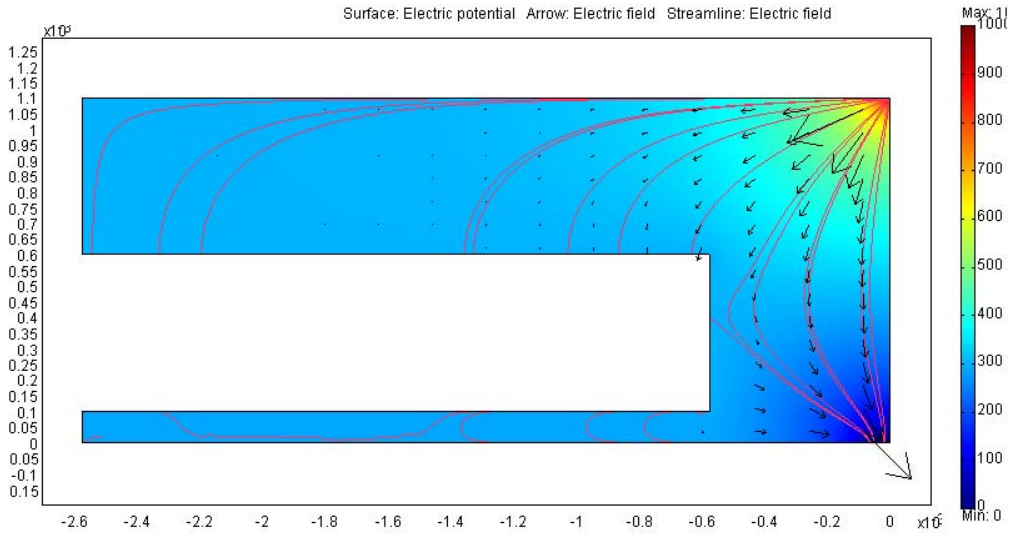
Surface: Electric potential Arrow: Electric field Streamline: Electric field
x10³
1.25
1.2
1.15
1.1
1.05
1
0.95
0.9
0.85
0.8
0.75
0.7
0.65
0.6
0.55
0.5
0.45
0.4
0.35
0.3
0.25
0.2
0.15
0.1
0.05
0
0.05
-0.1
0.15
-2.6 -2.4 -2.2 -2 -1.8 -1.6 -1.4 -1.2 -1 -0.8 -0.6 -0.4 -0.2 0
x10⁻⁶
Max: 1
1000
900
800
700
600
500
400
300
200
100
0
Min: 0

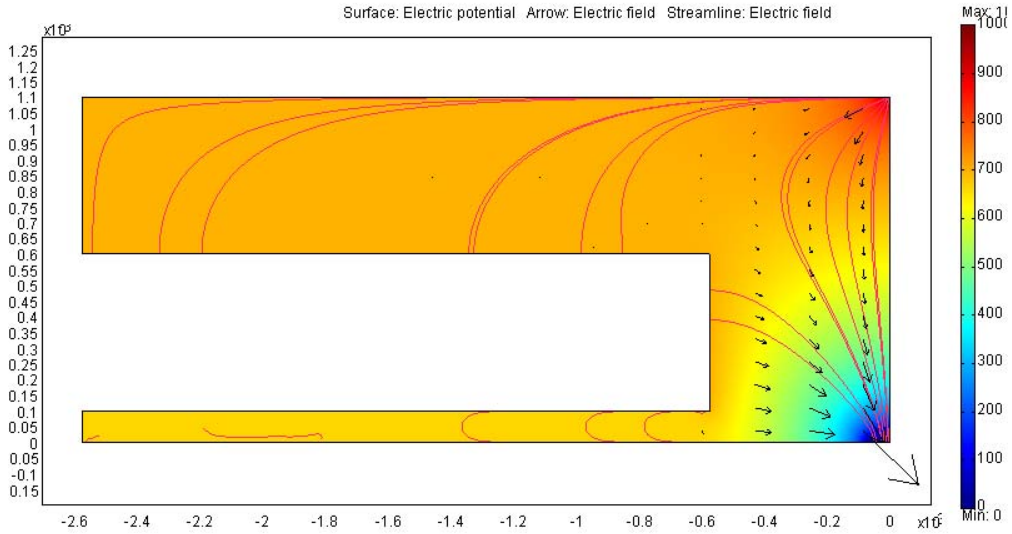
Surface: Electric potential Arrow: Electric field Streamline: Electric field
x10³
1.25
1.2
1.15
1.1
1.05
1
0.95
0.9
0.85
0.8
0.75
0.7
0.65
0.6
0.55
0.5
0.45
0.4
0.35
0.3
0.25
0.2
0.15
0.1
0.05
0
0.05
-0.1
0.15
-2.6 -2.4 -2.2 -2 -1.8 -1.6 -1.4 -1.2 -1 -0.8 -0.6 -0.4 -0.2 0
x10⁻⁶
Max: 1
1000
900
800
700
600
500
400
300
200
100
0
Min: 0

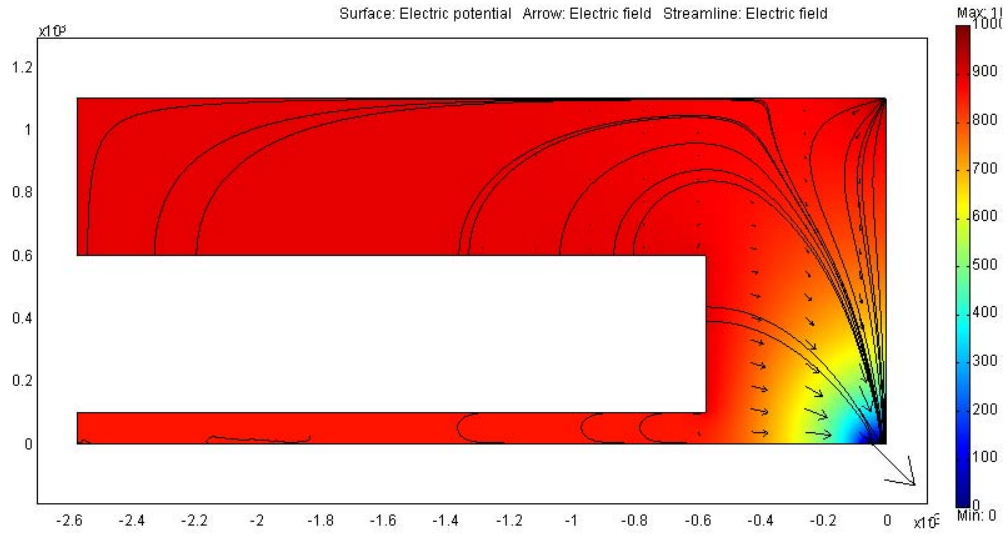

Figure 6-17 Varying by-pass voltages effect on middle cross-field focusing model; from top to bottom the by-pass voltages were 300V, 700V and 900V respectively, while the electrospray voltage is 1000V.

Figure 6-17 demonstrates the FEMLAB simulation results of varying by-pass voltage from 300V to 900V on the middle cross-field focusing model. Clearly, with higher by-pass voltage, the electric field from the electrospray source to the grounded plate was better-refined.

Table 6-1 Focusing area radius for two model using different by-pass voltage

	Horizontal Cross-field model	Middle cross-field model
By-Pass voltage (V)	Focusing area radius (um)	Focusing area radius (um)
100	N/A	84
300	>75*	68
500	72	53
700	52	36
900	31	15

*The radius was limited by the target geometry, not by the electric field

The focusing area of the electric field coming from the electrospray source can also be roughly measured by analyzing the FEMLAB simulation results. As listed in Table 6-1, the middle cross-field focusing method can achieve higher concentration than that predicted by the horizontal cross-field model. It also offers the theoretical proof that higher concentration may be achieved by inserting a by-pass ring in between the electrospray source and the grounded target.

6.6 Conclusions

This chapter explored the use of a pre-structured MALDI target to improve the homogeneity of the sample by reducing the size of deposited sample. Simply shortening the distance between the electrospray tip and the counterelectrode can not generate stable spray performance. Therefore, a new method, using the cross-field to confine the electric field from the electrospray source to the grounded target, was proposed and verified by FEMLAB simulations. The numerical simulations showed that as by-pass voltage (or horizontal electric field) increases, more confinement on the vertical electric field resulted in a better focusing effect, leading to smaller size of sample deposited by the electrospray method.

Based on the simulation of the horizontal cross-field focusing model, a line-type prestructured MALDI target, in which an isolated line created by CNC milling on PCB board, demonstrated improved MALDI MS data sensitivity for low abundant sample, i.e., low to 1fmol. Meanwhile using electrospray deposition on a standard steel plate can only detect >10 fmol sample at the same conditions. The point-structured target, which utilized 2-dimensional focusing instead of 1-dimensioanl focusing on the line-type prestructured

target, was fabricated by embedding gold wire in PCB board to obtain the isolated conductive pad. The resulted MALDI-MS data showed that using this method, low to 50 amol sample can be detected. However, due to poor compatibility between the present MALDI instrument and our customized target, some limitations from the instrument also constrained higher detection capacity and high single-to-noise ratio, which is addressed in detailed.

To further explore the prestructured target, a middle cross-field focusing model was proposed, offering higher concentration effect in theoretical design. It gave the potential direction to further improve the concentration effect and achieve high detection sensitivity.

Chapter 7 Conclusions and Future Work

7.1 Conclusions

The presented polymer microfabrication method involved template fabrication, hot embossing and different bonding techniques such as thermal bonding, solvent bonding and so on, as well as macro-to-micro integration. Due to low cost, polymer substrates with simple fabrication techniques facilitate mass production of disposable microfluidic devices. Several polymer materials were used in this study to form microfluidic networks, including PC, PMMA, PDMS, COC etc. Also different machining methods such as CNC milling and low speed sawing were explored.

An electrospray tip on a polymer-based microfluidic device was designed to interface to the online ESI-MS or the off-line MALDI-MS. This technique utilizes the high hydrophobicity of porous membrane to prevent fluid from spreading along the flat surface and has demonstrated good electrospray performance. Several different membranes and bonding techniques were considered according to their properties, and the final winner was PTFE membrane with 70% porosity and 0.22 μm pore size thermally bonded to the flat surface of PC or COC chip. The characterization of a single-channel electrospray tip was further investigated to understand the electrospray principle. The main application of this electrospray tip was to deposit protein/peptide sample on a

stainless steel plate followed by MALDI-MS. Electrospray deposition method improves the homogeneity of the deposited sample, and reduces the size of the deposition to further increase the local density of sample spot resulting in higher sensitivity.

Utilizing a similar principle, a multi-channel electrospray tip array was explored for future parallel analysis. The challenge in multi-channel electrospray tip array was to standardize flow resistances for all channels. This proved difficult for multiple reasons such as varying channel exit shapes due to mechanical milling, different pore collapse of porous membrane due to the heat and pressure during the thermal bonding, uniformity due to fabrication process (e.g., hot embossing, thermal bonding) etc. Efforts were made to optimize the mechanical milling and membrane bonding. A novel method, referred to as embedded capillary method, was first applied to reduce the debris clogging the channel exit during the mechanical milling and sawing utilizing different material properties of fused silica capillary and polymer. This method combined with the optimized milling and membrane bonding technique shows promising potential for parallel analysis, such as coupling high throughput multiplexed separations to MS.

A gel electrophoresis microfluidic network was designed to couple with MALDI-MS via electrospray interface. Denatrured protein-SDS complexes can be separated by the sieving mechanism of gel electrophoresis according to different m/z ratio. Following with MALDI-MS can further improve the sensitivity and resolution of the whole system, which can be used as an alternative technique to two-dimensional SDS PAGE. Replaceable gel solution, especially PEO, was first considered in this project due to good separation performance demonstrated in other groups. Although PEO gel showed some

results, band broadening due to hydrodynamic force in the system and lack of sample pre-concentration prior to the separation step resulted in poor separation. Hence, highly cross-linked gel was used instead, photopatterned in-situ in the desired area. Functionalization of the polymer surface and corresponding surface chemistry were studied in this work. Cross-linked polyacrylamide gel was covalently bonded to the sidewalls of polymer microfluidics after surface treatment of the inside channels. First, polyacrylamide gel was manufactured in a PDMS microchannel to test the gel chemistry and performance. Using the same technique, 8% (%T) polyacrylamide gel was formed in the separation channel in COC chips and acted as separation medium. PC/PMMA chips were found unfit for photografting and photoiniated polymerization due to their poor transmission in the UV range. Further protein separation can be calibrated using the gel electrophoresis in COC chips.

In the optimization of electrospray technology interfaced to MALDI-MS, reducing the tip-to-counterelectrode spacing in electrospray minimized the size of the deposited sample spot, about 550 μm in diameter with 1mm in tip-to-counterelectrode spacing, resulting in an increase in the local density of sample. However, further reducing the spacing down to 450 μm caused instability of electrospray performance, since a large amount of residues remained on the surface of the target, eventually interrupting the continuous electrospraying. Another strategy to improve the sensitivity of low-abundance sample is to use electric field to focus the charged molecules on a small size due to electrophoretic movement of charged molecules. Different by-pass voltages and misalignment for line structure and pointed structure effect on the sample size have been

demonstrated by FEMLAB simulation. A line structure target was fabricated on a PCB board by CNC milling. The lower limit of detection of 10 fmol peptide can be achieved by air-dried method. Using the line structure (or 1-dimensional focusing) can detect low to 1 fmol peptide. The fabrication of pointed-structure (or 2-dimensional focusing) involved inserting a gold wire into the PCB board fixed with epoxy and the following mechanical polishing. Using this customized target, a low-abundance sample down to 50amol sample can be detected. The limitations to this design were also addressed. A new method, the middle cross field focusing model, was proposed with demonstrated FEMLAB simulation. The results showed an improvement in further reducing the deposition size and offered the potential to achieve higher concentration of sample and better detection limit.

7.2 Contributions

Polymer-based microfluidics have a major impact on a range of bioanalytical instrument, in particular for protein analysis, an area of critical interest to biotechnology and pharmaceutical companies interested in the identification of biomarkers, new diagnostic tools, and drug development. The literature provides only a few examples of how to successfully couple standard capillary CGE with mass spectrometry, and essentially no insight into the specific challenges involved in coupling μCGE to MS. Thus the demonstration of this capability contributes uniquely to an economically- and societally-important area of research.

The significant contributions from the dissertation research include:

- Development of novel ultra-rapid plastic microfluidic device fabrication technology
- Development of a low-cost microfluidic ESI source based on porous polymer membranes capable of providing stable electrospray at flow rate below 10 nL/min
- Demonstration of a multichannel microfluidic ESI array capable of simultaneous electrospray from channels spaced less than 200 μm apart, capable of high-throughput and parallel deposition of biomolecules onto a MALDI target plate.
- Development of a microchannel gel electrophoresis separation system coupled with mass spectrometry via electrospray interface; Replaceable and cross-linked gel both are explored in polymer-based microfluidics.
- Development of a novel concentration method for MALDI-MS, further improving the performance of electrospray prepared method by using the electric field focusing effect, capable of the detection of low abundance sample below 100 amol.

7.3 Future Work

The remaining research involves optimization of protein separations via cross-linked polyacrylamide gel electrophoresis and further optimization of multichannel electrospray tips for multiplexed analysis from a single microfluidic chip which multiplexed MGE coupled with MALDI-MS. Specific goals for each direction are described in the following.

7.3.1 Microchannel Gel Electrophoresis System

The microchannel gel electrophoresis device should be further investigated for optimizing several key performance criteria, namely:

1. Model proteins separation calibration

Using the optimizing gel system, several model proteins will be used as analytes to calibrate the sensitivity and resolution of the device by on-chip fluorescence detection. The movements of model proteins should be monitored. Specific phenomena including differential mobility stacking during protein plug injection and band broadening during separation should be investigated in detail.

2. Demonstration of μCG-ES coupled to MALDI-MS

On-chip separated model proteins should be delivered to an electrospray tip to deposit the separated bands onto a MALDI target so that off-line MALDI mass spectral analysis can be performed. Before MALDI optimization, single channel ESI-MS from the μGE-ES should be characterized to determine the optimal flow rate and working voltage.

In addition, other techniques combination such as IEF coupled to MS etc, also can apply the same microfluidics technology via the electrospray interface.

7.3.2 Electropsray Tip Arrays

The μCG-ES system results in two fundamental contributions to the field of microfluidic bioanalytical technology. The first contribution is the integration of μCG with ES in a single integrated chip. The second contribution lies in the polymer membrane

electrospray technology. This fundamentally new approach of electrospray ionization or deposition enables the development of electrospray tip arrays that may be used for multiplexed analysis. This dissertation research addresses the optimization of multichannel electrospray tips for coupling high throughput multiplexed separations to MS. Future work should further explore the potential of coupling multiplexed separation to MALDI-MS via multiplexed electrospray tip array.

Other sample preparation techniques can be integrated with MS by the interface of multiplexed electrospray tip array. For example, the hydrophobic PTFE membrane showed the ability to absorb Trypsin due to hydrophobic interaction. Combined with multiplexed electrospray tip array technology, on-line protein digestion can be integrated with MS without cross-contamination. Further work should further explore the potential of the integration of other sample preparation techniques with MS

Bibliography

1. Smith, R.D., “Advanced Mass Spectrometric Methods for the Rapid and Quantitative Characterization of Proteomes”, *Comparative and Functional Genomics* **2002**, 3, 143-150

2. Shen, Y., Toli, N., Masselon, C., Smith, R. D. et al, “ Nanoscale Proteomics”, *Analytical and Bioanalytical Chemistry* **2003**, 378 (4), 1037-1045

3. Eriksson, J. and Fenyo, D, “Protein Identification in Complex Mixtures”, *Journal of Proteome Research* **2005**, 4, 387-393

4. Anderson, N.L and Anderson, N. G., “The Human Plasma Proteome: History, Character, and Diagnostic Prospects”, *Molecular and Cellular Proteomics* **2002**, 1 (11), 845- 867

5. Raymond, S. and Weintraub, L., “Acrylamide Gel as a Supporting Medium for Zone Electrophoresis”, *Science* **1959**, 130, 3377, 711

6. Shapiro, A. L., Vinuela and E., Maizel. J.V., “Molecular Weight Estimation of Polypeptide Chains by Electrophoresis in SDS-polyacrylamide Gels”, *Biochemical Biophysics Research Communication* **1967**, **28**(5), 815–820

7. Laemmli, U. K., “Cleavage of Structural Proteins During the Assembly of the Head of Bacteriophage T4”, *Nature* **1970**,2227(5259), 680-685

8. O’Farrell, P.H., “Separation Techniques Based on the Opposite of Two Counteracting Forces to Produce a Dynamic Equilibrium”, *Science* **1985**, 227, 1586-1589

9. Gygi, S.P., Corthals, G.L., Zhang, Y., Rochon, Y. and Aebersold, R., “Evualation of two-dimensional gel electrophoresis-based proteome analysis technology”, *Proceedings of the National Academy of Sciences of the United States of America* **2000**, 97(17), 9390-9395

10. Olivares, J. A., Nguyen, N. T., Yonker, C. R. and Smith, R. D.,“ On-line Mass Spectrometric Detection for Capillary Zone Electrophoresis”, *Analytical Chemistry* **1987**, 59, 1230-1232

11. Manz, A., Garber, N. and Widmer, H. M., " Miniaturized Total Chemical Analyses Systems. A Novel Concept For Chemical Sensing", *Sense and Actuator B: Chemistry* **1990**, 1, 244-248

12. Figeys, D. and Pinto, D., "Protomics on a Chip: Promising Development", *Electrophoresis* **2001**, 22, 208-216

13. Lion, N., Rohnear, T.C., Dayon, L., Arnaud, I.L. et al., "Microfluidic Systems in Proteomics", *Electrophoresis* **2003**, 24, 3533-3562

14. Marko-Varga, G., Nilsson and J., Laurell, T., "New Directions of Miniaturization within the Biomarker Research Area", *Electrophoresis* **2004**, 25, 3479-3491

15. Loo, J.A., Udseth, H.R and Smith, R, D., "Peptides and Proteins Analysis by Electrospray Ionization-Mass Spectrometry and Capillary Electrophoresis- Mass Spectrometry", *Analytical Biochemistry* **1989**, 179(2), 404-412

16. Nordhoff, E., Kirpekar, F. and Roepstorff, P., " Mass Spectrometry of Nucleic Acids", *Mass Spectrometry Review* **1997**, 15, 67-138

17. Limbach, P.A., "Indirect Mass Spectrometric Methods for Characterizating and Sequencing Oligonucleotide", *Mass Spectrometry Review*, **1997**, 15, 297-336

18. Huber, C.G. and Oberacher, H. "Analysis of Nucleic Acids by On-line Liquid Chromatography Mass Spectrometry", *Mass Spectrometry Review* **2001**, 20: 310-343

19. Li, J., Thibault, P., Bings, N. H., Skinner, C., D., Wang, C., Colyer, C. and Harrison, J., "Integration of Microfabricated Devices to Capillary Electrophoresis-Electrospray Mass Spectrometry Using a Low Dead Volume Connection: Application to Rapid Analysis of Proteolytic Digests", *Analytical Chemistry* **1999**, 71, 3036-3045

20. Kameoka, J., Oath, R., Ilic, B., Czaplewski, D., Wachs, T. and Craighead, H.G., "An Electrospray Ionization Source for Integration with Microfluidics", *Analytical Chemistry* **2002**, 77, 5897-5901

21. Xue, Q., Foret, F., Dunayevskiy, Y.M., Zavracky, P. M., McGruer, N. E. and Karger, B. L., "Multichannel Microchip Electrospray Mass Spectrometry", *Analytical Chemistry* **1997**, 69, 426-430

22. Ramsey, R. S. and Ramsey, J. M., "Generating Electrospray from Microchip Devices Using Electroosmotic Pumping", *Analytical Chemistry* **1997**, 69, 1174-1178

23. Huikko, K., Ostman, P., Grigoras, K., Tuomikoski, S., Tiainen,V. M., Soininen, A., Puolanne, K., Manz, A., Franssia, S., Kostiainen, R. and Kotiaho, T., "Poly (dimethylsiloxane) Electrospray Devices Fabricated with Diamond-like Carbon-Poly(dimethylsiloxane) Coated Su-8 Masters", *Lab on A Chip* **2003**, 3, 67-72

24. Desai, A., Tai, Y., Davis, M. T. and Lee, T. D., "A MEMS Electrospray Nozzle for Mass Spectroscopy", in *International Conference on Solid State Sensors and Actuators* **1997**, 927-930

25. Tang, K., Lin, Y., Matson, D. W., Kim, T. and Smith, R. D., "Generation of Multiple Electrosprays Using Microfabricated Emitter Arrays for Improved Mass Spectrometry Sensitivity", *Analytical Chemistry* **2001**,73, 1658-1663

26. Schultz, G. A., Corso, T. N., Prosser, S. J. and Zhang, S., " A Fully Integrated Monolithic Microchip Electrospray Devices for Mass Spectrometry", *Analytical Chemistry* **2002**, 72, 4058-4063

27. Wen, J., Lin, Y., Xiang, F., Matson, D. W., Udseth, H. R., Smith, R. D., "Microfabricated Isoelectric Focusing Devices for Direct Electrospray Ionization-Mass Spectrometry", *Electrophoresis* **2000**, 21,191-197

28. Rohner, T.C., Rossier, J. S. and Girault, H. H., " Polymer Microspray with an Integrated Thick-film Microelectrode", *Analytical Chemistry* **2001**, 73, 5353-5357

29. Gobry, V., van Oostrum, J., Martinelli, M., Rohner, T., Rossier, J.S. and Girault, H.H., "Microfabricated Polymer Injector for Direct Mass Spectrometry Coupling", *Proteomics* **2002**, 2, 405-412

30. Deng, Y., Henion, J., Li, J., Thibault, P., Wang, C. and Harrison, D. J., "Chip-based Capillary Electrophoresis/Mass Sepctrometry Determination of Carnitines in Human Urine", *Analytical Chemistry* **2001**, 73, 639-646

31. Kameoka, J., Craighead, H.G., Zhang, H.W. and Henion, J., "A Polymeric Microfluidic Chip for CE/MS Determination of Small Molecules", *Analytical Chemistry* **2001**, 73, 1935-1941

32. Deng, Y. Z., Zhang, N. W. and Henion, J., " Chip-based Quantitative Capillary Electrophoresis /Mass Spectrometry Determination of Drugs in Human Plasma", *Analytical Chemistry* **2001**, 73, 1432-1439

33. Li, J., Wang, C., Kelly, J. F., Harrison, D. J. and Thibault, P., "Rapid and Sensitive Separation of Trace Level Protein Digests Using Microfabicated Devices Coupled to a Quadrupole-time-of-flight Mass Spectrometry", *Electrophoresis* **2000**, 21, 198-210

34. Zhang, B., Liu, H., Harger, B.L. and Foret, F., "Microfabricated Devices for Capillary Electrophoresis-electrospray Mass Spectrometry", *Analytical Chemistry* **1999**, 71, 3258-3264

35. Lazar, I. M., Ramsey, R. S., Jacobson, S. C., Foote, R. S. and Ramsey, J. M., "Novel Microfabricated Device for Electrokinetically Induced Pressure Flow and Electrospray Ionization Mass Spectrometry", *Journal of Chromatography A* **2000**, 892, 195-201

36. Zhang, B., Foret, F. and Karger, B. L., "A Microdevice with Integrated Liquid Junction for Facile Peptide and Protein Analysis by Capillary Electrophoresis/ Electrospray Mass Spectrometry", *Analytical Chemistry* **2000**, 72,1015-1022

37. Li, J., Kelly, J. F., Chernushevich, I., Harrison, D. J. and Thibault, P., " Separation and Identification of Peptides from Gel-Isolated Membrane Proteins Using a Microgavricated Device for Combined Capillary Electrophoresis/ Nanoelectrospray Mass Spectrometry", *Analytical Chemistry* **2000**, 72, 599-609

38. Karas, M., Bachmann, D. and Hillenkamp, F., "Influence of the Wavelength in High-Irradiance Ultraviolet Laser Desorption Mass Spectrometry of Organic Molecules", *Analytical Chemistry* **1985**, 57, 2935-2939

39. Karas, M. and Bahr, U., “Laser Desorption Ionization Mass Spectrometry of Large Biomolecules”, *Trends in Analytical Chemistry* **1990**, *9*, 321-325.

40. Devoe, D. L. and Lee, C. S., “Microfluidic Technologies for MALDI-MS in Proteomics”, *Electrophoresis* **2006**, 27, 3559-3568

41. Karas, M. and Hillenkamp, F., “Laser Desorption Ionization of Proteins with Molecular Masses Exceeding 10,000 Daltons”, *Analytical Chemistry* **1988**, 60, 2299-2301

42. Weinberger, S.R., Boernsen, K.O., Finchy, J.W., Roberstson, V. and Musselman, B.D., *Proceedings of the 41th Annual ASMS Conference on Mass Spectrometry and Allied Topics*, **1993,** San Francisco, May 31-June 5, 775a.

43. Vorm, O., Roepstorff, P. and Mann, M., "Improved Resolution and Very High Sensitivity in MALDI TOF of Matrix Surfaces Made by Fast Evaporation", *Analytical Chemistry* **1994**, 66, 3281-3287

44. Nicola, A., Gusev, A.I., Proctor, A., Jackson, E. K. and Hercules, D. M., "Application of the Fast-evaporation Sample Preparation Method for Improving Quantification of Angiotensin II by MALDI", *Rapid Communication on Mass Spectrometry* **1995**, 9,1164-1171

45. Dai, Y.Q., Whittal, R.M. and Li, L., "Two-Layer Sample Preparation: an Effective Method for MALDI-MS Analysis of Complex Peptide and Protein Mixtures", *Analytical Chemistry* **1999**, 71, 1087-1091.

46. Zheng, J., Li, N., Ridyard, M., Dai, H., Robbins, S. M. and Li, L., “Simple and Robust Two-layer Matrix/Sample Preparation Method for MALDI MS/MS Analysis of Peptides’, *Journal of Proteome Research* **2005**, 4, 1709-1716

47. Strupat, K., Karas, M. and Hillenkamp, F., "2, 5-Dihydroxybenzoic acid: a new matrix for laser desorption-ionization mass spectrometry", *Int. J. Mass Spectrom. Ion. Proc.* **1991**, 111, 89-102

48. Perera, I. K., Perkins, J. and Kantartzoglou, S., “Spin-coated Samples for High Resolution Matrix Assisted Laser Desorption/Ionization Time-of-Flight Mass Spectrometry”, *Rapid Communication on Mass Spectrometry* **1995**, 9, 180-187

49. Hensel, R.R., King, R.C. and Owens, K.G., "Electrospray Sample Preparation for Improved Quantitation in MALDI TOF MS", *Rapid Communication on Mass Spectrometry* **1997**, 11,1785-1793

50. Hanton, S., Clark, P. and Owens, K., "Investigations of MALDI Sample Preparation by TOF SIMS", *J. Am. Soc. Mass Spectrom.* **1999**, 10,104-111

51. Axelsson, J., Hoberg, A-M. , Waterson, C., Myatt, P., Chield, G.L., Varney, J., Haddleton, D.M. and Derrick, J., "Improved Reproducibility and Increased Signal Intensity in MALDI as a Result of Electrospray Sample Preparation", *Rapid Communication on Mass Spectrometry* **1997**, 11, 209-21

52. Kochiling, H.J. and Biemannn, K., “Novel Sample Preparation for MALDI”, P*roceedings of the 43rd Annual ASMS Conference on Mass Spectrometry and Allied Topics: Atlanta*, **1995,** *GA*, May21-26, 1225

53. Schuerenberg, M., Luebbert, C., Eickhoff, H., Kalkum, M. et al, “Prestructured MALDI-MS Sample Support”, *Analytical Chemistry* **2000**, 72, 3436-3442

54. Redeby, T., Roeraade, J. an dEmmer, A., “Simple Fabriation of a Structured Matrix-assisted Laser Desorption/Ionization Target Coating for Increased Sensitivity in Mass Spectrometric Analysis of Membrane Proteins”, *Rapid Communication on Mass Spectrometry* **2004**, 8, 1161-1166

55. Xiong S., Ding, Q., Zhao, Z., Liu, S. et al, “ A New Method to Improve Sensitivity and Resolution in Matrix-Assisted Laser Desorption/ Ionization Time of Flight Mass Spectrometry”, *Proteomics* **2003**,2,265-272

56. Gundry, R.L., Edward, R., Kole, T.P., Sutton, C. an dCotter, R., “ Disposable Hydrophobic Surface on MALDI Targets for Enhancing MS and MS/MS Data of Peptide”, *Analytical Chemistry* **2005**, 77,6609-6617

57. Muscate-Magnussen, A., Rohl, H., Pickartz, J., Zhu, X. et al, "A New Approach of Liquid Sample Handling on MALDI Plates Enabling Advanced High Throughput Proteomics Applications", *52nd ASMS Conference*, **2004,** Nashville, TN

58. Little, D.P., Cornish, T.J., O'Donnell, M.J., Braun, A. et al., "MAIDI on a Chip: Analysis of Arrays of Low-Femtomole to Subfemtomole Quantities of Synthetic Oligonucleotides and DNA Diagnostic Products Dispensed by a Piezoelectric Pipet", *Analytical Chemistry* **1997**, 69, 4540-4546

59. Ekstrom, S., Ericsson, D., Onnerfjord, P., Bebgtsson, M. et al., " Signal Amplification Using "Spot-on-a-Chip" Technology for the Identification of Proteins via MALDI-TOF MS", *Analytical Chemistry* **2001**, 73, 214-219

60. Ekstrom, S., Nilsson, J., Helldin, G., Laurell, T. and Marko-Varga, G., " Integrated Selective Enrichment Target--a Microtechnology Platform for Matrix-assisted Laser Desorption/Ionization-Mass Spectrometry Applied on Poretin biomarkers in Prostate Diseases", *Electrophoresis* **2004**, 25, 3769-3777

61. Aerni, H. -R., Cornett, D. S. and Caprioli, R.M., "Automated Acoustic Matrix Deposition for MALDI Sample Preparation", *Analytical Chemistry* **2006**, 78, 827-834

62. Wallman, L., Ekstrom, S.,Marko-Varga, G., Laurel, T. and Nilsson, J., " Autonomous Protein Sample Processing on-chip Using Solid-phase Microextraction, Capillary Force Pumping, and Microdispensing", *Electrophoresis* **2004**, 25, 3778-3787

63. Gustafsson, M., Hirschberg, D., Palmberg, C., Jornvall, H. and Bergman, T., "Integrated Sample Preparation and MALDI Mass Spectrometry on a Microfluidic Compact Disk", *Analytical Chemistry* **2004**, 76, 345-350

64. Musyimi, H.K, Narcisse, D.A., Zhang, X., Stryjewski, W., Soper, S.A. and Murray, K.K., "Online CE-MALDI-TOF MS Using a Rotating Ball Interface", *Analytical Chemistry* **2004**, 76, 5968-5973

65. Liu, J., Tseng, K., Garcia, B., Lebrilla, C.B. et al, "Electrophoresis Separation in Open Microchannels. A Method for Coupling Electrophoresis with MALDI-MS", *Analytical Chemistry* **2001**, 73, 2147-2151

66. Brivio, M., Fokkens, R., Verboom, W. an dReinhoudt, D.N., "Integrated Microfluidic System Enabling (Bio)chemical Reactions with On-line MALDI-TOF Mass Spectrometry", *Analytical Chemistry* **2002**, 74,3972-3976

67. Gustafsson, M., Hirschberg, D., Palmberg, C., Jornvall, H. and Bergman, T., "Integrated Sample Preparation and MALDI Mass Spectrometry on a Microfluidic Compact Disk", *Analytical Chemistry* **2004**, 76, 345-350

68. Ekstrom, S., Wallman, L., Malm, J., Becker, C., et al., "Integrated Selective Enrichment Target –am Microtechnology Platform for Matrix-assisted Laser Desorption/ionization-Mass Spectrometry Applied on Protein Biomarkers in Prostate Diseases", *Electrophoresis* **2004**, 25, 3769-3777

69. Wheeler, A.R., Moon, H., Kim, C.J., Loo, G. A. and Grallel, R.L, " Electrowetting-based Microfluidics for Analysis of Peptides and Proteins by Matrix-Assisted Laser Desorption/Ionization Mass Spectrometry", *Analytical Chemistry* **2004**, 76,4833-4836

70. Hjertén, S., "High-Performance Electrophoresis: the Electrophoretic Counterpart of High-Performance Liquid Chromatography"**,** *Journal of Chromatography A* **1983**, 270, 1-6

71. Taylor, J.R., Zafirato C.D. and Dubson, M. A., "Modern Physics for Scientists and Engineers," **2004,** Prentice Hall, Upper Saddle River

72. Heiger, D. N., Cohen A. S. and Karger, B. L., "Separation of DNA Restriction Fragments by High Performance Capillary Electrophoresis with Low and Zero Cross-linked Polyacrylamide Using Continuous and Pulsed Electric Fields", *Journal of Chromatography A* **1990**, 516, 1, 1-298,

73. Carrihlo, E., Ruiz-Martinez, M. C., Berka, H., Smirnov, I. , Goetzinger, W., Miller, A. W. , Brady, D. and Karger, B. L., "Rapid DNA Sequencing of More Than 1000 Bases per Run by Capillary Electrophoresis Using Replaceable Linear Polyacrylamide Solutions", *Analytical Chemistry* **1996**, 68, 3305-3313,

74. Madabhushi, R.S., Vainer, M., Dolnik, V.,Barker, S., Harries, D.L. and Mansfield, D. W., "Versatile Low-viscosity Sieving Matrices for Nondenaturing DNA Separations Using Capillary Array Electrophoresis", *Electrophoresis* **1997**, 18, 104-111,

75. Fung E. N. and Yeung, E. S. "High-Speed DNA Squencing by Using Mixed Poly (ethylene oxide) Solutions in Uncoated Capillary Columns", *Analytical Chemistry* **1995**, 67, 1913-1919,

76. Westermeier, R., "Electrophoresis in Practice: A Guide to Theory and Practice", **1993**, 2nd Edition, Wiley Company, 17-19, 28-29

77. Seymour, R.B. and Carraher, C.E., "Polymer Chemistry, An Introduction", **1981**, Mercel Dekker, NY,

78. Odian, G., "Principles of Polymerization", **1991**, 3rd Edition, Wiley,

79. Hsieh, H.L. and Quirk, R.P., " Anionic Polymerization, Principles and Practical Application", **1996**, Mercel Dekker, NY,

80. http://www.specialchem4polymers.com/tc/Organic-Peroxides-Polymerization-Initiator/index.aspx?id=4402

81. Fisher, J.P., Dean, D., Engel, P.S. and Mikos, A. G., "Photoinitiated Polymerization of Biomaterials", *Annual Review Material Research* **2001**, 31, 171-181

82. Yu, C., Xu, M. , Svec, F. and Fréchet M. J., "Preparation of Monolithic Polymers with Controlled Porous Properties for Microfluidic Chip Applications Using Photoiniated Free-Radical Polymerization", *Journal of Polymer Science Part A: Polymer Chemistry* **2002**, 40 (6), 755-769

83. Yu, C., Davey, M. H., Svec, F., and Fréchet, M.J., "Monolithic Porous Polymer for On-chip Solid-phase Extraction and Preconcentration Prepared by Photoinitiated in Situ Polymerization within a Microfluidic Device", *Analytical Chemistry* **2001**, 73.5088-5096

84. Eccleston, G. M., Swarbrick, J. and Boylan, J.C., "Encyclopedia of Pharmaceutical Technology", **1992**, Marcel Dekker, New York, 444

85. Dole, M., Mach, L.L., Hines, R.L. and Mobley, R.C., "Molecular Beams of macroions", *Journal of Chemical Physics* **1960**, 49, 2240-5243

86. Whiteside, C.M., R.N. Dreyer, M. Yamashita and J.B. Fenn, "Electrospray interface for Liquid Chromatrographs and Mass Spectrometers", *Analytical Chemistry* **1985**, 57, 675-679

87. Fenn J.B., Mann, M., Meng, C. K. and Wong, S. F., "Electrospray Ionization for Mass Spectrometry of Large Biomolecules", *Science* **1989**, 246 (4926), 64-71

88. Fenn J.B., Mann, M., Meng, C. K. and Wong, S. F., "Electrospray Ionization-Principle and Practice", *Mass Spectrometry Reviews* **1990**,9,37-90

89. Schulz, F., Franzka, S. and Schmid, G., "Nanostructured Surfaces by Deposition of Metal Nanoparticles by Means of Spray Techniques", *Advanced Functional Materials* **2002**, 12, 532-536

90. Kebarle, P., "A Brief Overview of the Present Status of the Mechanisms Involved in Electrospray Mass Spectrometry", *Journal of Mass Spectrometry* **2000**, 35, 804-817

91. Cole, R.B., "Some Tenets Pertaining to Electrospray Ionization Mass Spectrometry", *Journal of Mass Spectrometry* **2000**, 35, 763-772

92. Loeb, L.B., Kip, A. F., Hudson, G.G. and Bennett, W.H., "Pulses in Negative Point-to-Plane Corona", *Physical Review* **1941**, 60(10), 714-722

93. Pfeifer, R.J. and Hendricks, C.D., "Parametric Studies of Electrohydrodynamic Spraying", *AIAA J*., **1968**, 6, 496

94. Kebarle, P. and Ho, Y., "In Electrospray Ionization Mass Spectrometry: Fundamentals Instrumentation and Applications", **1997**, John Wiley &Sons, New York, 3-63

95. de la Mora, J.F. and Locertales, I.G., "The Current Emitted by Highly Conductive Taylor Cones", *Journal of Fluid Mechanics* **1994**, 260,155-184

96. Schmelzensen-Redeker, G., Lütfering, L. and Röllgen, F.W., "Desolvation of ions and molecules in thermospray mass spectrometry", *International Journal of Mass Spectrometry and Ion Processes* **1989,** 90: 22, 139-150

97. Nehring, H., Thiebes, S., Lütfering, L. and Röllgen, F.W., "Cluster Ion Formation in Thermospray Mass Spectrometry of Ammonium Salts", *International Journal of Mass Spectrometry and Ion Processes* **1993**, 128:33, 123-132

98. Iribarne, J.V. and Thomson, B.A., "On The Evaporation of Small Ions From Charged Droplets", *Journal of Chemical Physics* **1976**,64(6), 2287-2294

99. Thomson, B.A. and Iribrane, J.V., "Field Induced Ion Evaporation From Liquid Surfaces At Atmospheric Pressure", *Journal of Chemical Physics* **1979**, 71(11), 4451-4463

100. Terry, S.D., Jermann, J.H. and Angell, J.B., "A Gas Chromatographic Air Analyzer Fabricated on a Silicon Wafer", *IEEE Transactions on Electron Devices* **1979**, 26 (12), 1880-1886

101. Harrison, D.J., Fluri, K., Seiler, K., Fan, Z., Effenhauser, C. and Manz, A., "Micromaching a Miniaturized Capillary Electrophoresis-Based Chemical Analysis System on a Chip", *Science* **1993**, 261, 895-897

102. Jacobson, S. C., Hergenroder, R., Moore, A.W., Jr. and Ramsey, J. R., **"**Precolumn Reactions with Electrophoretic Analysis Integrated on a Microchip", *Analytical Chemistry* **1994**, 66, 4127-4132

103. Becker, H. and Gartner, C., "Polymer Microfabrication Methods For Microfluidic Analytical Applications", *Electrophoresis* **2000**, 21, 12-26

104. Rohr, T., Ogletree, D. F., Svec, F. and Frechet, J., 'Surface Functionalization of Themoplastic Polymers for the Fabrication of Microfluidic Devices by Photoinitiated Grafting', Adv. Fun. Mat. 2003, 13, 4, 264~270

105. Zheng, J. , Li, N. , Ridyard, M., Dai, H., Robbins, S. M. and Li, L., "Simple and Robust Two-layer Matrix/Sample Preparation Method for MALDI MS/MS Analysis of Peptides', *Journal of Proteome Research* **2005**, 4, 1709-1716

106. Efimenko, K., Wallace, W. E. and Genzer, J. "Surface Modification of Sylgard-184 Poly (dimethyl siloxane) Networks by Ultraviolet and Ultraviolet/Ozone Treatment", *Journal of Colloid and Interface Science* **2002**, 254, 306-315

107. Lyons, C.S., Strobel, M. and Mittal, K. L., "Plasma Surface Modification of Polymers: Relevance to Adhesion", **1994**,VSP, 113-121

108. Brydson J., "Plastics Materials", **1999**,Butterworth Heinemann, seventh edition, 82~84

109. Khang, D., Yoon, H. and Lee, H., "Room-Temperature Imprint Lithography", *Advanced Materials* **2001**, 13 (10), 749-752

110. Esch, M. B., Kapur, S., Irizarry, G. and Genova, V., "Influence of Master Fabrication Techniques on the Characteristics of Embossed Microfluidic Channels", *Lab on a Chip* **2003**, 3, 121-127

111. Boothroyd, G. and Knight, W. A., "Fundamentals of Machining and Machine Tools", **1989**, 2nd Edition, Marcel Dekker Inc., New York

112. http://www.osmolabstore.com/OsmoLabPage.dll?BuildPage&1&1&1026

113. http://www.whatman.com/products/?pageID=7.57.293

114. http://www.osmolabstore.com/OsmoLabPage.dll?BuildPage&1&1&984

115. http://www.millipore.com/catalogue.nsf/docs/C7631

116. http://www.osmolabstore.com/OsmoLabPage.dll?BuildPage&1&1&607

117. Wang, Y., Cooper, J. W. , Lee, C. S. and Devoe, D., " Efficient Electrospray Ionization From Polymer Microchannels Using Integrated Hydrophobic Membranes", *Lab on a Chip* **2004**, 4, 363-367

118. Wang, Y., Zhou, Y., Balgley, B. M., Cooper, J. W., Lee, C. S. and Devoe, D. L. "Electrospray Interfacing of Polymer Microfluidics to MALDI-MS", *Electrophoresis* **2005**, 26, 3631-3640

119. Rohner, T.C., Rossier,J. S. and Girault, H. H., "Polymer Microspray with An Integrated Thick-film Electrode", *Analytical Chemistry* **2001**, 73, 5353-5357

120. Salas-solano, O., Carriho, E., Kotler, L., Miller, A. W., Geoetzinger, W., Sosic, Z. and Karger, B. L., " Routine DNA Sequencing of 1000 Bases in Less Than One Hour by Capillary Electrophoresis with Replaceable Linear Polyacrylamide Solution", *Analytical Chemistry* **1998**, 70, 3996-4003

121. Li, D., "Electrokinetics in Microfluidics", **2004**, ELSEVIER B.V

122. Pantankar, N.A. and Hu, H., "Numerical Simulation of Electroomostic Flow", *Analytical Chemistry* **1998**, 70, 1870-1881

123. FEMLAB 3 Chemical Engineering Module User's Guide, Comsol AB

124. Li, Y., Buch, J. , Rosenberger, F., Devoe, D. L. and Lee, C. S. , " Integration of Isoelectric Focusing with Parallel Sodium Dodecyl Sulfate Gel Electrophoresis for Multidimensional Protein Separations in a Plastic Microfluidic Network", *Analytical Chemistry* **2004**, 76,742-748

125. Alarie, J.P, Jacobson, S.C. and Ramsey, J.M., " Electrophoretic Injection Bias in a Microchip Valving Scheme", *Electrophoresis* **2001**, 22,312-317

126. Liu, S., Shi, S., William, W.J. and Mathies, R.A., " Optimization of High-speed DNA Sequencing on Microfabricated Capillary Electrophoresis Channels", *Analytical Chemistry* **1999**, 71, 566-573

127. Geschke, O., Henning, K. and Tellman, P., "Microsystem Engineering of Lab-on-a-chip Devices", **2004**,Wiley-VCH

128. Nguyen, N. and Wereley, S.T., "Fundamentals of Applications of Microfluidics", **2002**, Artech House

129. Wallenborg, S.R. and Bailey, C.G., "Separation and Detection of Explosives on a Microchip Using Micellar Electrokinetic Chromatography and Indirect Laser-induced Fluorescence", *Analytical Chemistry* **2000**, 72, 1872-1878

130. Mikkers, F.E.P., Everaerts, F.M. and Verheggen, T.P.E. M., "Concentration Distributions in Free Zone Electrophoresis," *Journal of Chromatography* **1979**, 169, 1-10

131. Burgi, D.S., and Chien, R.L., "Optimization in Sample Stacking for High Performance Capillary Electrophoresis," *Analytical Chemistry* **1991**,63,2042-2047

132. Jung, B., Bharadwaj, R. and Dantiago, J.G., "Thousand-Fold Signal Increase Using Field Amplified Sample Stacking for On-chip Electrophoresis", *Electrophoresis* **2003**, 24, 3476-3483

133. Duffy, D. C., Macdonald, J. C. , Schueller, O. and Whitesides, G. M., "Rapid prototyping of Microfluidic Systems in Poly (dimethylsiloxane)", *Analytical Chemistry* **1998**, 70, 4974-4984

134. Rohr, T., Ogletree, D., Svec, F. and Frechet, J.," Surface Functionalization of Thermoplastic Polymers for the Fabrication of Microfluidic Devices by Photoniatated Grafting", *Advanced Functional Materials* **2003**, 13 (4), 264-270

135. Hu, S., Ren, X., Bachman, M., Sims, C.E., Li, G.P., and Allbritton, N., "Surface Modification of Poly(dimethylsiloxane) Microfluidic Devices by Ultraviolet Polymer Grafting", *Analytical Chemistry* **2002**, 74, 4117-4123

136. Zamergister, R.A. and Tarlov, M.J., "UV Graft Polymerization of Polyacrylamide Hydrogel Plugs in Microchannels", *Langumuir* **2003**,19,6901-6904

137. Herr, A. E. and Singh, A. K., "Photopolymerized Cross-linked Polyacrylamide Gels for On-Chip Protein Sizing", *Analytical Chemistry* **2004**, 76, 4727-4733

138. Throckmortotn, D. J., Shepodd, T. and Singh, A. K., "Electrochromatography in Microchips: Reserved-phase Separation of Peptides and Amino Acids Using Photopatterned Rigid Polymer Monoliths", *Analytical Chemistry* **2002**, 74, 784-789

139. Decker, C. et al., " UV-radiation curing of acrylate/epoxide systems", *Polymer* **2001**,42, 5531-5541

140. Xiong, S., Ding, Q., Zhao, Z., Chen, W., Wang, G. and Liu, S., " A New Method to Improve Sensitivity and Resolution in Matrix-assisted Laser Desorption/Ionization Time of Flight Mass Spectrometry", *Proteomics* **2003**, 3, 265-272

141. Wang, Y., Zhou, Y., Balgley, B. M., Cooper, J. W., Lee, C. S. and Devoe, D. L., "Electrospray Interfacing of Polymer Microfluidics to MALDI-MS", *Electrophoresis* **2005**, 26, 3631-3640

142. Benzi, R., Biferale, L., Sbragaglia, M., Succi, S. and Toschi, F., "Mesoscopic Modelling of Heterogeneous Boundary Conditions for Microchannel Flows", *Journal of Fluid Mechanics*, **2006**, 548, 257-280

143. Yang, L., Yao, T., Huang, Y., Xu Y. and Tai, Y., "Marching Velocity in Capillary Meniscuses in Microchannels", *15th IEEE International Conference on Micro Electro Mechanical Systems (MEMS)*, **2002**, 93-96